The influence of a coupled formulation on the fluid dynamics in a large scale journal bearing.

by

Jacobus Malan Crous

Submitted in partial fulfilment of the requirement for the degree

Masters of Science (Applied Science)

In the

Department of Mechanical and Aeronautical Engineering

Faculty of Engineering, School of the Built Environment and Information Technology

2014

The influence of a coupled formulation on the fluid dynamics in a large scale journal bearing.

By

Jacobus Malan Crous

Supervisors:	Prof P. S. Heyns and Dr. J. Dirker
Department:	Mechanical and Aeronautical Engineering
University:	University of Pretoria
Degree:	Masters of Science (Applied Science – Mechanics)
Keywords:	Non-linearity, Fluid dynamics, Strong coupled formulation, Weak coupled formulation, Viscoelastic fluids, Non-Newtonian fluids, Journal bearings

Summary

In the pursuit of more accurate diagnostics of turbo machinery sophisticated rotor and bearing models are to be developed in order to better understand the dynamics of the rotor-bearing system. This study is concerned with such bearing models.

Four distinct fluid models are developed: The first two have a viscous fluid formulation, where fluid dependencies enter the momentum equations primarily through the viscosity of the fluid. The last two have a viscoelastic fluid formulation where dependencies enter the equations through an additional differential constitutive relation. This constitutive relation is strongly coupled with the momentum equation.

The dependencies included in the formulation of the fluid are: pressure, shear rate and temperature. The coupling of the fluid models is subject to the dependencies present in the formulation. Uncoupled, weakly coupled and strongly coupled formulations are compared in this work.

The formulated models are solved numerically using the Finite Volume Method in the open source program OpenFOAM. These models were newly implemented in OpenFOAM as part of this study. The models are validated by comparing results with various known analytical solutions.

A region of the bearing is subsequently analysed, where the dependencies of the lubricant are most prominent. In this region the influence of a weak and strong coupled formulation of the fluid dynamics in the oil film was considered.

In this study it is shown that both weak and strong couplings influenced the fluid behaviour significantly. It is shown that when these dependencies are no longer isolated in the mere adjustment of fluid properties is inadequate to account for the influence of dependencies.

The weak coupled formulation shows the difference between the coupled and uncoupled formulations. The weak coupling influence the fluid dynamics to the same extent as the pressure dependency in the region considered. The departure from the classical formulation is however observed to be uniform in the case of a weak coupling.

The difference between the uncoupled and strongly coupled formulation was not as great as in the weakly coupled case. Although the difference was less, it was seen that the presence of the strong coupling was about 40% of that of the temperature dependency in the region considered. The change in flow, for the strong coupled formulation, was non-homogenous compared to the classical formulation.

The influence of the coupling is therefore different in nature. The weak coupling changes the flow more than the strong coupling compared to the classical formulation. The strong coupling introduce a new characteristic to the fluid behaviour not seen with the weak coupled formulation.

Lastly it is shown that in order to model the bearing adequately, the fluid model and the coupling of the governing equations are not trivial. Great care must be taken in both the fluid model used as well as the formulation of the coupled equations.

Acknowledgements

I would like to thank the following people and institutions that have helped me to complete this thesis:

- Dr. Oliver Oxtoby, Dr. Onno Ubink and Dr. Johan Heyns for their invaluable inputs and for the fruitful discussions.
- The Centre for Asset Integrity Management group at the University of Pretoria for supporting me financially though all the studies.
- My dear wife for her prayers, support and encouragement.

Table of Contents

Nomenclature

Symbols

a , b	Constants of the Carreau fluid
$a_{T,p}$	Shift factor
c	Bearing clearance
C_1 , C_2	Constants for WLF-equation
D	Bearing diameter
D/Dt	Material derivative
De	Deborah number
e	Eccentricity of journal centre to bearing centre
f_i	Body force, component i
i, j, k	Index of component (Einstein notation)
k	Thermal conductivity
K_s	Shear constant
L_c	Characteristic length of flow domain
p	Pressure
Q	Heat generation term in energy equation
R_B	Radius of bearing
R_J	Radius of journal
Re	Reynolds number
t	Time
T	Temperature
T_0	Reference temperature
Ta	Taylor number
v_i	Velocity, component i
V	Velocity
x_i	Special vector (Cartesian coordinates), component i

Greek symbols

α	Mobility constant
β	Ratio of solvent viscosity to total viscosity
$\dot{\gamma}_{i,j}$	Rate-of-deformation tensor, component i, j
$\delta_{i,j}$	Dirac delta function
$\delta/\delta t$	Upper convected derivative
ϵ	Eccentricity ratio
η	Viscosity
η_0	Zero shear viscosity
η_p	Polymer viscosity
η_s	Solvent viscosity
η_t	Total viscosity (sum of solvent and polymer viscosity)
θ	Angle measure along circumference of the bearing
λ_1	Relaxation time
λ_2	Characteristic relaxation time
μ	Viscosity, Dynamic viscosity
ρ	Density
$\sigma_{i,j}$	Cauchy stress tensor, component i, j
$\tau_{i,j}$	Extra stress tensor, component i, j
$\tau_{pi,j}$	Polymeric extra stress tensor, component i, j
ϕ	Energy partitioning coefficient

Φ	Time duration of process
ψ	Barus law constant
ω	Angular velocity
ψ	Barus law constant

Abbreviations

BEM	Boundary Element Method
CFD	Computation Fluid Dynamics
CV	Control Volume
DEVSS	Discrete Elastic Viscous Split Stress
ESKOM	Electricity Supply Commision
FDM	Finite Difference Method
FEM	Finite Element Method
FSI	Fluid Structure Interaction
FVM	Finite Volume Method
LES	Large Eddy Simulation
OpenFOAM	Open Field Operation And Manipulation
PISO	Pressure Implicit with Splitting of Operator
WLF	Williams-Landel-Ferry

Chapter 1: Introduction

The maintenance of steam turbines is an important matter and the neglect of which can result in very expensive catastrophic failures and even result in the loss of life. On the other hand the cost involved in the down-time of turbines due to scheduled maintenance is huge and therefore unnecessary maintenance costs millions. There is therefore a need for fault detection in such systems to determine the severity of faults and how they develop over time so as to find the best time to perform maintenance.

The condition of a turbo generator is, for this reason, constantly monitored through various means to give an indication of the overall condition of the system. In the case of turbo generators non-contact eddy current probes, situated at the bearings, are typically used to measure the vibration signals. This continuous monitoring of the system gives information regarding the condition of the system and allows one to monitor fault development in time.

This study form part of a comprehensive program to investigate to what extent more information can be extracted from the vibration signals measured by the eddy current probes. By numerically simulating the rotor-bearing system and inducing faults in the system, the response of the system to these faults can then be studied.

The focus of this study is specifically on the journal bearings models. A set of four detailed bearing models was developed in order to determine how these models behave in the presence of various fluid dependencies. This study attempts to determine how the flow characteristic of the various fluid models are influenced when the velocity field is weakly or strongly coupled with the energy equation and, in some cases, the stress field. The bearing models vary in sophistication. However all four of the aforementioned bearing models are more sophisticated than the classical Reynolds equation.

In order to study the influence of the coupled fields on the fluid behaviour, the following assumptions are relaxed compared to the classical Reynolds equation, to obtain more realistic models:

- In deriving the Reynolds equation, the inertia terms are neglected assuming that the viscosity of the fluid dominates the flow. This greatly simplifies the mathematical model since the nonlinearity of general fluid dynamic problem arises from these terms. The issue with these terms is that a viscous flow dominated by its inertia terms will be unstable. It is also known that under these conditions propagation of instabilities is amplified (White 2006), which leads one to the conclusion that considering these terms is essential when considering the response to the system.
- The viscosity of the lubricant is no longer considered to be constant but is rather modelled as a function of shear rate, temperature and pressure. Each of these either causes the fluid viscosity to increase or decrease. The viscosity of the bearing is crucial to the performance of the bearing. If it is decreased substantially (due to, for instance, a rise in temperature) it could lead to catastrophic failure of the rotor-bearing system. The eccentricity of the bearing is also expected to change with the change in viscosity as a low viscosity would results in a higher eccentricity ratios. (The eccentricity ratio is a measure of how much the centre of the journal is shifted from the bearing centre, where, 0 implies that the centres are aligned and 1 would imply contact between the journal and the bearing).

- The dependence of viscosity on temperature is diminished in practice by adding various polymers to the oil. These additives, being long polymer chains, affect the flow since the fluid properties of the oil are changed. In this study the influences of these additives are included. In order to do this, some of the bearing models are extended to include the behaviour of viscoelastic fluids. Temperature, pressure and shear rate dependencies are also considered for these extended models.

The purpose of the bearing model in the context of the rotor-bearing system is to determine the forces on the journal. The forces generated in the bearing are due to the motion of the journal as well as forces acting on the rotor. The bearing model must therefore allow one to determine the transfer of the forces from the rotor to the bearing and the bearing to the rotor. The system therefore presents a complex interaction between the rotor and bearings. The starting point to study this system is to ensure that models representing the bearings are sophisticated enough to capture the nonlinear behaviour observed in the bearings. In this study the following is to be determined: how does the nonlinearity introduced by weak or strong couplings of the governing equations affect the different bearing models. In addition, if we know that the introduction of a dependency affects the operating conditions in the bearing in a specific way for the uncoupled system, would this dependence be affected by a coupling of the governing equations? Furthermore, if the coupling does affect the bearing model, would this influence be the same in all the bearing models considered? The reason why these questions cannot be easily answered is due to the superposition principle breaking down in the face of non-linear dynamics. By fully coupling the governing equations, a strong nonlinearity is introduced to the system (Christensen 2013).

Once the models that represent this complex system have been developed, the dynamics and characteristic responses of the system can be studied for various operating conditions. When the limitations of the models and the dynamics of the system are understood, it is a relatively simple task to look at the manifestations of fault mechanics in the system. Therefore before studying the complete dynamics of the rotor-bearing system, one must first understand how each individual model is affected by the various dependencies. This is not trivial since the influence of each dependency could potentially vary from one bearing model to another.

This study does not offer an exhaustive model of bearings or rotor-bearing interaction. It rather represents a first step in the direction of providing an answer regarding economical yet accurate bearing models: Viscoelastic fluid models in the context of steam turbine journal bearings are extremely resource intensive, whereas less sophisticated models might not be able to accurately express the flow characteristics present in the bearing. To this end it would be very beneficial to the further development of turbo generator diagnostics to find that for this particular case, a simple linear adjustment to a less sophisticated model would give sufficiently accurate results.

The aim of the study is therefore to examine the nonlinearity introduced by coupling the governing equation fully and looking at how the various dependencies will manifest in the context of the different models.

1.1 Problem statement

In most research projects pertaining to the dynamics of rotor-bearing systems, only very simplified bearing models are used due to the complexity of the systems being modelled. The first simplification is usually to approximate the three dimensional system as a two dimensional system. From there, other simplifications like constant viscosity, isothermal conditions, simplified cavitation model, steady state conditions and laminar flow are also commonly made.

These assumptions typically lead to the Reynolds equation, or variations of the Reynolds equation. These variations are more general models than the classical Reynolds equation and are formulated to address a specific short coming of the classic bearing model. The Reynolds equation is a partial differential equation describing the pressure distribution in thin films. For more general cases the Reynolds equation is solved numerically using either the finite difference, finite element or finite volume methods, since the analytical solutions are limited to very particular cases (such as very long or very short bearings).

Concerning oil-film journal bearings, much more sophisticated models have been developed. Models that address most of the short-comings of the Reynolds equation have been formulated. One area that is still lacking however is to study the difference between the individual bearing models as well as looking at how various dependencies would behave when the governing equations are coupled.

With the advancements in computational power available, the focus of this work is to construct more substantial models of an oil film journal bearing. This was done by breaking away from the conventional Reynolds equation for modelling the pressure distribution in the bearing and rather use more general flow equations, specifically using Cauchy's equations of motion as a starting point. Using these general equations, different bearing models are developed and then compared to each other, specifically regarding the interaction between the various governing equations.

One might wonder whether this is necessary. It might seem unnecessary to examine the nonlinearities that arise due to the coupling of the equations.

In a recent article (W. Li et al. 2011) a simple short bearing model as part of a rotor-bearing-seal model to study the response of the system at various operating speeds. The simple model showed the complexities of the non-linear system considered. However, how much would these results be affected by using a different bearing, rotor or seal model, and, how representative is this model of the real world situation? How much does the coupling of the governing equations change the characteristics of the flow?

As far as the bearing model goes, it is the object of this study to consider this question in order to determine the complexity and sophistication of the bearing model needed to capture the relevant physics.

The problem is approached as a coupled multi-field and coupled multi-physics problem (Markert 2010). It is in the context of this coupling that the bearing models are considered.

Accurately diagnosing fault mechanisms from the observed system response is the criterion for choosing the level of sophistication required.

The dissertation is structured as follows:

The remainder of chapter one provides a broad view of what has been done in lubrication theory and what has been done in recent years to advance the classical theory of lubrication to a more general theory. The advancements in numerical algorithms that are able to deal with these more advance models are then considered. Finally the dynamics of rotor-bearing systems are considered since these offer the background for studying the bearing models that have been developed in the past as well as those developed in this study.

Chapter two deals with the theoretical background and the mathematics needed for the development of the numerical solvers used in this study.

Chapter three deals with the numerical solvers' development form a mathematical point of view, implementation in OpenFOAM and benchmarking of these solvers against analytical solutions to determine the accuracy of the various fluid models developed.

Finally chapter four reports on the application of the developed models to a test case which captures the important physics of a bearing under the operating condition applicable to the context of this study. This test case was chosen in view of the focus of the study: to determine the behaviour of different fluid models in the presence of various dependencies when the governing equations a coupled. Due to the severe amount of computational resources required to model a full scale steam turbine journal bearing, a simpler test case was chosen (see section 4.1 for more details).

1.2 Literature survey

The literature survey comprises four sections:

In the first section the bearing models as well as how these models have developed as far as solution methodology is concerned, are considered.

The second section looks at the expansion of bearing models to include factors that influence the fluid film properties.

The third section is concerned with relevant numerical methods developed to solve complex flow problems. These methods are applied to various kinds of flow problems, the reason this is included in the literature review is that these methods are employed in this study to construct the various bearing models.

Finally the fourth section is concerned with the influence of the bearings on the dynamics of a rotor.

1.2.1 Bearing Models

The theory of lubrication was originally formulated and discussed by Reynolds, who expanded on work done by Rayleigh and Stokes (Szeri 2011). Since then analytical solutions to the Reynolds equation

have only been found for very specific cases: firstly isothermal bearings that are either of infinite length or has negligible length (Vignolo et al. 2011).

Approximations and analytical techniques are used at present to expand the existing analytical solutions to more general operating conditions (Georgescu et al. 2001; Vignolo et al. 2011; X. K. Li et al. 2011). While these solutions remain useful, their generality cannot be compared to the numerical solutions that arose due to the development of the digital computer.

Li et al. (2011) gained useful insight by means of an analytical solution that was obtained. They showed by means of perturbation theory that the viscoelastic effects in bearings are dependent on the minimum film thickness. The upper convected Maxwell constitutive model was used in this study. They reported a significant influence on the pressure distribution due to viscoelastic effects in their application and confirmed their calculations by experimental results.

Expanding the generality through combining analytical and numerical techniques was also accomplished. Mukherjee used an infinite series solution to solve the pressure field and obtained an infinite set of differential equation from the Reynolds equation (Mukherjee 1974). Using numerical integration it was able to compute the forces and the torques on the journal. This approach generalized the existing bearing models to take into account the inclination of the journal.

In the same year the curvature of the lubricant film (this would be the same as the curvature of the bearing) in the convergent-divergent zone was studied. Achieving greater accuracy in predicting the load-carrying capacity, friction losses and lubricant consumption through the numerical solution of a derived analytical expression from the Reynolds equations (Kvitnitsky et al. 1976).

Pure numerical solutions were also developed with different purposes in mind. Performance curves and design procedures have been outlined through the use of numerical solutions. Using the finite difference method the Reynolds equation was solved for a journal bearing with supply ports (Majumdar 1969). Singhal (1981) looked at the relaxation methods for iterative solvers and convergence criteria when using the finite difference method. Using the finite difference method the misalignment of a journal in the bearing in pressurized journal bearings was modelled (Kayar & Khalil 1983).

One of the major drawbacks with the analytical solutions is that they are two dimensional. Li et al. (1999) described the importance of three dimensional effects in bearings that are dynamically loaded. They first looked at the difference between the results obtained using the Reynolds equation ,when solved with the long and short bearing approximations, and that of solving the full set of governing equations. They considered bearings with different aspect ratios (bearing length to diameter): L/D = 10/1, 1/1, 1/10. They then used the models to predict the force acting on the journal perpendicularly and the torque resisted by the film. The numerical results were compared to the long bearing solution and found to be in good agreement. The results were seen to come closer and closer as the eccentricity ratio of the journal increases. This was not the case for the short bearing as there was quite a large discrepancy between the results. They pointed out that the reason for this is that in the case of the long and short bearing approximation when determining the forces in the bearing and on the film it is done with only the determined pressures obtained with the Reynolds equation. When working with the Cauchy equations of motion, however, there is an additional term computed that arise from the stress tensor which was neglected when only the pressure distribution is used to compute the forces.

The contribution of this stress tensor is more prominent in the short bearing case. In addition to this, it was also noted that the finite bearing takes side leakage into account. This is not done in the case of the short or long bearing approximations. The implication of this is that the predicted force in the finite bearing tends to be less than what is predicted by the other two approximations. This implies that the behaviour of the finite bearing does not just simply lie somewhere in between these extremes, but is influenced by additional factors that affect the operating conditions of the bearing. These additional factors are neglected when the long and shot bearing approximations are used.

Li et al. (1999) were not the first to realize the limitations of the analytical solutions in this regards. In early computational work on journal bearings the finite difference method was extensively used (Majumdar 1969; Mukherjee 1974; Singhal 1981; Kayar & Khalil 1983), however, analyses have also been done using the Boundary Element Method (BEM) and/or the Finite Element Method (FEM) (Li, Davies, et al. 2000; Li et al. 1999; Davies & Li 1994; Li, Gwynllyw, et al. 2000; Gwynllyw & Phillips 2008; Kohno et al. 1994), as well as the Finite Volume Method (FVM)(Gertzos et al. 2008; Jagadeesha et al. 2012).

Advances in oil technology have introduced new complexities to the field of lubrication, to the extent that Li et al. (2000) claims that lubricants with polymer additives have rendered lubrication theory inapplicable. This is specifically seen with synthetic oils which contain long polymer chains that when added to the base oil give rise to non-Newtonian flow behaviour (Chhabra & Richardson 2011). Due to the realization that the assumptions made in deriving the Reynolds equation are at times very crude, there is a need to develop models that include more dependencies of the lubricating oil (Stachowiak & Batchelor 2013).

1.2.2 Expanding the classical Reynolds model of lubrication

There are numerous variables that influence the operation of a journal bearing system. One of the most important factors is the viscosity of the lubricant used. The viscosity, in turn, is influenced primarily by the temperature, pressure and shearing rate of the lubricant film in the bearing. According to Mang and Dresel (2007) these are the three main dependencies that influence the viscosity. The temperature and the shearing rate will cause shear thinning behaviour in the film while an increase in pressure will result in shear thickening (Li, Gwynllyw, et al. 2000).

To gauge the dependence of viscosity on temperature the viscosity scale was introduced in 1928. The purpose of this scale is to give the viscosity dependence on the oil relative to other base oils. A base oil with viscosity index 0 would imply a very small dependence of the viscosity on the temperature, where as if an oil has an index 100 the opposite would be true. The turbine oils considered in this study has VIs (viscosity indices) ranging from 95 to 105. It is therefore quite clear that temperature dependence is very significant.

Furthermore, Mang and Dresel (2007) also mentioned that viscosity dependence on pressure is an effect that is frequently underestimated in lubrication applications. Due to the exponential dependence of viscosity on pressure it follows that the viscosity can rapidly increase due to an increase in pressure. He also notes that the VI improvers, added to the lubricant, can have a significant effect on the pressure dependence of the viscosity.

Binding et al. (1999) showed the importance of taking pressure dependence into account when modelling journal bearings. They demonstrated that viscoelastic effects become prominent at high pressures. The pressure dependence of a fluid can therefore enhance other dependencies that would not be significant at ambient pressures.

The importance of taking the non-Newtonian fluid behaviour of the oil into account has also been highlighted (Walters et al. 1997) . This specifically refers to the viscosity's dependence on the shear rate.

When considering the classical lubrication model of Reynolds it is important to note that all of the aforementioned dependencies of viscosity are ignored when deriving the classical Reynolds equation (Stachowiak & Batchelor 2013). In order to extend the generality of the classical lubrication theory, two approaches are commonly seen in the literature: Firstly the Reynolds equation is reformulated using a control volume approach to extend the classical theory to include the desired dependencies and effects that are to be modelled. This extension of the models might also include describing certain dependencies using semi-empirical models. Secondly the assumptions of the Reynolds equations are deemed too restrictive for certain cases (Gwynllyw & Phillips 2008) and therefore by back-tracking to more general fluid equations, the problem is reformulated .

In a theoretical paper Ramesh et al. (1997) set out to extend the classical Reynolds equation to include some of the complexities introduced through the development of oil technology and seen in practice. They extended the classical Reynolds equation to include thermal effects, specifically: the dependency of viscosity on temperature, the effect of surface roughness on the hydrodynamic pressure distribution and cavitation that arise in the diverging section of the wedge when the film thickness increases locally. The cavitation model was also modified to take surface roughness into account.

Continuing along this line of research, the power law has been used to model the lubricant as a non-Newtonian fluid (Nagaraju et al. 2003). In this study the influence of the power law index on the performance of the bearing was considered. The Reynolds equation was extended to include the effects of shear thinning, by modelling the fluid as a power law fluid, and surface roughness. Cavitation and thermal effects were however not modelled. This study was less concerned with the extension of classical lubrication theory to a more general theory as the previous one. The reformulated Reynolds equation was then discretized using the finite volume method.

Jagadeesha et al. (2012) extended this work even further by using the generalized Navier-Stokes equations with a viscous non-Newtonian model. The governing equations that was used for the flow was more general and included the inertia terms while deriving the classical Reynolds equation these terms are normally neglected. This extension alone introduced a non-linearity into the equations, since the inertia terms in the equations were highly non-linear (Ferziger et al. 2008). By including these terms, it is no longer possible to describe the flow as being just a viscous dominant flow. This would only be the case for low journal speeds. In addition to the above, the following was also included into the model: (1) Three dimensional mixing of the lubricant due to surface roughness was considered. This is very significant since the previous work done was primarily done with two dimensional equations since flow variables are averaged out across the film. (2) A more general viscous non-Newtonian flow model was used to describe the flow. This model is able to predict the behaviour of Herschel-Belkley fluids. In this study (by Jagadeesha et al.) journal bearing performance characteristics

are derived and presented for various bearing aspect ratios. This study was conducting using the software package Fluent which is a finite volume method based package.

An extension of the model developed by Jagadeesha et al. has been constructed by the reformulation of the Reynolds equation using a viscoelastic constitutive relation. The fluid can therefore be described as having a shear dependent viscosity, normal stress difference and a relaxation time associated with it. By discretizing the reformulated Reynolds equation by the finite difference method is can be solved numerically. Through such an analysis it was found that the maximum pressure in the bearing predicted for a Newtonian fluid differs from the viscoelastic fluid. The maximum pressure for the Newtonian model was shown to be either more or less than the viscoelastic model, depending on the angular velocity of the journal (Haosheng & Darong 2005).

Another useful extension of the classical Reynolds equation that is worth noting for this research is the extension of the theory to a three dimensional model that takes journal misalignment into account due to the deformation of the rotor shaft. The pressure distribution can be substantially different from the classical theory depending on the severity of the misalignment. The location of the minimum and maximum film thickness changes depending on eccentricity ratio of the bearing as well as journal misalignment. It follows that the location of the maximum pressure also changes as a function of these two variables. Interestingly it was found that the load capacity, attitude angle, amount of oil leakage and friction coefficient is independent of journal misalignment (Sun & Changlin 2004).

The latter approach is useful in expanding the generality of lubrication theory. The shortcoming of this model, however, remains: the inertia terms of the fluid film are neglected from the model (the work done by Jagadeesha et al. is an exception). The severity of this shortcoming is better understood in the light of the Taylor-Couette problem. The Taylor-Couette problem is essentially a stability analysis of the fluid between two concentric rotating cylinders (Owens & Phillips 2002). In order to analyse the stability of the flow the Taylor number is defined as (in the case where the outer cylinder is stationary):

$$Ta = 2Re^2 \left(\frac{c}{R_J}\right) \tag{1.1}$$

where Re is the Reynolds number of the flow, describing the ratio of inertia forces to viscous forces (White 2006), c is the clearance of the bearing and R_J is the radius of the inner cylinder. The Taylor number presents a similar ratio to the Reynolds number; however it is translated to a cylindrical domain. The Taylor number becomes important since it increases as the bearing size increases, mainly due to the bearing clearance increasing for larger bearings (Lisyanskii et al. 2006). The journal bearings for steam turbines have Reynolds numbers of 20 000 under normal operating conditions (Uhkoetter et al. 2012). The inertia terms in this kind of flow would be dominant and the flow would be fully turbulent. Similarly the Taylor number the steam turbine bearings considered in this study corresponding to transitional flow would be around 6 400. The corresponding Taylor number for the aforementioned case studied by Uhkoetter et al. is two orders of magnitude higher than this. In order to adequately model this kind of problem, it is necessary to break away from the Reynolds equation and consider a reformulation of the problem.

A three dimensional multiphase bearing model that takes turbulence, temperature and mixing of the lubricant into account was developed by Uhkoetter et al. (2012). The multiphase model was developed in order to understand the influence of cavitation in heavy duty steam and gas turbines. It was

concluded that when modelling these kinds of bearings a cavitation model is essential. The multiphase model had to be modified from the more common formulation to deal with the high shear rates encountered in this case. Although a multiphase model was employed, the film was still assumed to be incompressible and the lubricant Newtonian. Despite these assumptions the work gives very good insight into the shortcomings of the classical Reynolds model as well as providing very good visualizations of the flow within these large scale bearings.

In considering the formulation of problem in order to include the inertia terms of the flow, a significant amount of work was done by Davies, Gwynllyw, Phillips and Xi. In their research they use more generalized flow models. This allows them to construct more sophisticated bearing models.

Modelling concentric cylinders at high eccentricity ratios they were able to look at the influence of various factors that influence the operating conditions of the bearings. By modelling the fluid as a viscoelastic fluid, using the White-Metzner constitutive relation, they showed that the relaxation time of the lubricant can significantly affect the load carrying capacity of the bearings, even showing increased load carrying capacity of up to 20%, due to the difference in normal stresses (Davies & Li 1994). In later studies less general fluid models were used. This would usually entail a generalized Newtonian formulation with a non-Newtonian viscosity relation (this is also called a viscous formulation, since the non-Newtonian viscous part of the flow is modelled while neglecting any elasticity of the fluid).

Continuing the inclusion of various constitutive models into the context of lubrication theory, Grecov and Clermont (2005) applied a stream-tube method as well as domain decomposition to model lubricants that have Newtonian properties, non-Newtonian properties (by using the generalized Newtonian model as the constitutive relation) and viscoelastic fluid properties. For the modelling of the viscoelastic fluids the Upper Convected Maxwell model was used as well as the K-KBZ integral constitutive relation that deals with fluids that have a high relaxation time, therefore having a greater dependence on the fluid's previous states.

Looking at the temperature and pressure dependencies of viscosity it has been shown that pressure thickening behaviour is dominant at high eccentricities. This implies that shear thickening of the lubricant is dominant at high eccentricities, unlike the usual shear thinning behaviour of a temperature dependence(Davies & Li 1994).

By analysing the effect of thermal boundary conditions on the temperature of the film it was shown that a Dirichlet boundary conditions on the journal and Biot (or Robbins) boundary condition on the bearing casing gave the best results for modelling automotive bearings(Davies & Li 1994). However it has since been shown in independent research, that the adiabatic thermal boundary condition for the bearing casing is more accurate when the film is in the turbulent range (Stachowiak & Batchelor 2013). The Biot number in the Biot boundary condition constructs a boundary condition that is a linear interpolation between the Dirichlet and Neumann boundary conditions. If the Biot number is small the boundary condition will tends to the Neumann boundary condition and vice versa. In this way it was shown that the choice of boundary condition can significantly influence the maximum temperature in the lubricating film and therefore the dominance of the temperature dependence of the viscosity of the bearing (Li et al. 2000). If shear thinning is dominant in the bearing the viscosity of the bearing will decrease and therefore the eccentricity of the bearing will increase. If bearings are therefore not designed with this in mind, temperature rises in the bearing could lead to bearing failure.

In general it was shown that treating bearings with a thermal analysis yields lower load carrying capacities of about 6% than predicted by an isothermal analysis.

The first study by Davies and Li (1994) considered a steady state and a two dimensional problem, while in subsequent studies analysis of the transient dynamics have been performed as well as looking at the factors that influence the dynamics of the journal. The most significant were found to be three dimensionality (Li et al. 1999) and temperature of the lubricant(Li, Davies, et al. 2000).

The influence of neglecting the third dimension, either axially (as is the case in the long bearing approximation) or circumferentially (as is done with the short bearing approximation) was considered under both steady state conditions and transient dynamical conditions. Analysing the results by computing the force and torque acting on the journal for the steady state conditions showed good agreement between the numerical results and the long bearing approximation. The short bearing approximation, however, did not validate the numerical results. The reason they give to explain this is the neglecting of the extra stress terms of the Cauchy stress tensor when computing the forces on the journal. When just the trace of the stress tensor was used to compute the pressure distribution it was found to be in agreement with the short bearing approximation. This shows that the pressure distribution of both the short and the long journal bearing in the limit compares well with the numerical results (Li et al. 1999). This is a very important result since this shows that although the pressure distribution in the bearing might be predicted accurately, care must be taken in computing the force from only the pressure. This further also shows that when the force on the bearing is to be computed, it is not merely a superposition of the two approximated solutions. One cannot compute the long bearing solution and the short bearing solution and interpolate between them to find the force acting on a bearing that is not described by either of them. For transient cases the journal paths were considered while varying the load applied to the journal as well as the aspect rations of the bearings. It was shown that the aspect ratio significantly affect the eccentricity ratio at which the journal will operate.

The effect of viscoelastic fluid model and relaxation times of the lubricant was studied for various gap sizes of the bearing on the dynamics of journal bearings. It was found that for an Oldroyd-B fluid (a fluid described by a non-linear differential constitutive relation), an increase in the relaxation time of the lubricant would result in higher load carrying capacities of the bearing. This was however not the case with the linear PTT lubricant[1] for which a decrease in load carrying capacity was observed for higher relaxation time. This is, however, not the only dependence that the lubricant exhibited: it was also seen that an increase in the shear and extensional parameters of the PTT model would result in increasing shear thinning of the lubricant as well as shear hardening. These conclusions are drawn by looking at the orbital paths and eccentricities of the bearings in its dynamical state (Gwynllyw & Phillips 2008). This study is therefore an extension of the earlier one done by Davies and Li (1994), considering the influence of viscoelasticity on bearings operating under steady-state conditions.

In a more general context viscoelasticity has been shown, even at moderate Weissenberg numbers, to greatly influence the flow condition between two eccentric cylinders (Liu & Grecov 2011). The load

[1] Like the Oldroyd-B model, it is described by a non-linear differential constitutive relation. The PTT constitutive relation has an additional term, compared to the Oldroyd-B model, which described shear thinning and a bounded extensional viscosity

capacity of the bearing was shown to increase and the overall performance of the lubricant was improved when viscoelastic behaviour was present.

In all the above-mentioned studies it was assumed that the fluid film is incompressible. In a preliminary study the influence of compressibility of the lubricant was explored on journal bearings (Bollada & Phillips 2007). A simple Newtonian model with linear relations between density and pressure was used in order to determine the extent of the influence of compressibility. The analysis was done under steady-state conditions as well as the isothermal condition. It was, however, explicitly mentioned that these assumptions would be rectified in subsequent papers. The model would then also be extended to include a full cavitation model. The development of these models have been seen in literature, however, their application to journal bearings is still lacking (Lind & Phillips 2011; S. J. Lind & Phillips 2012; S. Lind & Phillips 2012).

In this preliminary paper, however, it was found, quite surprisingly, that the compressibility of the lubricant plays a significant role on the dynamics of the bearing even at Mach numbers as low as 0.02. It was seen that the compressibility of the lubricant would increase the load carrying capacity of the bearing due to the asymmetry of the pressure distribution. A mechanism that breaks this asymmetry would generate a resultant force that acts in the line that connects the centre of the bearing with the centre of the journal (Bollada & Phillips 2007).

In recent years there has been increased interest in using smart fluids for lubrication purposes. Electro-Rheological Fluids (ERFs) or Magneto-Rheological Fluids (MRFs) are both examples of this. The properties of these fluids change in the presence of a magnetic or electric field. In order to model these fluids in the context of lubrication theory the Bingham fluid model is used. Such a model was implemented in the Fluent environment in order to find the following performance characteristics of these lubricants: eccentricity ratio, attitude angle of the journal, pressure distribution, friction coefficient, lubricant rate of flow and maximum pressure given the length to diameter ratio of the bearing as well as the dimensionless shear number. The analysis performed was isothermal and incompressible. The flow was modelled using a generalized Newtonian formulation (Gertzos et al. 2008).

Most of the bearing models constructed through the reformulation of the film dynamics through the use of more general flow equations was applied to bearings found in the automotive industry. These bearings have dimensions that differ greatly form that considered in the present study. As mentioned previously, the size of the bearing would have a significant effect of the fluid dynamics of the fluid film. The conclusions made regarding dependence of the operating conditions on various fluid properties comes under scrutiny to determine which effect can simply be translated to the larger bearings as well as other fluid models.

The various factors that influence the lubricant film were highlighted in this section. These dependencies from the base of the study, since the influence of these dependencies on one another are considered in this study.

1.2.3 Recent developments in numerical techniques dealing with fluid flow

A large body of work exist for Computation Fluid Dynamics (CFD) as well as computational rheology. In this section therefore only the recent and relevant articles will be discussed. Due to the diversity of the field it would be very difficult to cover the development of the entire field.

The field of CFD and Computational Rheology has been developing rapidly with the increasing availability of computational power. This being said, although a large amount of work has been done in solvers for viscoelastic fluids, the generalization to compressible solvers is still under-developed (Bollada & Phillips 2007). In a recent study Phillips et al. (2012) showed that the generalization of a viscoelastic solver from an incompressible solver to a compressible solver is far from trivial. One of the main issues that arise is that the fundamental link between the velocity gradient tensor and the Cauchy stress tensor disappears once the fluid elements are no longer considered to conserve their volume. This clearly leads to various difficulties that should be addressed if a compressible model is to be developed (Bollada & Phillips 2012). Although the importance of such a model to the response of journal bearings cannot be discounted, the difficulties that arise due to such a formulation place it outside of the scope of this study. It is surely something that would have to be revised if one is to improve the current models.

Oliveira et al. (1998) used a finite volume based method to solve viscoelastic fluids with a differential constitutive relation. This model was then applied to two test cases: the entry flow problem and the bounded and unbounded flow past a cylinder. A Rhie-Chow inspired interpolation scheme was developed that required less storage space and was therefore more efficient. A second order scheme was used to discretize the convection terms: the linear upwind differencing scheme (LUWD), which is an extension of the upwind differencing scheme (UDS). The scheme is extended by taking two upstream values into account instead of just one. This leads to a stable and robust numerical model that gave good results compared when with experiments.

In studying viscoelastic flows, a semi-Lagrangian finite volume scheme with a staggered grid arrangement has been applied to contraction flows. A differential Oldroyd-B constitutive relation was used to describe the viscoelastic behaviour of the fluid. The Lagrangian nature of the scheme was incorporated into the finite volume context in order to trace particles over a single time step. This is done by means of a particle following transformation, using the latter transformation the convection terms in the momentum equation as well as the constitutive relation was evaluated. This numerical scheme was found to be stable and bypasses the numerical diffusion difficulties associated with the upwind differencing scheme (Phillips & Williams 1999).

The computation of non-isothermal viscous and viscoelastic fluid models in contraction geometries was considered by Wachs et al. (2002). In this work three fluid models were compared: a Newtonian fluid model, a generalized Newtonian fluid model with thinning viscosity and a viscoelastic fluid model with a differential constitutive relation. The shear thinning of the generalized Newtonian model is described by the Carreau model. The differential constitutive relation used for the viscoelastic fluid is the Upper Convected Maxwell relation. All these fluids were modelled as having a temperature thinning viscosity, described by the William-Landel-Ferry equation. The three fluid models were then compared to one another by looking especially at the length of the recirculating flow region at various contraction ratios of the contraction geometry. A further comparison was done by looking at how the

temperature dependence of each of these models affects the size of this recirculation zone. The numerical discretization was done with the finite-volume method using a staggered grid arrangement (Wachs et al. 2002).

In their study Wachs et al. (2002) used the EVSS (Elastic Viscous Stress Splitting) formulation in order to stabilize the numerical solver. The problem that arises from the explicit evaluation of the stress tensor in time is that it leads to constraints on the time step size having to be extremely small. If the time step size is not chosen sufficiently small the solver diverges rapidly. This formulation splits the viscous and elastic parts of the tensor and allows one to evaluate part of it implicitly in time and therefore achieve greater accuracy. The formulation is not restricted to a particular discretization method but rather can be applied directly to the general governing equations in its continuous form. This method has been extended to the DEVSS (Discrete Elastic Viscous Stress Splitting), which is an easier formulation to implement (Gucnette & Fortin 1995) and has been adopted in work related to viscoelastic flows (Habla et al. 2012; Omowunmi & Yuan 2013; Favero & Secchi 2009). In this extension an elliptical term is added to the governing equations which can then be evaluated implicitly in time. This additional term strengthens the diagonal dominance of the matrix obtained from the discretized set of equations. This in turn increases the stability of the numerical scheme.

In the context of OpenFOAM, an open source CFD package, Favero et al. (2009) developed a viscoelastic module in which some of the more commonly used differential constitutive relations are available. These constitutive models include: the UCM (Upper Convected Maxwell), Oldroyd-B, Giesekus, PTT (Phan-Thien-Tanner), FENE-P and FENE-CP (Finitely Extensible Nonlinear Elastic) fluid models. The P refers to Peterlin, whose idea forms the basis of the FENE-P and FENE- CP models. In addition, some derivations of the Pom-Pom models with both single and multimode form are included in this module. The advantage of using OpenFOAM to develop such a module is that it is able to handle non-orthogonal, unstructured meshes as well as dynamic meshes therefore allowing one to apply these flow models to complex geometries. It also has a wide variety of already programmed interpolation and discretization schemes (Favero & Secchi 2009). In a paper by Faverco and Secchi (2009), the solver was applied to 4:1 contraction geometries using only the Giesekus constitutive model. In another paper (Mu et al. 2012) this idea was extended to three dimensional contraction geometries and extended to include the PTT and FENE-P constitutive relations. OpenFOAM was, however, not used in the aforementioned study but rather a finite element method package was used.

Non-isothermal viscoelastic flows have been considered in the OpenFOAM environment by Habla et al. (2012). They studied Oldroyd-B fluids with temperature dependencies modelled by the William-Landel-Ferry equation and used the same fluid properties as the Wachs et al. (2002) study. A 4:1 contraction geometry was used to study the stress in the fluid at various Deborah numbers. In order to study the stress field more accurately an interpolation scheme obtained through a second order linear regression scheme was used.

Two-phase flow models have also been implemented in OpenFOAM. Looking at two-phase turbulent flows modelled with a LES (Large Eddy Simulation) model. Several cavitation models were simulated which have great significance in marine turbines as well as power turbines (Bensow & Bark 2010).

Two-phase flow models have also been developed for viscoelastic flows using the volume-of-fluid method. This solver is also able to simulate the surface effects of the fluid. The models have the following differential constitutive relations available: Oldroyd-B, Giesekus, FENE-P, FENE-CR, PTT,

Pom-Pom and XPP models. Using this, free surface effects such as the Weissenberg and the Die Swell effect have been studied. Comparison to several experiments was also done and found to be in good agreement (Habla et al. 2011).

The time dependent non-linear dynamics of polymer solutions were studied with respect to the effect of model parameters, the inertia of the fluid and the contraction ratio in microfluidic contraction flow. This study was also done in OpenFOAM and critically compares the rheometric material function of the FENE-CP model to that of the LPTT (Linear Phan-Thien-Tanner) model (Omowunmi & Yuan 2013).

Due to the complexities of the fluid dynamics considered in the present study and the small body of literature available on the coupling of these general fluid equations, numerical techniques from various areas of CFD are employed. These numerical techniques, their development and application were presented in this section.

1.2.4 Rotor-bearing systems

Journal bearings, in the context of steam turbines, are not isolated units operating by themselves, but rather form the support structure for the rotor. It is therefore important to note that the study of journal bearing dynamics is crucial when studying the dynamics of the rotor bearing system (Szeri 2011).

The acoustic emissions form a journal bearing has given some insight as to how sensitive the dynamics of the bearings are with respect to the material properties of the system. The magnitude of the applied load, the flexibility of the bearing casing and the viscosity of the lubricant all influence the acoustic behaviour of the bearing. This would influence the response of the rotor-bearing as a whole (Bouaziz et al. 2012).

The load carrying capacity of the journal bearing is usually computed by integrating the pressure distribution obtained through the Reynolds equation (Szeri 2011; Luneno & Aidanpää 2010). In order to reduce the complexities and the computational power required to deal with the full Reynolds equation, the short or long bearing solution is usually used to compute the forces acting on the rotor (Avramov & Borysiuk 2011; Luneno & Aidanpää 2010; W. Li et al. 2011).

Chaotic behaviour in journal bearing orbital paths have been reported. This was due to a nonlinear treatment of the restoring force in the bearings, while looking at the dynamics of flexible rotors (Chen 1998). It was seen that the angular velocities at which chaotic behaviour is very prominent corresponds to the operating conditions for many systems of this kind. One of the primary factors that contribute to this chaotic behaviour is the nonlinear suspension provided by the journal bearings. This would result in broad band vibration in the system. It is therefore necessary to consider the influence of the journal bearings on the response of the entire system.

A third order Taylor expansion was used by Sawicki and Rao (2001) in order to evaluate the nonlinear dynamic coefficients for a given position of the journal in the orbital path. The need for a nonlinear analysis of this kind is necessary in cases where the vibration amplitude of the journal is large. In this case the reaction force from the bearing is nonlinear. The reaction force of the bearing must therefore

be computed with higher order techniques since the linear theory is inadequate in predicting the reaction force of the film to the journal.

Luneno and Aidanpää (2010) considered the different results obtained by linear and non-linear analyses on the rotor bearing system. They found that the linear model was unable to give the correct orbital paths for the shaft in the bearing if the eccentricity ratio or the angular velocity of the shaft becomes too high. The linear model predicted elliptical journal orbits that grow bigger as the speed of the journal increases. The linear model was, however, unable to predict deviations from the elliptical journal orbit behaviour that is present at higher angular velocities. At eccentricity ratios larger than 0.6 the oil film behaviour became highly nonlinear, at which point the linear model was not sufficient to predict dynamic responses in the system.

A similar study was performed where the differences between the linear and nonlinear models were considered in its ability to predict the orbital paths of the journal (Moreira et al. 2000). The bearing model used, however, was different: a modified Reynolds equation was used that employed a semi-empirical model for the turbulent shear stress at the wall of the journal and the bearing casing. The bearing model was isothermal, two dimensional and incompressible. It was seen, however, that the nonlinear model compared well with experimental results.

The nonlinear dynamics of an asymmetric rotor was studied by Avramov and Borysiuk (2011). Using the short bearing solution to model the dynamic forces that the bearings exert on the rotor, and taking into account the gyroscopic moments which act on the disk, the response of the rotor was studied for various angular velocities. By looking at the Hopf bifurcation point by means various techniques they found mono-harmonic and poly-harmonic vibrations. In light of this analysis concluded that a linear analysis of the rotor-bearing system is unable to describe the complexities of the system under self-sustained vibrations.

Hamilton's principle was used by Li et al. (2011) to construct a novel nonlinear model of the rotor-bearing-seal system, improving the previous models. The system was modelled in terms of the kinetic and potential energies of the shaft and disk. Work was then done on the system by means of bearing forces acting on the shaft and forces from the steam acting on the rotor. The model is quite simple as it uses a five node finite element model to describe the rotor and disk and uses the short bearing theory to model the bearing forces. Looking at Bifurcation maps, time-history diagrams, Poincare maps, Fourier transforms of the response and trajectory maps of both the bearing and the disk they showed that the system had highly nonlinear behaviour as the angular velocity of the shaft increases above 700 rad/s.

The nonlinear dynamics in shaft lines due to coupling misalignment was studied by Pennacchi et al. (2012) using a more sophisticated approach as far as the rotor model is concerned. A detailed finite element model was constructed for the rotor which was supported by journal bearings modelled by the Reynolds equation. The journal bearing model was then solved using the finite differencing method. This allowed for a more elaborate dynamic analysis on the system and allowed them to diagnose coupling misalignments in the rotor by looking at the higher order harmonic components of the response (Pennacchi et al. 2012).

The dynamic analysis of journal bearings are complicated further by various dependencies such as: heat transfer and pressure (Davies & Li 1994; Solghar & Gandjalikhan Nassab 2011), type of lubricant

used (Li, Gwynllyw, et al. 2000; Gwynllyw & Phillips 2008; X. K. Li et al. 2011), the diameter to length ratio (Li et al. 1999), the surface roughness of the bearing surface (Jagadeesha et al. 2012), compressibility of the fluid film (Bollada & Phillips 2007), turbulence in the fluid film (Solghar & Gandjalikhan Nassab 2011) and cavitation (Wang et al. 2011). These factors influence the orbital path of the journal in the bearing; it would therefore have a direct influence of the response of the system as was shown in most of the articles sighted above.

A modified form of the Reynolds equation was used by Jagadeesha et al. (2012) to look at the transient response of non-Newtonian journal bearings taking into account the roughness of the bearing surface. This model was solved using the finite element method. The power law was used to describe the non-Newtonian fluid film, the effect of transverse and stationary surface roughness was then studied on the bearing orbital path. It was found that surface roughness has a significant effect on the operating conditions of the bearing. Generally it was seen that surface roughness benefits the operating conditions as the minimum film thickness in the bearing is increased or unaffected, but never decreased, by these two types of surface roughness considered.

A stability analysis was performed by Mongkolwongrojn and Aiumpronsin (2010). They showed that the stability of the rotor's response is strongly influenced by the bearings. This is affected by the surface roughness of the bearing, the lubricant used as well as the rigidity of the metal liner of the bearing. It was shown that transverse surface roughness patterns results in a more stable system compared to longitudinal roughness patterns. Further more stability was shown to increase with a decrease in length diameter ratio of the bearing.

The influence of cavitation on the dynamics of journal bearings was studied by Wang et al. (2011). Considering the difference between the Reynolds boundary condition on the pressure field, which forces the pressure to be zero in the diverging section of the bearing where cavitation is expected, and an improved Elron cavitation model. The bearing was subjected to dynamic loads and it was found that the cavitation model used can significantly affect the journal orbital and the response of the bearing. Additional damping is provided by the cavitation mechanism. This damps dynamic responses in the system as seen by analysing the orbital path of the journal in dynamically loaded cases (Li, Davies, et al. 2000).

A fully coupled bearing-rotor system was simulated by Liu et al. (2010). Using a monolithic Fluid Structure Interaction (FSI) method the deformation of both the bearing and the rotor was simulated. A simple cavitation model was employed that varies the properties of the lubricant according to the pressure of the lubricant in the diverging section of the bearing. This model was used to compute the orbital path of the journal for varying degrees of dynamic instability. The elastic dynamics of the rotor and the bearing was considered, the elasticity of the material of the rotor and bearing were seen to significantly influence the orbital path of the journal. The study showed the extent to which modelling errors can influence the predicted results for highly nonlinear systems (Liu et al. 2010).

The literature on rotor-bearing systems shows emphatically the non-linearity of these systems. Predicting the evolution of these non-linarites (i.e. the development of the dynamics in the rotor-bearing system) becomes obscure when all the non-linarites are not accounted for or not allowed to interact with one another. (Due to the super-position principle breaking down one can no longer model systems individually and extrapolate the behaviour of the systems in the presence of other factors influencing the operating conditions). The accurate prediction of the dynamics of the rotor-

bearing system hinges on adequately modelling and accounting for interaction of the non-linarites present in the system.

1.2.5 Summary

Looking at the complexity of the work done in the past decade in the field of tribology it is evident that the classical and linear models are no longer sufficient to model all the complexities in the system. This can further be seen when looking at the response in literature to develop exceedingly sophisticated nonlinear models to investigate the dynamics of the rotor-bearing systems. In addition to the nonlinearities introduced through the dynamics of the system, additional factors that are essential to the construction of an accurate model demands more complex models to capture the physical laws governing the dynamics of the system. The issue that arise in the realm of nonlinear mechanics is that the superposition principle is not applicable. Caution should therefore be taken when looking at a single dependency and extrapolating the effect it has to the general nonlinear system. A single dependency would not necessarily influence the general system in the same way when other dependencies are present. The literature cited above showed definitively that nonlinear dynamics are common in the kinds of problems considered in this study. This implies that to merely extrapolate results from one model to another would be quite naïve. There is thus merit in looking at how well the dependencies translate from one model to another when the models considered are not uncoupled, but rather strengthens the non-linearity further by coupling the governing equations with one another.

In this study we will therefore not be looking to consider the influence of various dependencies on the bearing operating conditions individually. Rather we want to compare various models that take into account various nonlinearities and look at how these nonlinearities behave in the presence of one another.

Chapter 2: Models and Theory

The modelling of a journal bearing is not a simple matter. There are numerous mechanisms of heat generation and deformation, amongst many others, which influence the operating conditions of the bearing. Although the modelling of a bearing becomes exceedingly complex if one considers all mechanisms influencing its performance, it is always important not to lose sight of what is the information that needs to be extracted from the model. Once one has a clear view of the output parameters that one needs to extract from the model, it is easier to determine which of the aforementioned mechanisms are most important to capture in the model.

Due to the adhesion of the oil to the surface of the journal, the oil is dragged by the rotating journal to form a converging and diverging regions in the pressure field. The converging region is where the film thickness decreases due to the eccentricity of the journal; this causes an increase of pressure in this region. As the fluid passes through the narrow gap the pressure starts decreasing, this is due to the film thickness increasing again. The decrease in pressure could cause cavitation of the oil film if the pressure drops below the saturation pressure of the oil for the particular operating temperature. The pressure in this region (diverging region) would usually not be much lower than atmospheric pressure (if the bearing is not pressurized). The existence of these regions is essential for effective lubrication as this induced pressure field is what supports the loading on the bearing.

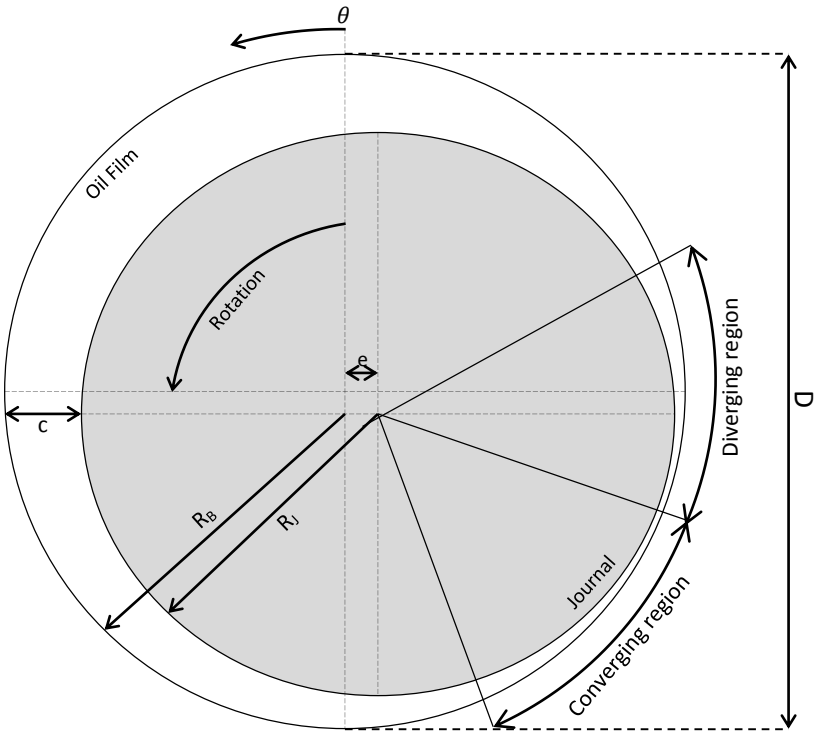

Figure 1: Schematic of a Journal Bearing

Figure 1 is a simple representation of a bearing. The eccentricity, indicated by e on the figure, is the offset of the journal from the centre line of the bearing. The clearance of the bearing, denoted by c,

is the difference between the journal radius and the bearing radius. The eccentricity ratio, denoted in the text by ϵ, is the ratio between the eccentricity and the clearance of the bearing.

$$\epsilon = \frac{e}{c} \tag{2.1}$$

The direction of θ is indicated. The reference point of θ (the point on the circumference where $\theta = 0$) is set to correspond to the zero pressure point before the maximum pressure is encountered (the point of zero pressure does not vary with eccentricity, as can be seen by the solution of the Reynolds equation presented in section 2.1.8). Setting this reference point will always yield the maximum pressure within the bearing between the angles 0^0 and 180^0 (this is also the reference point selected for θ in section 3.2.1).

For quick and simple calculation the Reynolds equation is usually used to determine the following bearing parameters, as mentioned in the book of Stachowiak and Batchelor (2013): (1) The pressure distribution, which is obtained by solving the Reynolds equation. (2) The load capacity which is computed from integrating the pressure field. (3) The friction force, obtained from the torque acting on the oil film, which in turn is computed from the pressure field. (4) The mass flow rate of lubricant supplied to the bearing which is important in the effective design of bearings. If the mass flow rate is too high the fiction force is increased in the bearing. In the case where the mass flow rate is too low it could lead to metal to metal contact. This could lead to damage of the bearing and even breakdown of the system.

The Reynolds equation is derived from the Navier-Stokes equations. The revised assumptions in the development of the coupled formulation are:

1. The fluid is being modelled as a Newtonian fluid. This assumption is addressed by starting from two more general points. Firstly the oil is modelled as a shear thinning Non-Newtonian fluid. The equations of motion are a generalized Newtonian formulation and are more general than the Navier-Stokes equations. Secondly the oil is modelled as a viscoelastic fluid, and the Cauchy equations of motion are used with two different constitutive relations for describing the stress field in the fluid.
2. Fluid inertia is neglected (fluid inertia is still neglected with the Stokes formulation). As mentioned before, the Taylor number being high in steam turbine bearings indicate that the inertia forces will be dominant (opposed to the viscous forces). Furthermore in this study we are looking to develop a bearing model that would eventually be used to diagnose fault mechanisms. Since the response of the lubricant film is important to study the response of the rotor-bearing system it follows that the inertia terms must be included.
3. The viscosity is constant throughout the film. This assumption is crude since the viscosity is usually a function of temperature, pressure and shearing rate. The temperature and shearing of the fluid will have a shear thinning effect on the fluid and the pressure a shear thickening effect.
4. The uncoupling of the governing equations. The governing momentum and energy equations and the constitutive relation for the stress field (in the viscoelastic formulation) are all coupled, either by a weak or a strong coupling.

For the non-Newtonian model the temperature dependency of the viscosity implies a fully coupled system of equations: the momentum equation is dependent on viscosity which is dependent on temperature. The energy equation has a heat generation term due to viscous dissipation which is affected by the velocity gradients in the flow and the viscosity. The flow would therefore influence the amount of heat generated and the amount of heat generated will affect the flow though the viscosity dependence of the temperature. For the viscoelastic models the above holds, however an additional equation is added to the set of governing equations, the constitutive relation. The constitutive relation is fully coupled with the temperature and momentum equations. The momentum equation is dependent on the extra stress tensor which comes out of the solution of the constitutive relation. The temperature equation has an additional dependence in the viscous dissipation term on the extra-stress tensor. Finally the constitutive relations contain both convective and explicit temperature terms. This therefore also forms a fully coupled set of equations.

2.1Governing equations

2.1.1 Continuity equation:

The continuity equation or conservation of mass equation is (Temam and Miranville 2005):

$$\frac{\partial \rho}{\partial t} + \frac{\partial}{\partial x_j}(\rho v_j) = 0 \tag{2.2}$$

where ρ is the density of the continuum, t is time, v_j is the velocity component of the velocity vector. Einstein's notation is used with the index j indicating that the index j runs through all the vector components (in this case three) and the components are summed.

In this study the lubricant is assumed to be incompressible and therefore (2.2) reduces to:

$$\frac{\partial}{\partial x_j}(v_j) = 0 \tag{2.3}$$

This is an important assumption for the numerical solution, since the velocity field being free from divergence is vital to the solution algorithms used in this study (see appendix A.2 for more details).

2.1.2 Linear Momentum equations:

The linear momentum equations for a continuum are defined below (Temam and Miranville 2005). These are also called the Cauchy equations of motion (Reddy 2009):

$$\rho\left(\frac{\partial v_i}{\partial t} + \sum_{j=1}^{3} v_j \frac{\partial v_i}{\partial x_j}\right) = \frac{\partial \sigma_{ij}}{\partial x_j} + f_i \tag{2.4}$$

where i and j ranges from 1 to 3. The terms inside the bracket on the left hand side of (2.4) represent the change of the velocity at a point with respect to time and the convective flux at a point respectively. The first term on the right hand side is the divergence of the stress tensor (this stress tensor is also called the Cauchy stress tensor) and f_i is the body force acting on a volume element in the direction i.

The Cauchy stress tensor describes the stress in the fluid element due to surface tractions acting on the fluid element. For an incompressible fluid there is no dilation of the fluid element (in the case of the fluid being incompressible, the volume of the element will remain the same and the only deformation of the element will be due to shearing of the element).

The total stress tensor (or the Cauchy stress tensor) can be decomposed into its hydrostatic and deviatoric components as follows (Reddy 2009):

$$\sigma_{ij} = -\delta_{ij}p + \tau_{ij} \tag{2.5}$$

where $\delta_{i,j}$ is the Dirac delta function, p is the pressure and $\tau_{i,j}$ are the components of the extra stress tensor. The equation (2.5) is not solvable (numerically or analytically) since the system of equations is underdetermined. Therefore additional equations are needed to complete the set of equations and make the problem well-posed. This is provided in the form of a constitutive relation that describes the stress in the fluid as a function of the deformation of the fluid. This constitutive relation is crucial as it affects the entire model and is specific to the material modelled.

The theoretical complexity of modelling a viscoelastic continuum is that it has a 'memory'. That is the current state of the fluid is dependent on previous states of the fluid and not only on the current condition. Energy is therefore stored and released as the continuum undergoes loading and is released when the loading is no longer applied. This is contrary to fluids such as water or air where the energy applied to the fluid is dissipated through motion of the fluid. The greater the ability of the fluid is to store energy the greater its dependence will be on the history of the previous states. The extent to which a fluid is dependent on the previous history can be measured by the Deborah number, defined as (Szeri 2011):

$$De = \frac{\lambda_1}{\Phi} \tag{2.6}$$

where λ_1 is the relaxation time and Φ is the time duration of the process. When De is zero the continuum is a Newtonian fluid however if De is infinite the continuum is a Hookean solid (Owens & Phillips 2002). The Deborah number determines the complexity of the fluid that is to be modelled. When the Deborah number is small the viscous forces are dominant and therefore only viscosity dependencies are to be modelled. As the Deborah number increases the elastic behaviour of the fluid becomes more prominent. A constitutive relation of the fluid is required to describe the relationship between the velocity gradient tensor and the stress tensor as this relation is no longer linear, as is assumed for a Newtonian fluid. The fluid is now classified as being of differential type as the constitutive relation is described by a differential equation. For the synthetic oils considered in this study a differential fluid model is used (Szeri 2011).

The consistency, flow properties and viscosity of a lubricant are key parameters to the operation of the bearing. It is therefore very important how the fluid is modelled and which properties are included in the model (Mang & Dresel 2007). Due to the small relaxation times associated in literature with

synthetic oils used in journal bearings, differential constitutive models are sufficient to model the fluid behaviour (Gwynllyw & Phillips 2008).

2.1.3 Viscoelastic models:

Two viscoelastic models are used in this study. The two models are both of differential kind. Oldroyd type models are the simplest non-linear viscoelastic fluid models. The Oldroyd-B model is only suitable to model dilute polymer solutions (Owens & Phillips 2002). Due to the limitations of the Oldroyd-B model a second model, the Giesekus model, is included in this study. Compared to the Oldroyd-B model, the Giesekus model has an additional term in the constitutive relation which arises from taking the polymer orientation into account. The constitutive relations used for the viscoelastic fluids are of a general non-isothermal formulation. The more general form of the constitutive models to the author's knowledge has not yet been used in the context of journal bearings. The inclusion of this term is important in order to strongly couple the differential constitutive relation and the energy equation with one another.

Order fluids might seem like the most logical constitutive relations to use in looking for the next generalisation from generalized Newtonian fluids. The issue with these models is, however, that the third order models have a maximum allowable shear rate, which in the case of bearings is not an acceptable limitation. Second order models are also unstable in unsteady flow situations since the variations in Rivlin-Ericksen tensors must be slow (Owens & Phillips 2002). Although this particular study is not concerned with the unsteady flow conditions present in the bearing, considering the context of the study and future work these models are avoided as they are too limiting in the context of the overall problem that is being solved.

In the previous section the Cauchy stress tensor was separated into the pressure and the extra stress tensor. The constitutive models presented in the following sections deal with the extra stress tensor in various ways. Firstly the extra-stress tensor is separated into solvent and polymer stress contributions:

$$\tau_{ij} = \eta_s \dot{\gamma}_{ij} + \tau_{p,ij} \tag{2.7}$$

where the first term on the right hand side represents the Newtonian solvent contribution and the corresponding solvent viscosity, η_s. The tensor associated with the solvent stress contribution is the rate of deformation tensor, represented by (Reddy 2009):

$$\dot{\gamma}_{ij} = \left[\frac{\partial v_i}{\partial x_j} + \frac{\partial v_j}{\partial x_i}\right] \tag{2.8}$$

The second term on the right hand side of (2.7) is the polymer contribution to the stress. The constitutive relations now enter in order to deal with the polymer stress contribution in equation (2.8).

The constitutive relations used for the viscoelastic flow in this study are differential constitutive relations. These constitutive relations are non-linear due to the convective time derivative used. The time derivative used in these equations is the first convected derivative of the stress tensor (also called the Upper-convected derivative) defined as (Christensen 2013):

$$\frac{\delta \tau_{ij}}{\delta t} = \frac{\partial \tau_{ij}}{\partial t} + v_k \frac{\partial \tau_{ij}}{\partial x_k} - \tau_{kj} \frac{\partial v_i}{\partial x_k} - \tau_{ik} \frac{\partial v_j}{\partial x_k} \tag{2.9}$$

Here k is employed in the summation in the same way i and j was used before. This derivative is needed to formulate the non-linear constitutive model (such as the Oldroyd-B model) in contrast to the linear model which uses only the first term on the right hand side of equation (2.9) (The linear Jeffery's fluid model is an example of this). The convected derivative is formulated to have an independence of superposed rotation of the polymer in the fluid. The derivative therefore takes into account the motion of the particle through the solvent while neglecting the rotation of the polymer.

In order to deal with the non-isothermal problem and account for the coupling of the energy and the differential constitutive relation time-temperature superposition is applied (Zhmayev et al. 2008). For both of the constitutive relations used in this study these general forms are used to describe the stress field's dependence on temperature (Wachs et al. 2002). The approach here is adopted from the above cited work.

The momentum equation can be rewritten to explicitly contain the polymer and solvent flow contributions as follows:

$$\rho \left(\frac{\partial v_i}{\partial t} + \sum_{j=1}^{3} v_j \frac{\partial v_i}{\partial x_j} \right) = -\frac{\partial p}{\partial x_i} + \frac{\partial \tau_{p,ij}}{\partial x_j} + \frac{\partial}{\partial x_j} \left[\eta_s \dot{\gamma}_{ij} \right] \tag{2.10}$$

The body forces have been neglected since the only body force that would have an influence on the fluid is gravity, and since all the other forces would be much greater (such as shearing and pressure gradients) the force of gravity on the fluid can be neglected.

2.1.4 Giesekus model:

The Giesekus model is a generalization of the Oldroyd-B model. The Giesekus model has an additional term that allows the model to describe shear thinning behaviour. The model falls into a larger group of differential constitutive relations that modify the Oldroyd-B model in order to reduce the limitations of it. The constitutive relations, for the polymeric stress, are of the general form:

$$\tau_p + \lambda_1 \frac{\delta \tau_p}{\delta t} + f(\tau_p, \dot{\gamma}) = \eta_p \dot{\gamma} \tag{2.11}$$

Both τ_p and $\dot{\gamma}$ are tensors that describe the stress in the polymer chains and the rate-of-shear tensor respectively. The constants λ_1 and η_p are material properties and represent the relaxation time and polymer viscosity respectively (Owens & Phillips 2002). The right most function on the left hand side sets this model apart from the Oldroyd-B model. Both constitutive relations considered in this study can be derived from a molecular model consisting of dumbbells, connected by a spring, suspended in a Newtonian solvent. The Fokker-Planck equation is used to derive an equation describing the probability density of the polymer orientation in the suspension. One of the key aspects that set constitutive relation derived from this platform apart is the way in which the spring force between dumbbells are dealt with.

For the Giesekus model the added term in the constitutive relation is chosen to be:

$$f(\tau_p, \dot{\gamma}) = \alpha \frac{\lambda_1}{\eta_p} \tau_p^2 \tag{2.12}$$

The new scalar, α, in the added term is called the mobility constant. The addition of this term gives a fluid model that has a non-vanishing second normal stress difference, a bounded extensional viscosity as well as shear thinning behaviour (Giesekus 1982).

The non-isothermal formulation of the Giesekus model is (Zhmayev et al. 2008):

$$\tau_{p,ij} + \alpha \frac{\lambda_1}{\eta_p} \tau_{p,ij}^2 + \lambda(T) \frac{T_0}{T} \left[\frac{\delta \tau_{p,ij}}{\delta t} - \tau_{p,ij} \frac{Dln(T)}{Dt} \right] = \eta_p(T) \dot{\gamma}_{ij} \tag{2.13}$$

For the temperature dependence of viscosity and the relaxation factor the Williams-Landel-Ferry (WLF)-equation is used. In the case where relaxation time is divided by viscosity as is the case in the second term of the above equation, the shift function cancels out and therefore only the reference values are used for these mechanical properties in this term. This is indicated by not explicitly stating that these properties are functions of temperature.

2.1.5 Oldroyd-B fluid model:

An Oldroyd-B fluid is the simplest non-linear viscoelastic constitutive model and therefore it is the most logical step for a more general fluid model than the generalized Newtonian fluid. The model is arrived at by assuming that the polymers act as dumbbells connected by linear Hookean springs in a Newtonian solvent.

$$\tau_{ij} + \lambda_1 \frac{\delta \tau_{ij}}{\delta t} = \eta_0 \left[\dot{\gamma}_{ij} + \lambda_2 \frac{\delta \dot{\gamma}_{ij}}{\delta t} \right] \tag{2.14}$$

The constant on the left hand side is the relaxation time of the fluid, the viscosity on the right hand side is the total viscosity (that is the sum of the solvent viscosity and the polymer viscosity) and the second constant on the right hand side is the characteristic relaxation time of the fluid defined as (also see equation 4.7, for definition of β):

$$\lambda_2 = \frac{\eta_p \lambda_1}{(\eta_p + \eta_s)} = (1 - \beta)\lambda_1 \tag{2.15}$$

Using the definition of the characteristic fluid relaxation time, the Oldroyd-B constitutive relation and the splitting of the extra stress tensor it follows that the polymer contribution of the stress tensor can be computed from the Upper-Convected Maxwell equation (Owens & Phillips 2002):

$$\tau_{p,ij} + \lambda_1 \frac{\delta \tau_{p,ij}}{\delta t} = \eta_p \dot{\gamma}_{ij} \tag{2.16}$$

where the viscosity now refers to the polymer viscosity. The temperature dependence of the polymer contribution to the fluid is introduced as before with the Giesekus model. This dependence is described by the WLF-equation, which acts as a shift function on the viscosity and the relaxation time. This however is not yet a full coupling of the temperature and the stress field. The more general expression of the Oldroyd-B constitutive relation, fully coupled with the energy equation, can be obtained by setting the mobility parameter in the non-isothermal Giesekus model to zero (Thomas et al. 2004):

$$\tau_{p,ij} + \lambda(T)\frac{T_0}{T}\left[\frac{\delta\tau_{p,ij}}{\delta t} - \tau_{p,ij}\frac{Dln(T)}{Dt}\right] = \eta_p(T)\dot{\gamma}_{ij} \tag{2.17}$$

In this case all the mechanical properties have dependencies on temperature and pressure and are computed by applying a shifting factor to these fluid properties (see section 2.1.10 for details).

2.1.6 Generalised Newtonian fluid model:

The magnitude of the Deborah number can be seen as a measure of how dominant the polymer additives are in the fluid. In the case where the flow is dominated mostly by the solvent and therefore the elasticity of the fluid becomes negligible, the relaxation time of the fluid tends to zero (Szeri 2011). For both the Giesekus and Oldroyd-B constitutive relations, as the polymer contribution to the flow tend to zero, the constitutive relations reduce to:

$$\tau_{p,ij} = \eta_p\dot{\gamma}_{ij} \tag{2.18}$$

The solvent and the polymer viscosities are therefore no longer separated. It is then assumed that the extra-stress tensor is a linear function of the strain rates which leads to (Owens & Phillips 2002):

$$\tau_{ij} = \Lambda\delta_{ij}\frac{\partial v_k}{\partial x_k} + \eta\left[\frac{\partial v_i}{\partial x_j} + \frac{\partial v_j}{\partial x_i}\right] \tag{2.19}$$

The first term on the right hand side represents the volumetric expansion at a point. The stress tensor can therefore be expanded as:

$$\sigma_{ij} = -\delta_{ij}p + \Lambda\delta_{ij}\frac{\partial v_k}{\partial x_k} + \eta\left[\frac{\partial v_i}{\partial x_j} + \frac{\partial v_j}{\partial x_i}\right] \tag{2.20}$$

The equation of motion can be written as (White 2006):

$$\rho\left(\frac{\partial v_i}{\partial t} + \sum_{j=1}^{3} v_j\frac{\partial v_i}{\partial x_j}\right) = -\delta_{ij}\frac{\partial p}{\partial x_i} + \frac{\partial}{\partial x_j}\left[\eta\left(\frac{\partial v_i}{\partial x_j} + \frac{\partial v_j}{\partial x_i}\right) + \delta_{ij}\Lambda\frac{\partial v_k}{\partial x_k}\right] \tag{2.21}$$

The equation is left in terms of Cartesian coordinates, although initially one might think that cylindrical coordinates would be better suited for the problem. However due to the curvature of the two surfaces in the analysis the surfaces can be approximated as being straight. Comparing the curvature of the surfaces with the dimensions of the geometry it can be seen that the curvature of the surface becomes negligible. This justifies the choice. Writing these equations in cylindrical coordinates introduces extra terms into the equation which increases the complexity of the equations and consequently the computational time to solve the equations (Szeri 2011).

2.1.7 Stokes Flow:

A further simplification can be made for flows where the viscous part of the fluid dominates the flow. In this case the flow is assumed to have negligible effects form the inertia of the fluid. The Reynolds number is a measure of the ratio of inertial forces in the fluid to the viscous forces in the fluid (White 2006):

$$Re = \frac{\rho V L_c}{\eta} \tag{2.22}$$

For inertial effects to be negligible the Reynolds number must be much smaller than one (L_c refers to the characteristic length of the flow domain). If this is the case the inertia terms can be neglected from the equation of motion (White 2006):

$$\rho \frac{\partial v_i}{\partial t} = -\delta_{ij} \frac{\partial p}{\partial x_i} + \frac{\partial}{\partial x_j}\left[\eta\left(\frac{\partial v_i}{\partial x_j} + \frac{\partial v_j}{\partial x_i}\right)\right] \tag{2.23}$$

For Stokes flow it is common to neglect the term on the left hand side also. The reason for this is that if we assume that the inertial effects are small no sudden changes in velocity are allowed as this would suddenly increase the flow conditions to the point where the Stokes flow model breaks down. On physical grounds, in the case of this study, it therefore makes sense to neglect this term also. The term is retained however for the sake of the numerical computations: this term stabilizes the numerical solver and helps reach a converged solution quicker. Once steady state conditions are reached this term would disappear and therefore is only present while the solution has not converged.

The reason this model is added to the study is that it serves as a representative of the classical Reynolds equation which have been modified to take the various dependencies considered in this study into account. This model therefore serves as a crucial part of the study when the models are to be compared to one another.

2.1.8 The Reynolds equation and solutions:

The Stokes flow model presented in the previous section is simply the generalized Newtonian fluid model with inertia terms neglected. Starting at this point, the assumptions mentioned in the first section of this chapter are applied, and an order of magnitude analysis is done on the equation of motion (Szeri 2011). The result is the Reynolds equation for lubrication (Owens & Phillips 2002):

$$\frac{\partial}{\partial\theta}\left[(1+\epsilon\cos(\theta))^3\frac{\partial p}{\partial\theta}\right] + \left(\frac{R}{2L}\right)^2\frac{\partial}{\partial z}\left[(1+\epsilon\cos(\theta))^3\frac{\partial p}{\partial z}\right] = -6\eta\omega R^2\frac{\epsilon}{c^2}\sin(\theta) \tag{2.24}$$

The first term on the left hand side governs the circumferential pressure gradient whereas the second term governs the axial pressure gradients. The variable θ is runs along the circumference of the bearing and Z runs in the axial direction of the bearing. The right hand side of the equation represents the shear rate of the bearing (Szeri 2011).

Two cases exist where solutions can be found for this equation:

The first is the long bearing solution. The bearing is assumed to be of infinite length, this implies that there would be no pressure relief in the axial direction and hence the second term on the left hand side can be neglected. This assumption leads to an ordinary differential equation which can be solved to yield the pressure distribution (Owens & Phillips 2002):

$$p = p_0 + \frac{6\eta\omega R^2}{c^2}\frac{\epsilon\sin(\theta)\,(2+\epsilon\cos(\theta))}{(2+\epsilon^2)(1+\epsilon\cos(\theta)\,)^2} \tag{2.25}$$

The second solution is the short bearing solution. It is assumed that the bearing is short enough to allow pressure release in the axial direction to be dominant. The circumferential pressure gradient is assumed to be small enough to be neglected, yielding an ordinary differential equation that again can be solved to yield:

$$p = p_0 + \frac{3\eta\omega\epsilon \sin(\theta)}{c^2(1+\epsilon\cos(\theta))^3}\left(\frac{L^2}{4} - z^2\right) \tag{2.26}$$

These solutions have proven to be accurate for length to diameter ratios of 10:1 for the long bearing solution and 1:10 for the short bearing solution respectively.

2.1.9 Energy equation:

The energy equation follows from the first law of thermodynamics and therefore gives a differential description of internal energy at a point in terms of heat and work. The heat that is transferred in the system is heat generated in the oil due to viscous dissipation and it is transferred from the oil film to the journal and to the bearing casing through conduction and convection.

Assuming that there is no internal heat generation in the fluid apart from viscous dissipation and neglecting interdiffusional convection and the Dufour effect and assuming incompressibility of the fluid the energy equation reduces to (Faghri et al. 2010):

$$\rho C_p\left(\frac{\partial T}{\partial t} + \sum_{j=1}^{3} v_j \frac{\partial T}{\partial x_j}\right) = \frac{\partial}{\partial x_j}\left[k\frac{\partial T}{\partial x_j}\right] + \sigma_{ij}\frac{\partial v_i}{\partial x_j} \tag{2.27}$$

where C_p is the heat capacity, k is the thermal conductivity and T is the temperature.

The first term on the left hand side of the equation inside the brackets is the temporal change in the energy per unit volume and the second is the heat transferred by convection. The terms on the right hand side of the equation represents the heat transferred by thermal conduction and the heat generated due to viscous dissipation.

The viscous dissipation term is the contraction of two second rank tensors where the contraction of two vectors is defined as:

$$\bar{\bar{\sigma}} : \nabla\vec{V} = \sigma_{ij}\frac{\partial v_i}{\partial x_j} \tag{2.28}$$

where $\bar{\bar{\sigma}}$ and $\nabla\vec{V}$ are two tensors of the same rank. This term describes the heat generated as a result of the friction between the fluid layers. This is produced by the shear forces acting between the fluid layers.

In order to arrive at this equation it had to be assumed that the fluid is incompressible. Due to this assumption the viscous dissipation term can be simplified by splitting the Cauchy stress tensor into its hydrostatic and deviatoric components:

$$\sigma_{ij}\frac{\partial v_i}{\partial x_j} = (-\delta_{ij}p_i + \tau_{ij})\frac{\partial v_i}{\partial x_j} \tag{2.29}$$

Since the contraction of the two tensors (the Cauchy stress tensor and the velocity gradient tensor) produces a scalar (since the energy equation must be a scalar equation), multiplying the terms out and grouping all the terms in which pressure appears, yield:

$$-\delta_{ij}p\frac{\partial v_i}{\partial x_j} = p\,\nabla\cdot(\vec{v}) = 0 \tag{2.30}$$

The last term is zero due to the continuity equation (2.3). It follows therefore that for incompressible fluids, only the extra-stress tensor contributes to the viscous dissipation term and therefore the energy equation can be written as:

$$\rho C_p\left(\frac{\partial T}{\partial t} + \sum_{j=1}^{3} v_j\frac{\partial T}{\partial x_j}\right) = \frac{\partial}{\partial x_j}\left[k\frac{\partial T}{\partial x_j}\right] + \tau_{ij}\frac{\partial v_i}{\partial x_j} \tag{2.31}$$

This is the formulation employed in the viscous fluid solvers “genStokesFoam” and “ViscFoam”. These solvers are developed in the OpenFOAM environment (see section 3.1 for more detail).

An additional complication for the differential fluid models is the ability of the polymers to store mechanical energy (similar to compression and tension in springs). For instance, when the fluid undergoes constant shearing not all of the work done on the system will be dissipated immediately (which is typically the case with a Newtonian fluid). Heat generation in a viscoelastic fluid, by means of shear, is in part due to viscous dissipation and partly due to the compression and elongation of the polymers in the fluid. Mechanical energy stored in compressed or elongated polymers are partly dissipated by heat transferred from the polymer to the fluid. The heat generation by this mechanism is accounted for as follows (Habla et al. 2012; Wachs et al. 2002):

$$\mathrm{Q} = \tau_{s,ij}\frac{\partial v_i}{\partial x_j} + \phi\tau_{p,ij}\frac{\partial v_i}{\partial x_j} + (1-\phi)\frac{tr(\tau_{p,ij})}{2\lambda_1(T)} \tag{2.32}$$

The constant ϕ is called the energy partitioning coefficient and weights the heat generation from the polymer, due to viscous dissipation and mechanical dissipation. The heat source in the fluid is now also denoted by the scalar Q. The final form of the energy equation used in the viscoelastic fluid solvers is therefore:

$$\rho C_p\left(\frac{\partial T}{\partial t} + \sum_{j=1}^{3} v_j\frac{\partial T}{\partial x_j}\right) = \frac{\partial}{\partial x_j}\left[k\frac{\partial T}{\partial x_j}\right] + Q \tag{2.33}$$

where (2.32) will reduce to (2.29) if the polymer behaviour of the flow can be neglected or if the fluid is a generalised Newtonian fluid.

In their book, Stachowiak and Batchelor (2013) give a generic example of how prominent the conduction heat transfer mechanism is in the overall heat transfer process in the bearing. One might be tempted to neglect conduction heat transfer at high shaft velocities as convection should be the dominant heat transfer mechanism. Convection is indeed the dominant mechanism for heat transfer, however the conduction of heat is not negligible: in a thick film journal bearing with a shaft angular velocity of 3000rpm and a minimum film thickness of 0.1mm, total heat transfer through conduction

is about 17%. This implies an increase of 17% to the total heat transferred since thermal convection and thermal conduction occurs in series.

Heat transfer through both conduction and convection is therefore important and must be considered when modelling the heat transferred in the bearing.

2.1.10 Viscosity models:

In section 2.1.2 the linear momentum equation was presented. In this formulation viscosity was assumed to vary through space and have a dependence on the thermodynamic properties of the system. The constitutive relation of the fluid would therefore be incomplete without the formulation of this dependence. The viscosity is assumed to have a dependence on temperature, pressure and shear rate. The shear thinning behaviour of the fluid is modelled using the Carreau model (Wachs et al. 2002):

$$\eta(\dot{\gamma}) = \frac{\eta_0}{(1 + (K_s\dot{\gamma})^b)^a} \tag{2.34}$$

In section 3.2.3 it is shown that this model varies between power law model and the standard Newtonian model. The Cross law model is mimicked by imposing limits on the minimum and maximum viscosities. These minimum and maximum viscosities are chosen in order to set the minimum and maximum viscosity allowed when all the viscosities are factored in (Chhabra & Richardson 2011). Furthermore, this model for shear rate dependence of viscosity is only used for the generalised Newtonian fluid. In deriving the differential constitutive relations the solvent is assumed to be Newtonian. The Giesekus model describes shear thinning behaviour through the addition of the term that describes polymer orientation (see section 2.1.4).

The shear rate is defined as (Owens & Phillips 2002):

$$\dot{\gamma}^2 = 2\left[\left(\frac{\partial v_1}{\partial x_1}\right)^2 + \left(\frac{\partial v_2}{\partial x_2}\right)^2 + \left(\frac{\partial v_3}{\partial x_3}\right)^2\right] + \left(\frac{\partial v_1}{\partial x_2} + \frac{\partial v_2}{\partial x_1}\right)^2 + \left(\frac{\partial v_1}{\partial x_3} + \frac{\partial v_3}{\partial x_1}\right)^2 + \left(\frac{\partial v_3}{\partial x_2} + \frac{\partial v_2}{\partial x_3}\right)^2 \tag{2.35}$$

The WLF-equation is used to describe the temperature dependence of viscosity as well as the relaxation time of the fluid (Habla et al. 2012). The WLF-equation provides a shift factor that describes how the fluid properties changes due to temperature. The change of the fluid property is applied to the property at some reference temperature. Therefore the WLF-equation perturbs the value of the property around this reference value. The WLF equation is:

$$a_T = \exp\left(-\frac{C_1(T - T_0)}{C_2 + T - T_0}\right) \tag{2.36}$$

C_1 and C_2 are constants and T_0 is a reference temperature. The pressure dependence of the fluid is modelled in a similar way by the Barus law as (Li, Gwynllyw, et al. 2000; Owens & Phillips 2002):

$$\eta = \eta_0 \exp\left(-\frac{1}{3}\psi trace(\sigma)\right) \tag{2.37}$$

Minus a third of the trace of the Cauchy stress tensor is the effective pressure at a point in the fluid.

Due to the form of the Barus law and the WLF-equation, it is simple to combine these two dependencies into one shift factor as follows (Owens & Phillips 2002):

$$a_{T,p} = exp\left(-\frac{C_1(T-T_0)}{C_2+T-T_0} - \frac{1}{3}\psi trace(\sigma)\right) \tag{2.38}$$

This shift factor is applied to the shear rate dependence in the same way as before.

The shift is added to the Carreau model to give the three fold viscosity dependency on shear rate as follows (Wachs et al. 2002; Owens & Phillips 2002):

$$\eta(T) = \frac{a_{T,p}\eta_0}{(1+(a_T K_s \dot{\gamma})^b)^a} \tag{2.39}$$

The relaxation time describes the time needed for the viscoelastic fluid to return to its original state after a disturbance has occurred (Chhabra & Richardson 2011). This relaxation time will have a dependence on temperature and pressure, similar to that of the viscosity (Habla et al. 2012):

$$\lambda(T) = a_{T,p}\lambda(T_0) \tag{2.40}$$

2.1.11 Elasto-hydrodynamics:

Elasto-hydrodynamics include two important mechanisms that influence the operating conditions. The first is with regards to the viscosity model. This specifically includes the effect of pressure on the viscosity as was discussed in section 2.1.10. The second is the elastic deformation of the metal surfaces in the bearing.

Under high pressure conditions the fluid film has an increase in viscosity (this would increase the load caring capacity of the bearing) which significantly influences the operating conditions. The sudden thickening of the oil in a region results in a greater film thickness than what is predicted in the classical theory (Szeri 2011). If the film thickness varies in a region this will have a direct influence on the orbital path of the bearing. Since this is of great importance in this study it is therefore crucial to take these effects into account.

The second mechanism is the deformation of the bearing case due to the induced pressure field in the bearing. Although this is certainly an important effect to study when considering the transient behaviour of bearings (Stachowiak & Batchelor 2013), it is not considered in this study but is recommend as a crucial topic to be studied in a follow up study.

2.1.12 Cavitation:

Due to the converging and diverging section in the journal bearing it is known that in the diverging region sub atmospheric pressures can result. In gas lubrication this would not be a problem. However, with liquid films the pressure in the diverging region would frequently drop below the vapour pressure of the oil and consequently result in bubble formation. This formation can be accelerated by high temperatures occurring in the bearing due to viscous dissipation. The process of these bubbles forming is called gaseous cavitation. When these gas bubbles collapse there is a sudden spike in stress in the bearing, due to shock waves propagating form the area of collapse. This can cause permanent damage to the bearing structure (Stachowiak & Batchelor 2013).

Due to the formation of bubbles in the film, cavitation modelling has to deal with two issues: firstly to account for the change in viscosity and secondly the compressibility introduced to the system due to the bubble formation in the film.

It has been shown that liquids that have no contaminants can sustain negative pressures to a degree. However due to the large amount of wear in the system introducing impurities in the oil, the oil loses its ability to sustain negative pressures and cavitation would occur more frequently (Stachowiak & Batchelor 2013).

If cavitation occurs in a system it will have an effect on the response of the system. The cavitating region is compressible and acts as a damper in the response of the system (D. R. Gwynllyw, et al. 2000). It is therefore important in the stability of the system especially at high eccentricities.

The study of cavitation in the response of rotor-bearing systems is therefore important. Modelling cavitation requires considering multi-phase flow. The fluid is no longer considered to be incompressible and the density of the fluid is allowed to change throughout the film. In addition shock waves are produced in the film due to the collapse of the cavitation bubbles (Bensow & Bark 2010).

The complexities of modelling cavitation are therefore quite apparent. A general treatment of it is beyond the scope of this study. It is highlighted here due to its importance in the dynamics of the system as well as the need to consider it in further research.

2.2 Boundary Conditions

2.2.1 Momentum equation boundary conditions:

For the surfaces of the journal and the bearing casing a non-slip boundary condition holds:

At the journal surface:

$$\left|\vec{V}_{rel}\right| = |\vec{\omega}_{rotation}||\vec{r}| \tag{2.41}$$

At the surface of the bearing casing:

$$\vec{V}_{rel} = 0 \tag{2.42}$$

Two more boundary conditions are required for the axial direction. This choice is not trivial since this boundary condition can be affected by a fault mechanism in the seals. In the case where a three

dimensional bearing is modelled, the pressure at the ends of the bearing will be set to the atmospheric pressure or the pressure withstood by the seals at the ends of the bearing.

$$P_{Z=-L} = P_{Z=L} = 0 \; ; P_{Z=-L} = P_{Z=L} = P_{seal} \tag{2.43}$$

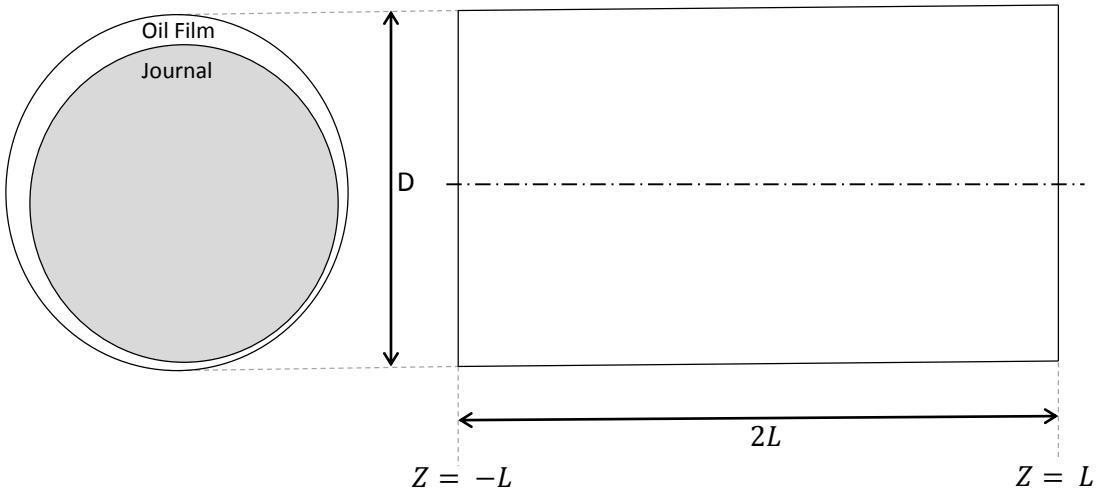

Figure 2: Front and side schematic of bearing

Figure 2 illustrates the front and side views of the bearing respectively. The Ends of the bearing (in the Z-direction) is indicated since this is where the boundary conditions (2.43) are applied.

In section 3.2.1 the bearing model considered is infinite in length and therefore the pressures at the ends of the bearing do not have to be set. This boundary condition applied in principle to the numerical case study described in section 4.1.

2.2.2 Energy equation boundary conditions:

The thermal boundary conditions in a bearing can potentially present just as much trouble as the governing equation when solving the problem. In ideal bearings an isothermal or adiabatic boundary condition is applied. The heat transfer is assumed to be dominant in the radial direction for such bearings.

The journal is assumed to be at constant temperature. This assumption is not entirely valid, however, it does give reasonable results when compared to experimental results (Szeri 2011). The assumption is based on the observation that heat is conducted in the axial direction within the journal. The amount of heat that is conducted along the axis is usually quite high due to the thermal conductivity of metal being high. The journal therefore would remain at a constant temperature. This boundary condition is employed in the current work.

The isothermal and adiabatic boundary conditions therefore refer to the boundary condition applied to the stationary surface, the bearing casing, rather than the journal. Although neither of these assumptions are entirely correct either, the following observations were made by Szeri (2011):

1) The isothermal analysis is seen to predict temperatures much lower than the adiabatic analysis.

2) When comparing the results to experiments the adiabatic analysis gave good agreement with the flow condition in the laminar regime whereas the isothermal analysis gave good agreement with the turbulent regime.

The boundary condition is therefore dependent on the flow regime. This is not surprising as it is generally known that heat transfer is enhanced in the turbulent flow regime (Faghri et al. 2010).

Oil is forced into the bearing through the oil inlet, the location of the inlet is specific to each bearing. Oil leaves the bearing in two ways: through an oil outlet (the location of which similarly to the inlet depends on the bearing specification) and oil flows out in the axial direction through leakage of the seals. (The amount to which this can occur depends on the bearing, seals and the age of the seals). The implication of this is that one needs to specify thermal boundary condition for each of these inlets and outlets. For the inlet the isothermal boundary condition is sufficient, since the oil that enters though the inlet is mixed in a reservoir and is then pumped through the system allowing for significant mixing and therefore a temperature of the oil at the inlet. This is subject to the assumption that there is no back flow into the inlet (the severity of this assumption will depend on the location and size of the bearing). The oil that exits though the outlet is set to have an adiabatic boundary condition. Due to the size of the outlet the oil that exits though it will conduct an insignificant amount of heat compared to the heat conducted though the structural part of the bearing. A similar argument holds for the oil that escapes due to oil leakage (Szeri 2011).

The boundary conditions applied to the test case in Chapter 4 is discussed in 4.1. For both the journal and bearing surface boundary conditions a constant temperature (Dirichlet) boundary condition is chosen. The primary reasons for this choice of boundary conditions are: (1) the temperature profile develops to a steady profile rapidly. The temporal development of the energy equation is quite costly. The time steps used in this work is of the order 1 ns, where the energy equation would usually require up to 20 seconds reach equilibrium. (2) The temperature profile also closely resembles the contour plot computed by Davies et al. (1994) in their work. This choice of boundary conditions therefore yields efficient and accurate solutions. (3) The Reynolds numbers reported for the flow within the bearing place the flow well within the turbulent regime (Uhkoetter et al. 2012). According to Szeri (2011) isothermal boundary conditions are better suited for the turbulent flow regime.

Chapter 3: Numerical solvers and benchmarks:

3.1 Constructing the Solvers

3.1.1 "genStokesFoam" and "ViscFoam" viscous fluid solvers

"genStokesFoam" is an inertia-less fluid solver developed in the OpenFOAM environment. The name is derived from the Stokes formulation of creep flow where inertia terms in the momentum equations are neglected. The stress field is described by a generalised Newtonian constitutive relation, which is a linear constitutive relation. The viscosity of the fluid is assumed to be a function of temperature, pressure and shear rate. The viscosity is therefore the property of the flow that couples the momentum and the energy equations: the velocity field is affected by changes in the fluid's viscosity which is a function of the temperature field. The temperature field is affected by the fluid's viscosity through the viscous dissipation term. The viscous dissipation term is formulated in terms of the fluid's viscosity and the velocity field. The governing equations are therefore fully (or strongly) coupled (Bird et al. 1977).

The "ViscFoam" fluid solver follows a similar formulation, with the only difference being the inclusion of the inertia terms in the momentum equation.

In order to solve these sets of equations numerically the PISO (Pressure Implicit with Splitting of Operator) algorithm is used. Details of the algorithm are included in appendix A (see A.2). The algorithm is outlined below, as it is implemented in the "genStokesFoam" and "ViscFoam" solvers respectively:

- Compute the velocity field form the initial pressure field or from the pressure field computed in the previous time step.
- Correct the pressure field by using the newly computed velocity field and applying the continuity condition to the equations (the number of pressure corrections varies with application).
- The velocity field is corrected based on the corrected pressure field.
- Correct the mass flux at the boundaries according to the preservation of mass in the system.
- Compute the temperature field from the energy equation using the new velocity field.
- Adjust the viscosity according to the pressure temperature and shear rate dependencies.
- Repeat the above until the momentum and energy equations have converged below a specified residual.

In this algorithm there are two correction steps: the pressure and velocity correction steps. These corrections are performed within each time step. The number of times each of these corrections is performed varies with application. In the OpenFOAM environment these two correction steps are referred to as corrections and non-orthogonal corrections respectively. The number of non-orthogonal corrections determines how many times the discrete Poisson equation is solved. Solving this equation yields the pressure correction that is applied to the pressure field. The number of corrections made to the pressure field is determined by the number of non-orthogonal correctors. The number of corrections (as referred to in OpenFOAM) determines the number of times the velocity field is corrected within a time step. This correction of the velocity field only follows when the

correction of the pressure field has been completed for the current time step. In this study it was found that when the eccentricity of the bearing was increased, the non-orthogonality of the mesh was also increased. As the non-orthogonality of the mesh was increased in the converging and diverging sections of the bearing, the number of pressure corrections needed to stabilise the fluid solver, was increased. This held for both the viscous and the viscoelastic solvers. Maintaining a balance between computational time and accuracy, however, is important, since applying more corrections than needed wastes computational resources (In sections 3.2.1 this was particularly important due to the change of the eccentricity ratio). The balance was established in this work by finding the smallest number of pressure corrections needed to reach a converged solution on the mesh for which mesh independence had been established.

The implementation of the momentum equation requires some consideration. The main concern is how to deal with the constitutive relation. When working with the Navier-Stokes equation this does not require much care as the Laplacian term can simply be evaluated implicitly and hence there is no cause for concern. The issue when dealing with more complex formulations is that only part of the constitutive relation can be evaluated implicitly. Therefore part of the constitutive relation is then termed with the source term and evaluated explicitly. Neglecting the proper evaluation of the constitutive relation gives rise to instabilities and consequently requires much more computational resources to achieve a converged solution.

The constitutive relation for the generalized Newtonian fluid was described in section 2.1.6 of chapter 2. By applying the divergence operator to equation (2.19) the following is obtained:

$$\frac{\partial \tau_{i,j}}{\partial x_j} = \frac{\partial}{\partial x_j}\left[\Lambda \delta_{i,j} \frac{\partial v_k}{\partial x_k} + \eta \dot{\gamma}_{ij}\right] \tag{3.1}$$

From the continuity equation for an incompressible fluid, given in equation (2.3), it follows that the first term inside the bracket on the right hand side will disappear. This term is sometimes retained in order to improve the stability, since continuity will not be satisfied initially. The principle, however, is still applied in other terms arising from the variation in viscosity. Applying the chain rule to what remains from (3.1) yields:

$$\frac{\partial}{\partial x_j}\left[\eta \dot{\gamma}_{i,j}\right] = \left(\frac{\partial \eta}{\partial x_j}\right)\dot{\gamma}_{i,j} + \eta \frac{\partial \dot{\gamma}_{i,j}}{\partial x_j} \tag{3.2}$$

The first term on the right hand side can be reduced further; however it is left as it is. Reducing it further will not impact on whether it is evaluated implicitly or explicitly, in OpenFOAM the gradient operator is always evaluated explicitly. These additional terms will disappear once the solution is converged. While the fluid solver is converging to a solution, these terms stabilises the fluid solver (Oliveira et al. 1998).

The divergence of the rate-of-deformation tensor can be simplified by using the continuity equation (2.3). This reduces the term to the Laplacian of the velocity field, which can be evaluated implicitly. The implemented constitutive relation then becomes:

$$\frac{\partial}{\partial x_j}\left[\eta \dot{\gamma}_{i,j}\right] = \left(\frac{\partial \eta}{\partial x_j}\right)\dot{\gamma}_{i,j} + \eta \frac{\partial^2 v_j}{\partial x_j^2} \tag{3.3}$$

where the first term on the right hand side is the outer product of a gradient vector and the rate of deformation tensor and is treated explicitly. The second term on the right hand side is the Laplacian of the velocity field and is treated implicitly.

The implicit and explicit evaluation of terms determines the stability and consequently the amount of computational resources needed to solve the problem. The stability of an explicit evaluation is dependent on the mesh size and the associated time step. If the mesh is fine the time step needs to be adjusted to be proportional to the mesh size. If the time step is not small enough, the solver becomes unstable. Decreasing the time step size increases the computational time. It is therefore beneficial to evaluate the discretized equation implicitly as far as possible (Versteeg & Malalasekera 2007).

The energy equation is much simpler to deal with as far as implicit and explicit evaluation of terms is concerned. The source term is the only term that is evaluated explicitly in OpenFOAM. The conduction term, which reduces to the Laplacian of the temperature field, along with the convection terms are all treated implicitly. The only remaining issue that might be of concern is whether viscous dissipation is a surface or a body source. When the energy equation is discretized by the finite volume method each of the terms is integrated over the surface or volume of the CV (control volume). The evaluation of viscous dissipation as a surface or volume source is therefore an important matter to consider.

The first law of thermodynamics is used in order to describe the change in the internal energy due to work done by or on the system and heat transferred to or from the system. This law can be rewritten in integral from as follows:

$$\frac{d}{dt}\int_{V(t)} \rho\left(\frac{1}{2}v^2 + e\right) dV = \int_{V(t)} \rho\bar{b}\cdot\bar{v} + \nabla\cdot(\sigma\cdot\bar{v}) + \nabla\cdot\bar{q}\; dV \tag{3.4}$$

Expanding the second term inside the integration operator on the right results in:

$$\nabla\cdot(\sigma\cdot\bar{v}) = \sigma{:}\nabla\bar{v} + \bar{v}\cdot(\nabla\cdot\sigma) \tag{3.5}$$

The dot product between the velocity and the momentum equation is taken to find an expression for the kinetic energy. Applying the Reynolds transport theorem to the resultant expression results in:

$$\frac{d}{dt}\int_{V(t)} \frac{1}{2}\rho v^2\, dV = \int_{V(t)} \bar{v}\cdot(\nabla\cdot\sigma) + \rho\bar{b}\cdot\bar{v}\, dV \tag{3.6}$$

Subtracting equation (3.6) from (3.4) while using the expression (3.5) and applying the assumption that the flow is incompressible yields:

$$\int_{V(t)} \rho C_p \frac{DT}{Dt}\, dV = \int_{V(t)} \sigma{:}\nabla\bar{v} + k\nabla^2 T\, dV \tag{3.7}$$

This clearly shows that the viscous dissipation term in the energy equation must be integrated over the volume and not over the surface of the CV.

3.1.2 "ThermOldBFoam" and "ThermGiesFoam" viscoelastic fluid solvers

The "ThermOldBFoam" and "ThermGiesFoam" are viscoelastic fluid solvers and are more sophisticated than the viscous fluid solvers. The viscoelastic fluid solvers take into account the elasticity of the fluid due to the polymer additives added to the viscous solvent. The formulation yields a strong coupling between the momentum, energy and stress fields. The complexity introduced through the additional coupled field requires a different numerical approach.

A segregated approach is used to deal with these couplings. This is done by linearising the nonlinear equation by assuming the coefficients of the partial differential equation remains constant. Once the linear problem is solved the results obtained from the linearised problem are used to solve the other equations (for instance the momentum equation is linearised and the constitutive relation and energy equation are solved for). At the end of the time step the coefficients that were assumed to be constant are updated using the newly computed results. This approach therefore solves two sets of equations: the linearised and the nonlinear forms of the governing equations. The solving of the linearised and nonlinear equations can be called the inner and outer iterations respectively. The outer iteration solves the nonlinear problem based on the solution of the linearised problem. The linear solution therefore serves as an approximation for the nonlinear problem in the temporal domain. In the OpenFOAM environment, the PISO loop will serve as the inner loop (where the equations are explicitly linearised) and the time steps will serve as the outer loop. Only when the solution has converged in the temporal domain will the nonlinear problem be sufficiently approximated (Ferziger et al. 2008).

In OpenFOAM there is a built-in function called ".relax()". This function fixes the coefficients of the set of discretised equations during the time step. Since pressure is the first field that is to be solved, this algorithm requires the pressure field from the previous outer iteration to be stored such that the momentum equation can be explicitly relaxed.

The algorithm therefore executes as follows:

- The shift factor is applied to both the viscosity and relaxation time.
- The nonlinear momentum equation is updated and linearised (relaxed).
- The linearised momentum equation is solved.
- The pressure correction equation is solved and the pressure field is corrected accordingly.
- The pressure equation is linearised (relaxed) in order to correct the momentum equation.
- The differential constitutive relation is updated and linearised (relaxed).
- The linearised constitutive relation is solved.
- The energy equation is solved for the temperature field using all the latest computed fields.

Dealing with the momentum equation is more complex than before, specifically in terms of stability due to diagonal dominance of the discrete set of equations weakening. This would require much smaller time step sizes compared to the viscous solver in order to obtain a converged solution. These difficulties arise since the divergence of the polymer stress tensor has to be evaluated explicitly in the momentum equation. In general the divergence operator can only be applied implicitly if the variable on which it is applied is being solved for. Since the velocity is solved for when evaluating the momentum equation it follows that the polymer stress tensor can only be evaluated explicitly when operators are applied to it. The stability can be improved therefore by strengthening the diagonal

dominance of the discrete set of equations. This is accomplished by applying the DEVSS (Discrete Elastic Viscous Split Stress) decomposition (Habla et al. 2012). With this technique an elliptic term is added to the momentum equation and is to be evaluated implicitly. The same term is then subtracted from the source term and is then evaluated explicitly. The momentum equation, originally given in equation (2.10) as presented in section 2.1.3 is repeated here for clarity after the term containing the solvent stress contribution is transferred to the left hand side:

$$\rho\left(\frac{\partial v_i}{\partial t}+\sum_{j=1}^{3} v_j\frac{\partial v_i}{\partial x_j}\right)-\frac{\partial}{\partial x_j}\left(\eta_s\dot{\gamma}_{ij}\right)=-\frac{\partial p}{\partial x_i}+\frac{\partial \tau_{\mathrm{p,ij}}}{\partial x_j} \tag{3.8}$$

The solvent viscosity is a function of temperature and pressure. Therefore the divergence of the solvent viscosity multiplied with the rate of deformation tensor is treated the same as it was treated in the generalized Newtonian formulation:

$$\rho\left(\frac{\partial v_i}{\partial t}+\sum_{j=1}^{3} v_j\frac{\partial v_i}{\partial x_j}\right)-\eta_s\frac{\partial^2 v_j}{\partial x_j^2}=-\frac{\partial p}{\partial x_i}+\frac{\partial \tau_{\mathrm{p,ij}}}{\partial x_j}+\dot{\gamma}_{ij}\frac{\partial \eta_s}{\partial x_j} \tag{3.9}$$

The DEVSS decomposition is now applied by adding and subtracting the Laplacian of the velocity field multiplied by the polymer viscosity to (3.9):

$$\rho\left(\frac{\partial v_i}{\partial t}+\sum_{j=1}^{3} v_j\frac{\partial v_i}{\partial x_j}\right)-\eta_t\frac{\partial^2 v_j}{\partial x_j^2}=-\frac{\partial p}{\partial x_i}+\frac{\partial \tau_{\mathrm{p,ij}}}{\partial x_j}+\dot{\gamma}_{ij}\frac{\partial \eta_s}{\partial x_j}-(1-\beta)\eta_t\frac{\partial^2 v_j}{\partial x_j^2} \tag{3.10}$$

Where the viscosity appearing in this equation is the total viscosity of the fluid, which is the sum of the solvent and polymer viscosities. The Laplacian term on the left hand side of the equation is evaluated implicitly, which can be done since the velocity field is being solved for, and the Laplacian on the right hand side of the equation is evaluated explicitly.

3.2 Validations

3.2.1 Simulating long bearings with "genStokesFoam"

In order to establish the validity of the simulated results, results from the "genStokesFoam" solver were compared to the long bearing solution of the classical Reynolds equation. In this benchmark the pressure distribution predicted by the numerical solution was compared to the analytical solution. The Reynolds equation is essentially a two dimensional Stokes formulation of the fluid in two dimensions, since the thickness of the film is neglected. It therefore follows that the solution predicted by the "genStokesFoam" solver, being a Stokes formulation of the fluid flow, should closely resemble the analytical solution of the Reynolds equation (see section 2.1.8). As the clearance of the bearing is reduced in the numerical solution it is expected that it will tend towards the analytical solution. The reduction of the bearing clearance simulates the numerical solution tending towards that of a two dimensional flow similar to that described by the Reynolds equation.

The reason for using the long bearing solution as a benchmark is that: since the bearing is assumed to be of infinite length, a two dimensional model can be used to model the bearing, this significantly reduces the amount of CVs (and therefore computational time needed) in the computational domain to achieve a converged solution. This is not the case with the short bearing solution where the bearing must be simulated in three dimensions and since the bearing cannot be made to have no length one would have to reduce the bearing length and see if the results tend to that of the short bearing theory. This implies that the individual cases need more computational power and the number of cases that must be run in order to show that the solver is correct is more.

The analytical result for the short bearing problem, given in equation (2.26), does contain a term that describes the length of the bearing. One might remark that this would therefore not require one to run numerous numerical cases where the length of the bearing is decreased in order to show validity of the numerical results. It is important to note that when this analytical solution is derived the Reynolds equation is reduced on the premise that the length of the bearing is negligible (Owens & Phillips 2002). Therefore one is left with the problem: what is negligible length of the bearing? Again one arrives at the problem that in order to definitively show the validity of the results multiple numerical solutions needs to be computed at various lengths of the bearing. These difficulties are circumvented by selecting the long bearing solution as a benchmark.

Phillips et al. (1999) showed that the long bearing theory gives good results in predicting the load bearing capacity of the bearing, which implies that it is able to correctly predict the pressure distribution.

To show that the “genStokesFoam” solver is indeed able to correctly predict the pressure distribution in the bearing the solver was used for two separate cases: Firstly the maximum pressure in the bearing predicted by the Reynolds equation for the long bearing case is compared to the computed value from “genStokesFoam”. Secondly the pressure distributions for the aforementioned models were compared for three different eccentricity ratios. It can be seen, by looking at the long bearing solution given by equation (2.25) that the nonlinear terms dominate at higher eccentricity ratio’s causing the pressure distribution to depart from the sinusoidal profile obtained at low eccentricity ratios. This benchmark exercise was therefore aimed at comparing the maximum pressure and the pressure distribution in the converging part of the bearing as the pressure profile tends away from the sinusoidal profile found at low eccentricity ratios.

The numerical solver becomes unstable when the control volumes used are much longer in one direction than the other. This is typically the case when the number of elements in the circumferential direction is not enough, the CV is then elongated in the direction of the flow. This causes the solution to diverge rapidly. When the bearing diameter is increased the number of circumferential elements must also be increased. When the mesh is refined in the radial direction, which could also happen when the bearing clearance is reduced but the number of elements in the radial direction is kept constant, a refinement in the circumferential direction must be made. For high eccentricity geometries the mesh skewness in the diverging and converging sections of the bearing becomes very high, and either mesh refinement or the number of pressure correctors must be increased. Both of these adjustments imply an increase in computational time. It was found that if the number of pressure corrections were increased from 2 to 3 for the $\epsilon = 0.4$, and 3 to 4 for the $\epsilon = 0.6$, the solution was stable and converged to below the specified residual.

The first comparison was done for a bearing with an eccentricity ratio of 0.2, radius of 0.1m, journal velocity of 10m/s and variable bearing clearance. Since the bearing simulated is assumed to be of infinite length the simulation was done in two dimensions. For all the cases in this section the fluid used was SAE 50W oil, specifications for this oil are found in White (2006). The only fluid property used was viscosity which is 95.34 mm^2/s. The meshes used to establish mesh independence are presented in Table 1:

Table 1: Mesh specifications for bearings with ϵ = 0.2 having different bearing clearances.

c = 1mm				
	Number of Control Volumes in:			
	Radial direction	Circumferential direction	Total	Difference[2]
Mesh1	20	750	56 924	
Mesh2	20	1000	75 924	2.45%
Mesh3	25	1500	143 904	1.66%
c = 0. 5mm				
	Number of Control Volumes in:			
	Radial direction	Circumferential direction	Total	
Mesh1	20	1500	113 924	
Mesh2	25	2000	191 904	1.95%
Mesh3	25	2500	239 904	1.08%
c = 0. 1mm				
	Number of Control Volumes in:			
	Radial direction	Circumferential direction	Total	
Mesh1	20	7500	569 924	
Mesh2	20	10000	759 924	1.43%
Mesh3	25	12500	1 199 904	0.682%

Table 1 shows the number of CVs required to reach a converged solution. It is seen that the number of CVs had to be increased as the clearance decreased, in order to reach a converged solution. The number of CVs in the radial direction is the same for the various clearances. The increase in the number of circumferential CVs is needed to decrease the aspect ratios of the CVs. Circumferential refinement is needed in order to assure stability of the solver.

The numerical result followed the expected trend, comparing the difference between the maximum and minimum predicted pressure, without accounting for cavitation. The results obtained are summarised in Table 2. (The error reported is a percentage error between the numerical and analytical solutions. The analytical solution is used as the reference value). The results presented are only those computed from the finest mesh for which mesh independence was established.

From Table 2 it is clearly seen that the numerical results tended towards the analytical result when the bearing clearance tended to zero. This implies that the numerical solution tends to the analytical solution as the approximation of no clearance between the journal and the bearing, made in deriving the analytical solution, is more closely resembled by the numerical case.

[2] The Percentage difference between the current mesh and the previous mesh.

Table 2: Comparison between numerical an analytical solution for various bearing clearances, ϵ = 0.2.

c [mm]	Analytical	Numerical	Error [%]
1	258	254	1.66
0.5	1033	1022	1.08
0.4	1614	1599	0.920
0.3	2869	2845	0.844
0.1	25829	25653	0.682

The long bearing theory, when cavitation is not accounted for, produced a negative minimum pressure that has the same magnitude as the maximum pressure within the converging region of the bearing. The "genStokesFoam" solver is for incompressible cases only and therefore the pressure is only meaningful if a gauge pressure is specified. By looking at the differences in the pressure field the benchmark becomes independent of the specified gauge pressure. The gauge pressure is set by selecting a control volume in the mesh that is at the pressure that is to be selected as the gauge pressure and setting this control volume as the reference for the pressure field. This can become quite tedious in the case where numerous meshes are used and finding the right control volume can be quite time consuming as well as introduce errors. Given the above considerations it was therefore concluded that looking at the pressure differences rather than the minimum and maximum pressures separately would be quicker and more accurate. In order to confirm the above, the gauge pressure was specified to be zero at 90^0 (along the circumference of the bearing). This was done each time the eccentricity was changed. In each case it was found that the pressure difference was independent of the gauge pressure set. The results for the pressure difference in a bearing for various clearances are shown in Figure 3.

Figure 3 shows that the numerical and analytical solutions for a long bearing are extremely close in predicting the pressure difference between the minimum and maximum pressures in the bearing. The data was plotted on a logarithmic graph simply because of the wide range in the magnitudes of the pressure difference.

To look at the shape of the pressure distribution the highest bearing clearance ratio (c = 0.001 m) was taken, because it is known (see Table 2) that the computed pressure at the minimum and maximum have the greatest error for this bearing clearance. Refer to Figure 4 giving the pressure distribution over the first half of the bearing. Only this half is reported on because of two reasons: Firstly by looking at the analytical solutions (the numerical solutions also show this) it is seen that the negative part of the pressure distribution has the same shape as the positive pressure distribution (this happens due to cavitation not being accounted for). Secondly due to cavitation occurring in practice we are not concerned with the accuracy of the negative pressure distribution. Since the governing equations describing the flow in the oil film resembles that of parabolic type, in this case, it follows that when the pressure distribution is integrated to give the force acting on the journal, the negative part of the pressure distribution can be disregarded (Owens & Phillips 2002).

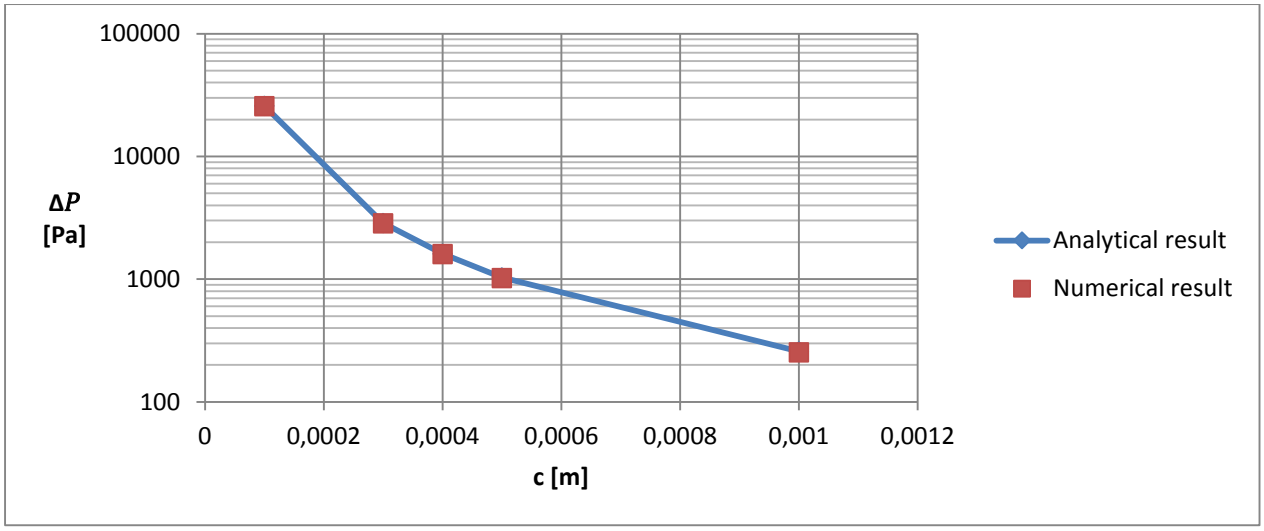

Figure 3: Comparison between the numerical and analytical solution of maximum pressures in bearings with varied clearances, ϵ = 0.2.

The pressure distributions are plotted against the angle (see Figure 4), theta, measured along the circumference of the bearing, see Figure 1 for range of θ (whether this is the pressure on the bearing casing or on the journal does not matter since the pressure difference across the oil film is negligibly small).

It is shown in Figure 4 that the pressure distribution changes as the eccentricity changes. This is due to the nonlinearity in the system becoming more dominant at higher eccentricity ratios. It can, however, be seen from all the pressure distributions that the greatest error in the numerical results is as the maximum pressure. The pressure difference, between the maximum and minimum pressures in the bearing, therefore gives a good indication to the accuracy of the overall pressure distribution for these eccentricity ratios. Figure 4 also shows that the pressure distribution predicted by the numerical solution is in good agreement with the analytical solution.

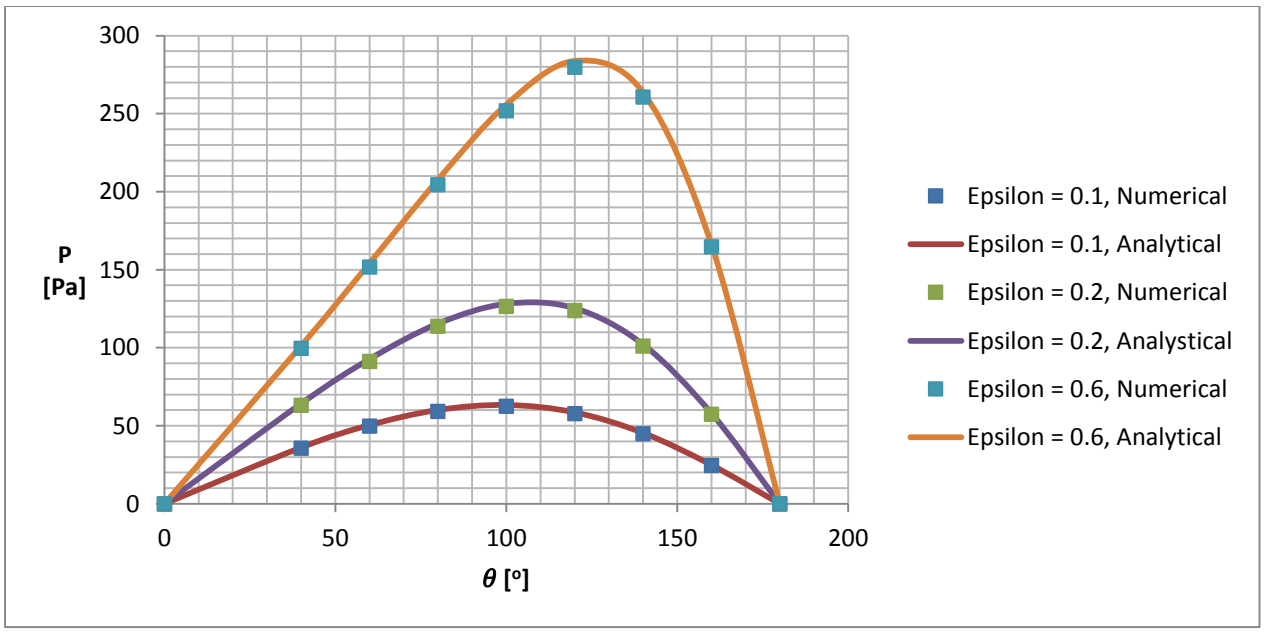

Figure 4: Pressure distributions for various eccentricities, c = 0.001 m. The graph is a plot of Pressure with respect to θ.

This section thus shows that the "genStokesFoam" solver, being a Stokes formulation of the flow, closely resembles the Reynolds equation in predicting the pressure distribution in the bearing. Care however must be taken to ensure that the numerical case resembles the assumptions made when deriving the Reynolds equation. The "genStokesFoam" solver, with an uncoupled formulation is therefore used in this study as a representative of the classical formulation.

3.2.2 Rotating concentric cylinders

The fluid flow between two concentric rotating cylinders is presented as a benchmark in the book of Owens et al. (2002). The benefit, highlighted in their book, of this benchmark is that the geometry is easy to construct. Furthermore no compensation is needed in terms of flow or thermal development. This implies that less computational resources are spent on the development of the flow conditions. The additional reasons for selecting this benchmark for this study is that there is a similarity between the benchmark and journal bearings and an analytical solution is known for this problem.

The flow can be solved analytically if the momentum and the energy equation are uncoupled (White 2006). The fluid properties are therefore modelled as having no dependence on pressure, temperature or shear rate.

In the previous section the long bearing solution was used to show that the "genStokesFoam" solver can predict the same pressure distribution as the classical Reynolds equation when the fluid is Newtonian. In the following benchmark two things are to be shown: Firstly it needs to be verified that the other solvers give the same result as the "genStokesFoam" solver when operating at low velocities and the fluid is approximately Newtonian. This shows that all the fluid models will reduce to the classical formulation if the same assumptions are made with regards to the flow characteristics and fluid properties. Secondly, to determine the accuracy of the temperature fields computed by the evaluation of the energy equations of each solver respectively. The computed results are in both cases compared to the analytical solutions.

The concentric cylinders are assumed to be of infinite length, heat transfer is therefore due to radial conduction. Heat is generated within the fluid domain due to viscous dissipation. This benchmark therefore checks the accuracy of the solvers in predicting the heat transferred, as well as heat generated due to viscous dissipation. Convection is also checked in this case since it is still being solved for, implying that although convection does not influence the amount of heat transferred for this case specifically, it must still be computed and the computed result must show that heat transferred by means of convection is negligible.

Assuming that the cylinders have infinite length implies that the geometry is two dimensional. Flow in the axial direction is therefore neglected. Since there is no pressure gradient in the radial direction and the boundaries of the cylinders are impermeable the flow can only be in the circumferential direction. For a fully developed Newtonian fluid the velocity profile is described by (White 2006):

$$v_\theta = r_0\omega_0 \frac{\left(\frac{R_1}{R} - \frac{R}{R_1}\right)}{\left(\frac{R_1}{R_0} - \frac{R_0}{R_1}\right)} + r_1\omega_1 \frac{\left(\frac{R}{R_0} - \frac{R_0}{R}\right)}{\left(\frac{R_1}{R_0} - \frac{R_0}{R_1}\right)} \tag{3.11}$$

where subscripts 0 and 1 refer to the inner and outer cylinder respectively. Since the velocity profile is known, it is used together with the assumptions mentioned earlier to find the analytical solution for the temperature profile in the fluid (White 2006):

$$\frac{T-T_0}{T_1-T_0} = PrEc\frac{R_1^4}{R_1^2-R_0^2}\left[\left(1-\frac{R_0^2}{R^2}\right)-\left(1-\frac{R_0^2}{R_1^2}\right)\frac{\ln\left(\frac{R}{R_0}\right)}{\ln\left(\frac{R_1}{R_0}\right)}\right]+\frac{\ln\left(\frac{R}{R_0}\right)}{\ln\left(\frac{R_1}{R_0}\right)} \quad (3.12)$$

The two non-dimensional constants that are used in the solution of the temperature field, the Prandtl number and the Eckert number, are defined as:

$$\mathrm{Pr} = \frac{\mu_0 c_p}{k_0} \;;\; Ec = \frac{U^2}{c_p T_0} \quad (3.13)$$

The Prandtl number is usually used for single or multiphase convective heat transfer calculations and is the ratio of the rate of diffusion of viscous effects to the rate of diffusion of heat. The Eckert number on the other hand is usually used in high speed flows and describes the ratio of the kinetic energy of the flow to the enthalpy change (Faghri et al. 2010).

In this case these constants are used to describe the viscous dissipation in the system. The first term on the right hand side of the temperature solution, equation (3.12), describes the heat generated due to viscous dissipation. The second term on the right hand side describes conduction heat transfer in the radial direction.

In order to have a well-posed problem, boundary conditions have to be set at the inner and outer cylinders. The inner boundary was chosen to be at T_0= 373.15K and the outer boundary was chosen at T_1= 273.15K. The inner cylinder's radius was 0.1m and the thickness of the domain in the radial direction was 0.01m. The fluid properties used for the fluid between the two cylinders was engine oil. Fluid properties were taken to be at 320K and were found in the book Faghri et al. (2010).

Table 3: Fluid properties used in this section.

Fluid property	Value
Cp	1.99 KJ/kgK
mu	0.141 Ns/m^2
k	0.141 W/mK

Non-slip boundary conditions were set for the momentum equation. The outer cylinder was chosen to be stationary and the angular velocity of the inner cylinder is varied. This was done to vary the prominence of the viscous dissipation term.

For this benchmark the same three meshes (mesh 1, 2 and 3, described in Table3) were used for all the test cases. In all the cases mesh independence was established. The meshes were hexahedral which means that the orthogonally of the meshes was high and therefore computational time was reduced since a single pressure correction was sufficient for the solution to converge. The refinement in each direction is given in terms of the amount of control volumes in that direction.

Table 4: Mesh specifications for concentric rotating cylinders.

	Refinement	
Mesh	Circumferential	Radial
1	75	15
2	100	20
3	150	30

For the pure conduction case the two cylinders were chosen to be stationary. The system of equations derived from the discretised domain was symmetric and therefore converged rapidly. The system was treated as being under steady state conditions. When the velocity field goes to zero the energy equations reduces to the pure conduction case:

$$k\nabla^2 T = 0 \tag{3.14}$$

The computed temperature profiles for each of the solvers were exactly the same, therefore only one set of data is presented in Table 5. The results presented in this section are only for those computed inside the fluid domain since the boundary conditions are held constant. No computation is performed at the boundary with regards to the temperature or velocity, since these values remained the same:

Table 5: Comparison of temperature profiles predicted numerically and analytically.

R [m]	Analytical [K]	Mesh1 [K]	Mesh2 [K]	Mesh3 [K]
0.101	362.710	362.696	362.697	362.704
0.103	342.136	342.121	342.123	342.131
0.105	321.960	321.943	321.942	321.951
0.107	302.162	302.137	302.148	302.151
0.109	282.732	282.717	282.719	282.724
Average Error[3] [%]		0.00542	0.00444	0.00248

In Table 5 the computed temperature values at different radial positions are presented for each of the meshes. This shows that for all three of the meshes the energy equation reduces to exactly the same form. This is a very good result as it indicates that all three energy equations reduce to give the same result if the solution is simple enough (since all the solvers gave exactly the same results). Mesh convergence is also clearly seen in this result as the error decreases with greater refinement of the mesh.

Relative motion of the cylinders generates heat in the fluid. This is due to friction between the layers because of this relative motion. The viscous dissipation would therefore increase as the velocity of the relative motion is increased. Due to the nonlinearity introduced through the inertia terms of the momentum equation the discrete system of equations are no longer symmetric and therefore the solution requires more computational time.

[3] The average error is that of the numerical result compared to the analytical result.

Next the angular velocity of the inner cylinder is set to be 10rad/s .At these speeds the viscous dissipation would be moderate; therefore the temperature profile would only be slightly affected by this term. Due to the velocity being low the results obtained from the Stokes formulation should be very similar to that obtained with the formulations that include the inertia terms. Mesh independence was established for each of the solvers. The results for mesh 3, the finest mesh, are presented Tables 6 and 7 for the different solvers respectively, first for the generalized flow solvers and then for the viscoelastic solvers.

Table 6: Comparison of velocity and temperature profiles, predicted by viscous solvers. V_{max} = 1m/s

	genStokesFoam		ViscFOAM		Analytical	
R [m]	**V [m/s]**	**T [K]**	**V [m/s]**	**T [K]**	**V [m/s]**	**T [K]**
0.101	0.8952	362.723	0.895242	362.685	0.8955	362.710
0.102	0.7917	352.379	0.791668	352.31	0.7918	352.373
0.103	0.6892	342.134	0.68924	342.046	0.6893	342.138
0.104	0.5878	331.983	0.58777	331.891	0.5879	331.999
0.105	0.4874	321.949	0.487426	321.864	0.4875	321.959
0.106	0.3880	312.014	0.38803	311.944	0.3881	312.014
0.107	0.2896	302.174	0.2896	302.124	0.2897	302.162
0.108	0.1922	292.427	0.192164	292.395	0.1922	292.402
0.109	0.0956	282.752	0.0956058	282.736	0.0957	282.731

Table 7: Comparison of velocity and temperature profiles, predicted by viscoelastic solvers. V_{max} = 1m/s

	ThemOldBFoam		ThermGiesFoam		Analytical	
Radial Direction	**V [m/s]**	**T[K]**	**V [m/s]**	**T [K]**	**V [m/s]**	**T [K]**
0.101	0.8952	362.991	0.8955	362.710	0.8950	362.867
0.102	0.7916	352.889	0.7918	352.373	0.7914	352.656
0.103	0.6892	342.814	0.6893	342.138	0.6890	342.511
0.104	0.5877	332.699	0.5879	331.999	0.5876	332.423
0.105	0.4874	322.581	0.4875	321.959	0.4872	322.392
0.106	0.3880	312.512	0.3881	312.014	0.3879	312.424
0.107	0.2896	302.55	0.2897	302.162	0.2894	302.505
0.108	0.1921	292.698	0.1922	292.402	0.1920	292.659
0.109	0.0956	282.906	0.0957	282.731	0.0954	282.868

The number of points at which the temperature and velocity were compared to the analytical solution is double to that of the pure conduction case. This is due to the temperature profile deviating from a linear form. Therefore more points are needed to capture the form of the temperature profile. The velocity profile is seen to change very slightly between the various solvers. Due to these small variations more points are also needed to compare these variations. The results presented in Tables 6 and 7 were compared to the analytical solution. For each solver the average error was calculated, these errors are presented in Table 8.

Table 8: Error between the analytical and numerical velocity and temperature profiles respectively. V_{max} = 1m/s

Solver	[%]Error of V	[%]Error of T
genStokesFoam	0.0292	0.104
ViscFoam	0.0292	0.122
ThermOldBFoam	0.0408	0.0362
ThermGiesFoam	0.261	0.0874

When the relaxation time of the Oldroyd-B constitutive models are small the constitutive relation describing the polymer stress reduces to a linear constitutive relationship:

$$\tau_{p,ij} \approx \eta_p \dot{\gamma}_{ij} \tag{3.15}$$

This implies that the constitutive relation is reduced to the generalised Newtonian formulation when the relaxation time of the fluid is negligible. This argument especially holds for the Giesekus model when the angular velocity of the inner cylinder is small. It becomes less simple in the next case where the velocity is increased. For this reason the Giesekus formulation was treated separately and these results are presented later in the section.

The angular velocity of the inner cylinder was then further increased to 100rad/s. The viscous dissipation term is much more dominant at this speed and therefore the temperature profile would be significantly affected by the heat generated in the film (referring to the more general case where the governing equation is coupled and therefore viscosity would be dependent on temperature). The results for the first three solvers on the finest mesh are presented in Table 9.

Table 9: Comparison of numerical and analytical velocity profiles.

	genStokesFoam	ViscFoam	ThermOldBFoam	Analytical
R [m]	**V [m/s]**	**V [m/s]**	**V [m/s]**	**V [m/s]**
0.101	8.952	8.952	8.955	8.953
0.102	7.917	7.917	7.920	7.918
0.103	6.892	6.892	6.895	6.893
0.104	5.878	5.878	5.880	5.879
0.105	4.874	4.874	4.876	4.875
0.106	3.880	3.880	3.882	3.881
0.107	2.896	2.896	2.898	2.897
0.108	1.922	1.922	1.922	1.922
0.109	0.956	0.956	0.956	0.957

It is seen from the results presented in Table 10 that viscous dissipation increased the maximum temperature in the fluid with almost 10^0C as compared with the results in Table 7. Comparing the velocity profiles of the 10rad/s case and the 100rad/s case it is seen that the velocity profile predicted by the “genStokesFoam” solver was just one order of magnitude larger.

Table 10: Comparison of numerical and analytical temperature profiles.

	genStokesFoam	ViscFoam	ThermOldBFoam	Analytical
R [m]	**T[K]**	**T[K]**	**T[K]**	**T[K]**
0.101	380.414	380.411	380.415	380.484
0.102	383.532	383.346	383.32	383.420
0.103	382.156	382.151	382.039	382.224
0.104	377.01	377.009	376.769	377.081
0.105	368.111	368.115	367.738	368.186
0.106	355.629	355.638	355.17	355.706
0.107	339.752	339.764	339.307	339.829
0.108	320.595	320.606	320.272	320.668
0.109	298.301	298.308	298.145	298.365

This is however not the case with the other two solvers. This shows the loss of linearity in the solution through the inclusion of the inertia terms. The results presented in table 8 were again compared to the analytical solution and an average error for each of the results was determined. These errors are presented in Table 11.

Table 11: Average errors of velocity and temperature profiles, compared with analytical solution.

Solver	[%]Error of V	[%]Error of T
genStokesFoam	0.0292	0.0208
ViscFoam	0.0307	0.0192
ThermOldBFoam	0.0201	0.0888

The temperature profiles for the three cases: the conduction case, the 10rad/s and 100rad/s angular velocity cases are presented in Figure 5.

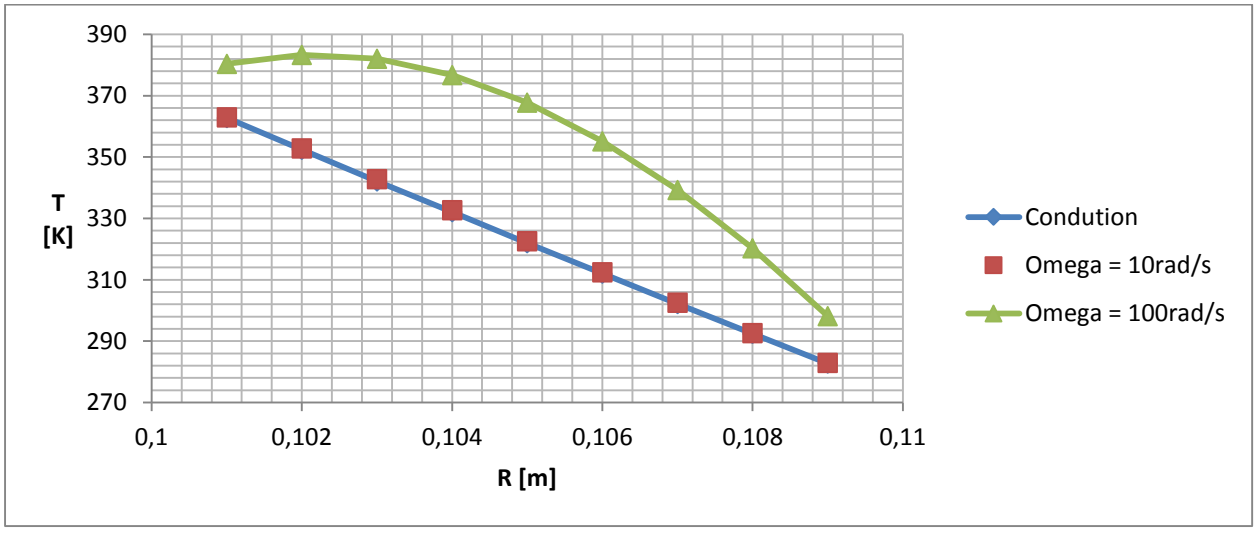

Figure 5: Temperature profiles with respect to radial position at three different angular velocity of the inner journal. Results presented was computed with "genStokesFoam".

The results presented in Figure 5 is for only the "genStokesFoam" solver since the differences of these solvers are so small one would not be able to see the differences between them on this kind of graph.

The temperature profiles of the conduction and 10rad/s angular velocity flow are very close to each other. For the 100rad/s angular velocity flow case temperature is higher than the previous two cases. The higher velocity increases the heat generated through viscous dissipation and therefore the temperature for the latter case is higher. Viscous dissipation would increase further if the angular velocity was increased further. For the operating condition of large steam turbine journal bearings viscous dissipation would therefore be much more dominant than in the cases presented here. The angular velocity of the journal is held constant between speeds of 300 - 400rad/s. This does not include the additional shear due to eccentricities of the journal. Therefore when considering the eccentricities of the journal in the bearing it is expected that viscous dissipation would play a greater role in heat generated in the bearing.

The results from the "ThermGiesFoam" solver were not as easily benchmarked as the previous solvers. The reason for this is due to the additional term in the constitutive relation, equation (2.13) of the form:

$$\frac{\alpha\lambda}{\eta_p}\,\tau_p^2 \tag{3.16}$$

The square in this term implies an outer product of the polymer stress tensor with itself. Considering just the shear entries of the tensor equation for the Giesekus model it follows that this product introduces a constant,α , times the square of the shear stress. It the context of this benchmark this implies that for shear stress less than unity this term will disappear much quicker than the other terms. On the other hand this term will dominate at high shear stresses since it grows much quicker than the other terms. Since this term models the shear thinning behaviour of the fluid the shear stress must be kept small in order to minimise shear thinning behaviour in the flow. The flow is solved when α is set to zero. This reduces the Giesekus model to the Oldroyd-B model. Since the Oldroyd-B model has been shown to be accurate it can be used to determine the validity of the Giesekus model. Thus a perturbation type approach is taken: The value of α was selected such that the added term in equation (3.16), the only term that distinguished the Giesekus model from the Oldroyd-B model, goes from being negligible to significant in the constitutive relation. The velocity profiles for these varied values of α are presented in Table 12.

Table 12: Velocity profiles as computed with the "ThermGiesFoam" solver at varied values of α.

α	0.15	0.01	0.001	0
R [m]	V [m/s]	V [m/s]	V [m/s]	V [m/s]
0.101	8.95301	8.96399	8.96537	8.96554
0.102	7.91534	7.9212	7.92222	7.92235
0.103	6.89589	6.89811	6.89859	6.89865
0.104	5.8865	5.88405	5.88368	5.88364
0.105	4.88699	4.88008	4.87887	4.87873
0.106	3.89622	3.88601	3.88413	3.8839
0.107	2.91183	2.90006	2.89782	2.89754
0.108	1.935011	1.92456	1.92251	1.92225
0.109	0.963578	0.95721	0.955934	0.955772

For the velocity profile slight shear thinning was observed close to the inner cylinder where velocity was the highest. The effect of the shear thinning is more drastically seen in the temperature profiles where shear thinning caused a decrease in viscous dissipation and therefore a lower maximum temperature. Figure 6 shows this as a graph of the temperature profiles plotted against radial direction.

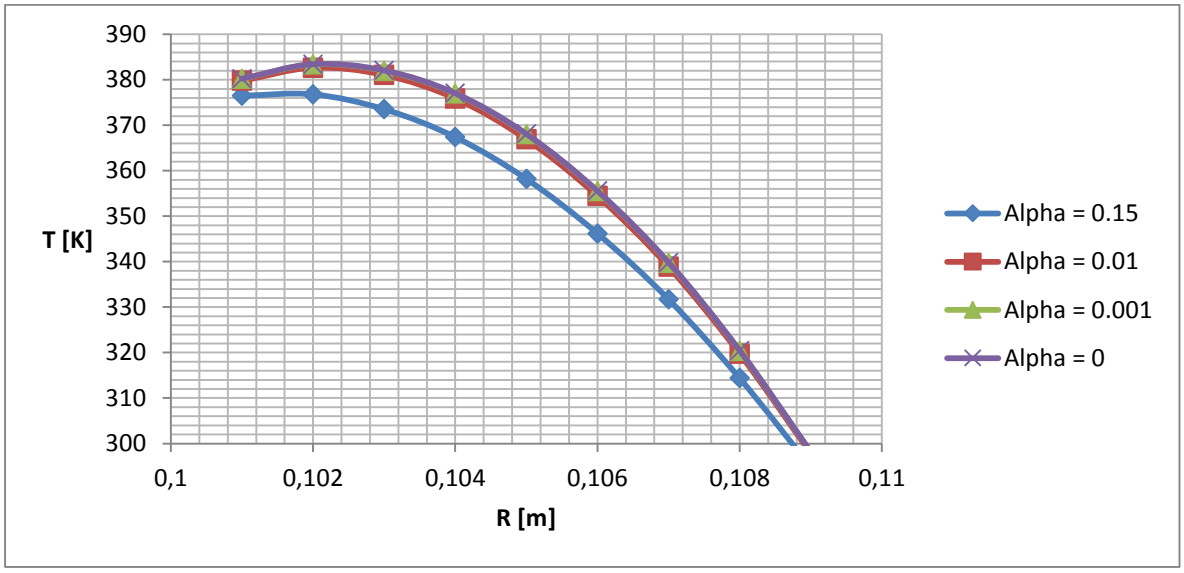

Figure 6: Temperature with respect to radial direction at α = 0, 0.001, 0.01, 0.15.

The temperature profiles predicted by the Giesekus model were compared to the Oldroyd-B model. The average difference between these profiles was determined and is presented in Table 13.

Table 13: Percentage difference between the results predicted by the Oldroyd-B model and different results from the Giesekus model.

α	[%] Difference
0.15	2.04
0.01	0.241
0.001	0.0147

From Table 12 and 13 it is clear that the Giesekus model's predicted results tend towards the Oldroyd-B model's results as α tends to zero.

Through the above cases it is seen that all four of the solvers were able to correctly predict the velocity and temperature profiles at various angular velocities. This benchmark therefore confirms that all four solvers are able to correctly reduce to the Newtonian fluid model when the material properties are chosen correctly. It furthermore shows that accurate evaluation of the energy equation.

3.2.3 Non-Newtonian flow benchmark with channel flows

In this section, the shear thinning behaviour of the viscous fluid formulations are validated. This is done by comparing the computed results of channel flows with known analytical solutions.

Channel flows, in this context, are flows between two stationary walls with a pressure gradient applied in one direction. The flow domain is assumed to be infinitely wide (the width of the channel is the direction perpendicular to the walls of the channel as well as the direction of the applied pressure gradient) and therefore the problem is reduced to a two dimensional case. The reason for choosing this benchmark is because analytical solutions for the power law model are easy to find. The use of Cartesian coordinates further simplifies the matter. Finally computationally this kind of problem is not very demanding as one is solving a two dimensional flow problem with a pressure gradient as its driving force.

The shear thinning behaviour in the bearing models was described by the Carreau model (see section 2.1.10). Finding an analytical solution for this particular model however was quite troublesome due to the integral that is to be evaluated when solving for the velocity profile from the momentum equation. Therefore in order to simplify the mathematics the following observation regarding the Carreau fluid model will help (the Carreau model is presented here again for the sake of clarity in the discussion):

$$\eta(\dot{\gamma}) = \frac{\eta_0}{(1 + (k_s\dot{\gamma})^a)^b} \tag{3.17}$$

If the shear rate is high ($\dot{\gamma} = 10$ would be an example of this), then the denominator can be approximated as:

$$(1 + (k_s\dot{\gamma})^a)^b \approx (k_s\dot{\gamma})^{ab} \tag{3.18}$$

This is the same form as the viscosity relation of a Power Law fluid. Therefore if the shear rate is high the fluid will tend towards the behaviour of a Power Law fluid.

In the case where the shear rate is low ($k_s\dot{\gamma} \ll 1$ would be an example of this) then the denominator can be approximated as:

$$(1 + (k_s\dot{\gamma})^a)^b \approx 1 \tag{3.19}$$

Therefore the fluid would behave as a Newtonian fluid. Using a simple shear flow example will not work, although one can very easily control the magnitude of the shear rate. Specifics for this are presented in the next section.

To derive the analytical solution a Power Law fluid is assumed. A steady flow as well as low velocity flow such that the inertia terms can be neglected is assumed. Under these conditions the momentum equation reduces to:

$$\frac{dp}{dx} = \frac{d}{dy}\left(m\left(\frac{du}{dy}\right)^{n-1}\right) \tag{3.20}$$

This is an ordinary differential equation and since the velocity field is assumed to be only in one direction the velocity in the equation above is a scalar quantity. Solving this equation is simple and yields the solution to the velocity profile:

$$u(y) = \left(\frac{n}{n+1}\right)\left(-\frac{1}{m}\frac{dp}{dx}\right)^{\frac{1}{n}}\left(\left(\frac{h}{2}\right)^{\frac{n+1}{n}} - y^{\frac{n+1}{n}}\right) \tag{3.21}$$

In order to simplify the analytical solution to be used to benchmark this aspect of the solver, a Power Law fluid is assumed. For a Power law fluid the analytical solution for the above case is simple. From the observations above we can conclude that a Carreau fluid will tend towards the behaviour of the power law fluid (for this specific case) when both of these models are tending towards the Newtonian case.

Both the "genStokesFoam" and the "ViscFoam" solvers were used for this benchmark. The fluid was modelled as being a shear thinning fluid. In order to show that the numerical solutions tend to the analytical solution of a Power Law fluid, the following powers for the Power Law fluid was selected: n= 0.6, 0.8 and 0.9. For the Carreau fluid it follows that: $1 - ab = n$. The value for k_s was chosen to be close to unity: 1.04. For this benchmark a was set to 2 for all cases and b was changed between 0.3, 0.2 and 0.1.

For the two solvers different domains were needed. The "ViscFoam" solver requires a much larger domain for the flow to fully develop. The reason for this is simply due to the addition of the inertia terms to the flow formulation. For the two solvers the domains used are presented in Table 14.

Table 14: Geometric specifications for domain used.

Solver	Length [m]	Height [m]
genStokesFoam	0.5	0.1
ViscFoam	12	0.1

The mesh specifications for the different domains are presented in Table 15.

Table 15: Mesh specifications for channel flow simulation.

genStokesFoam		
	Number of Control Volumes in:	
	x direction	y direction
Mesh 1	40	20
Mesh 2	60	30
Mesh 3	80	40
ViscFoam		
	Number of Control Volumes in:	
	x direction	y direction
Mesh 1	240	20
Mesh 2	320	30
Mesh 3	320	40

Mesh independence for each of the cases were established. The results for the finest mesh are presented and compared to the analytical solution. According to the discussion above the difference between the numerical and analytical solution should become smaller as n tends to unity. The percentage difference between the power law (analytical) and Carreau model (numerical) solutions are presented in Table 16.

Table 16: Percentage error between the velocity profiles predicted from the power law fluid and the Carreau fluid.

	Error [%]		
	n=0.6	*n*=0.8	*n*=0.9
genStokesFoam	5.28	0.104	0.0412
ViscFoam	5.17	0.297	0.118

The results presented in Table 16 show that the computed results from both solvers tended towards the analytical solution (3.21) as *n* tends to 1. It is therefore concluded that the shear thinning behaviour described by the Carreau model as implemented in these solvers is correct. This benchmark therefore shows the ability of the viscous solvers to describe shear thinning behaviour.

3.2.4 Viscoelastic flow benchmark with Couette flows

In this final section of chapter three the validity of the viscoelastic solvers to predict the stress field in the fluid is validated. In this benchmark the two viscoelastic solvers are validated against the analytical solution of a Couette flow.

The Couette flow problem is a simple shear problem, where (in this case), a rectangular domain is selected for the flow. The important boundary condition is set at the top wall, since this wall is moving at a fixed velocity. The bottom wall is stationary and the other boundaries in the domain are treated as zero gradient pressure and velocity boundary conditions.

The reason why Couette flow was chosen is twofold: firstly this flow is still in the context of journal bearings since the shearing of the fluid is one of the primary factors that influence the flow condition in a bearing (see introduction of chapter 4). Also, it is selected because analytical solutions can be found for these flows. Analytical solutions for these general flow models are quite rare compared to Newtonian flow models.

For the velocity profile we note that although the constitutive relation enters the set of governing equations the momentum equation reduces to:

$$\frac{\partial}{\partial x_j}(\tau_{ij}) = 0 \tag{3.22}$$

Due to the geometry of the problem the above reduces to a single equation:

$$\frac{\partial}{\partial y}(\tau_{xy}) = 0 \tag{3.23}$$

this is the component in the stress tensor that describes the shear stress. From this it follows that the shear stress is constant for the flow. The velocity profile will also look the same as for that of a Newtonian fluid: linear, hence a straight line. In order to evaluate the validity of the solvers the velocity profile is compared with the analytical result. Furthermore although the stress components in the tensor are constant for this case it is still possible to find it analytically. It thus gives a checking mechanism with which to validate the solved stress field.

For the Oldroyd-B model, the constitutive relation gives the following equation for the Couette problem (Owens & Phillips 2002):

$$\tau_{xx} = 2\eta_0(\lambda_1 - \lambda_2)\dot{\gamma}^2 \tag{3.24}$$

$$\tau_{xy} = \eta_0\dot{\gamma}_{xy} \tag{3.25}$$

where the viscosity in the above equations refers to the zero shear viscosity. The $\dot{\gamma}$ in the first equation represents the magnitude of the rate of shear tensor, where as in the second equation it refers to the second component of the rate of shear tensor.

The same mesh specifications were used for both the solvers. Mesh independence was established for each of the cases. The mesh specifications are presented in Table 17.

Table 17: Mesh specifications for viscoelastic Couette flow simulation.

	Number of Control Volumes	
	x direction	y direction
Mesh 1	200	20
Mesh 2	300	30
Mesh 3	400	40

Mesh independence for each of the cases was established.

The viscosity was kept at $\eta = 0.00104878$ mm²/s, the first relaxation time was chosen to be 0.01 s and the second was neglected. The shear rate was kept constant at $\dot{\gamma}_{xy} = 10$ 1/s by setting the top wall to move at a constant velocity of 1 m/s. For the Oldroyd-B fluid the stress components were compared to equations (3.24) and (3.25). The results of this comparison are presented in Table 18.

Table 18: Comparison between analytical and numerical solutions of tensor components. Oldroyd-B fluid model used.

	τ_{xy}	τ_{xx}
ThermOldBFoam	0.010487	0.00020975
Analytical	0.0104878	0.000209756
Error [%]	0.0076285	0.002860548

For the Giesekus model the analytical expression of each stress component was not derived. The equations obtained from the constitutive relation are used directly. Three equations are derived from the constitutive relations. Since all the various components of the polymer stress tensor feature in these equations it implies that the error of each term will contribute to the overall error. The aforementioned equations are:

$$\tau_{xx} - 2\lambda_1(\tau_{xy}\dot{\gamma}_{xy}) + \frac{\alpha\lambda_1}{\eta}\left(\tau_{xx}^2 + \tau_{xy}^2\right) = 0 \tag{3.26}$$

$$\tau_{xy} - \lambda_1 \tau_{yy} \dot{\gamma}_{xy} + \frac{\alpha \lambda_1}{\eta} \tau_{xy} (\tau_{xx} + \tau_{yy}) = \eta \dot{\gamma}_{xy} \quad (3.27)$$

$$\tau_{yy} + \frac{\alpha \lambda_1}{\eta} (\tau_{yy}^2 + \tau_{xy}^2) = 0 \quad (3.28)$$

These equations are derived from the first, second (and fourth since the tensor is symmetric) and fifth tensor components.

When the mobility constant in the Giesekus model is small the fluid will behave like an Oldroyd-B fluid. For this reason the Couette flow problem for the Giesekus model was investigated for different values of the mobility constant. The term that introduces the shear thinning of the fluid will become more dominant and therefore the stress field will move away from that predicted with the Oldroyd-B model. The fluid properties and problem set up is the same as before, however, the relaxation time is increased to 0.1 s in this case.

Three values of the mobility constants are chosen for the Giesekus model that would change the significance of the shear thinning behaviour of the model. These constants are $\alpha = 0.001, 0.01, 0.15$. The results computed are compared to the three equations obtained from the Giesekus model and presented in Table 19.

Table 19: Numerical solution of tensor component for Giesekus fluid model. Solution of equation 3.26-3.28 presented as computed from numerical solution.

α	τ_{xx}	τ_{xy}	τ_{yy}	Eq (3.26)	Eq (3.27)	Eq (3.28)
0.15	0.012933	0.008135	-0.00096	1.04E-06	0.010488	7.57E-10
0.01	0.019917	0.010196	-9.91E-05	1.17E-06	0.010488	4.26E-10
0.001	0.020864	0.010457	-1.04E-05	1.93E-06	0.010488	-2.99E-10

The reported tensor components, columns two to four, in Table 19 were computed by the "ThermGiesFoam" solver. Columns five to the end of the same table show the result when these computed components are substituted into the left hand side of equations (3.26) to (3.28). For equations (3.26) and (3.28) the values were shown to be close to zero and therefore these equations are satisfied, given the numerical error. For equation (3.27) the result were shown to be very close to the right hand side of this equation, where the analytical result is 0.0104878. From the above it is concluded that the results predicted by the "ThermGiesFoam" solver are in good agreement with the analytical values. As the value of the mobility constant decreases the significance of shear thinning decreases and the fluid behaviour tends to that predicted by the Oldroyd-B model (this is seen by comparing the results form Table 18 and Table 19).

In sections 3.1.1-3.12 a brief overview of the models developed were given. Since these models were newly developed in the OpenFOAM environment the validity of these models had to be established. This was done systematically through the remainder of the chapter. In sections 3.2.1 and 3.2.2 both the validity of the flow and temperature field predicted by all the solvers were established. It was shown in section 3.1.1 that the most basic fluid solver "genStokesFoam" was able to accurately predict the pressure distribution in the bearing if the simulated bearing was similar to the one assumed when the long bearing solution is derived. The uncoupled Stokes formulation of the flow can be used as a representative of the classical Reynolds formulation of the problem. In section 3.2.2 the error of the

flow field and the temperature field of all the solvers were shown to be less than 0.3% off from the analytical solution. After this it was still necessary to show that the shear thinning behaviour predicted by the “genStokesFoam” and “ViscFoam” solvers respectively were accurate when compared to an analytical result. This validity of the latter solvers was established in this regard in section 3.2.3. Finally for the two more sophisticated models the predicted stress field had to be validated. The accuracy of the stress field implies the ability of these solvers to predict viscoelastic behaviour. The tensor components that describe the stress field are computed by solving the differential constitutive relation for either the Oldroyd-B model or the Giesekus model. The results predicted by these solvers showed very good agreement with the analytical solution. Therefore the ability of the solvers to correctly predict the fluid behaviour was established.

Chapter 4: Application

In the previous chapter the fluid models were developed and validated. In this chapter these models are applied in order to study the non-linearity introduced through the various dependencies. The dependencies themselves are not the focal point of these applications; rather the applications show how these dependencies translate from one fluid model to another and how a coupled formulation affects the results predicted by each fluid formulation. The influence of these dependencies has been stated repeatedly in literature as well as their influence on the operating condition on bearing models (see section 1.2.2). An application that captures the operating condition within the bearing is developed and the different fluid formulations are compared in order to access the extent of the influence a coupled formulation would have.

Since the focus of the applications is not to predict the operating condition of a bearing accurately, a less sophisticated application can be used to show the effect of the coupling of the various fields. A realistic fluid model predicting the flow condition in a steam turbine journal bearing is extremely resource intensive, this is another reason an alternative application is sought. The issue with large scale bearing is the journal and bearing diameter compared with the film thickness. Compared to the scale of the bearing the fluid film is extremely thin, however the circumference of the bearing is of the same order of magnitude as the bearing's axial length. This implies a very large but thin computational domain. The large circumferential length implies that a large number of CVs are needed to gain a stable solution (this problem was also encountered in section 3.2.1 when the clearance of the bearing was decreased an increase of CVs in the circumferential direction was required). The dimension of the large steam turbine bearings considered in this study has a diameter of 0.9 m and a length to diameter ratio of 1. This translates to about $4.3\text{x}10^9$ CV's in order to achieve a converged solution. This is a rough estimate based on the same aspect ratios of the CV's used in section 3.2.1, Table 1 for the coarsest mesh for a bearing with film thickness of 1 mm. This estimate assumes that the control volumes would have equal length and width. However the simulation conducted in 3.2.1 had a journal rotating at a much lower angular velocity. The eccentricity ratio was 0.2. For more severe operating condition more CVs would be required.

On the other hand the nonlinearity of the problem needs to be recognised: one needs to look at operating conditions that are similar to that found in a bearing. The nonlinearities of the problem make the system very complicated and therefore one cannot, with confidence, say whether effects observed in a particular case would hold in general.

In order to better understand the flow conditions in a bearing, one that can neither be regarded as being short nor long, the classical Reynolds equation was considered (see section 2.1.8):

$$\frac{\partial}{\partial\theta}\left[b_1(\theta)\frac{\partial p}{\partial\theta}\right]+\left(\frac{R}{2L}\right)^2\frac{\partial}{\partial z}\left[b_2(\theta)\frac{\partial p}{\partial z}\right]=\ b_3(\theta) \tag{4.1}$$

This equation shows three primary factors that influence the flow of the oil in a bearing: the axial pressure gradient, the circumferential pressure gradient and the shearing of the oil due to the rotating journal (see Figure 7). The first two are effects due to the geometry of the bearing and the last is due to the rotation of the journal. It is known that the position of the journal, and therefore the axial and circumferential pressure gradients, depend on the motion of the journal. The motion of the journal ,in

turn, determines the position of the journal (Li, Davies, et al. 2000). The interaction between the journal and the film is therefore a complicated nonlinear dynamics problem.

An application that has each of these factors: axial pressure gradient, circumferential pressure gradient and shear, in the correct measure will be a suitable representation of the problem (see Figure 8: Section of Film taken out of the converging section of bearing.). This assumes that the journal position has reached steady state conditions such that its position and therefore the axial and circumferential pressure gradients do not change significantly. This assumption is made only for the purpose at hand: to look at the translation of dependencies from one fluid model to another. The validity of this application to predict accurate results as far as general operating conditions of the bearing are concerned is not endorsed.

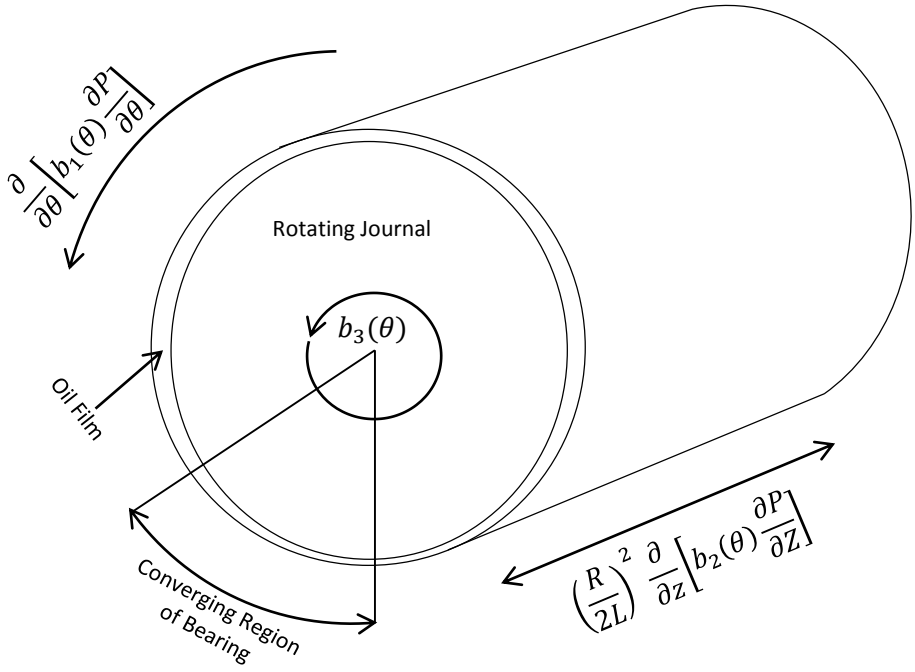

Figure 7: Bearing with terms from Reynolds equation that influence the flow indicated.

In section 3.2.1 (see Figure 4) it is seen that the maximum pressure in the bearing changes in both magnitude and position according to the eccentricity of the journal (the position of the maximum pressure shifts towards θ= 180^0 as the eccentricity of the bearing increases). It is in this region, of the maximum pressure, where the viscosity dependencies are the most influential. This is simply because both the pressure and temperature is a maximum in this region (Davies & Li 1994). (This assumes that the system has reached steady state conditions)

It is therefore reasonable to look at the converging region of the bearing (see Figure 7) since this is where the dependencies are the most severe. Hence it follows that if the dependencies in this area do not vary between the models, it will not differ anywhere else in the bearing. On the other hand, if the models do differ in this region this implies that one would carefully have to consider the model used when modelling these kinds of journal bearings. The pressure distribution in this section

determines the load carrying capacity of the bearing. The forces acting on the journal due to the pressure distribution is intricately related to the dynamics of the journal. Therefore, if the models predict different fluid behaviour in this region it will influence the behaviour of the entire system.

This chapter will proceed as follows: in section 4.1 the numerical case is developed and the fluid properties needed to accurately predict the fluid behaviour in this section are determined. In sections 4.2 and 4.3 the weak and strong coupled formulation of the problem is compared with an uncoupled formulation. After this, the results obtained are discussed.

Finally in chapter 5 conclusions are drawn on the influence of a coupled formulation opposed to an uncoupled formulation of the various fluid models. Recommendations for further research are also made.

4.1 The test case

In the previous section the reason for considering a region close to the maximum pressure was highlighted. A prismatic section of the film (see Figure 8) in this region is therefore considered and the test case was developed with the view of simulating the fluid dynamical behaviour in this region. The case presented in this section is only an approximation to the actual flow conditions. By taking out a piece of the oil film one loses a huge part of the bearing and therefore also part of the physics that would be present in a full scale bearing simulation. In order to compare the coupling of the various fluid models, the operating condition in the selected region needs to only be approximated. The approximation was developed with two particular aspects of the problem in mind: (1) The computational resources and time needed to simulated a large scale journal bearing accurately, taking all the dependencies highlighted thus far into account, would not be feasible. Particularly if one wants to look at the behaviour of the oil film without specifically computing the operating conditions of the bearing. (2) The approximation needs to capture the important factors that determine the fluid dynamics in the bearing credibly.

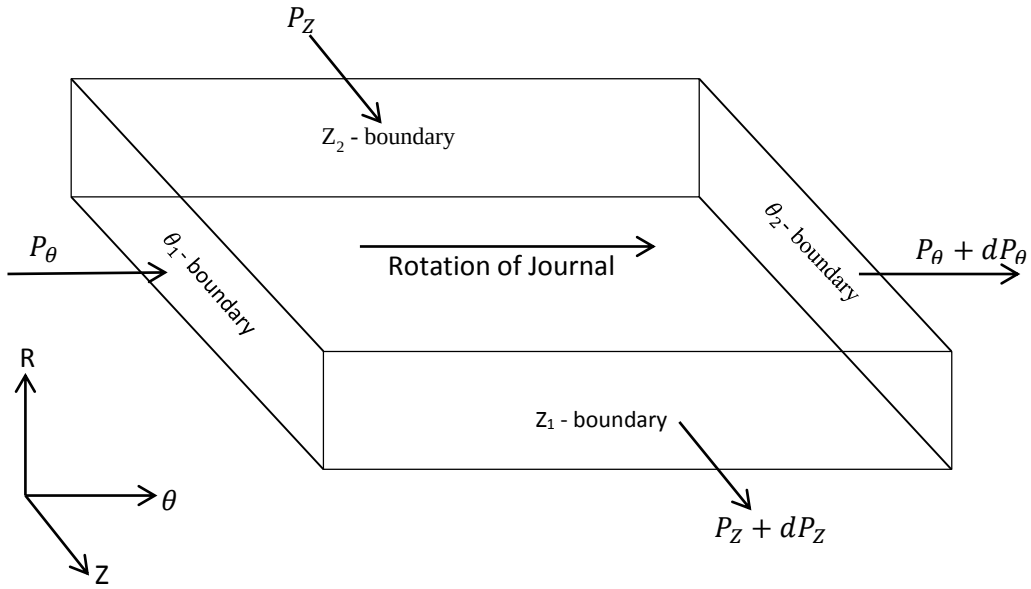

Figure 8: Section of Film taken out of the converging section of bearing.

In order for this to be the case each of the three factors, highlighted in the previous section (also see Figure 8 which indicates this), need to appear in the approximation to the same degree as it would in the corresponding section of the oil film. This presents another problem: how would one determine accurate boundary condition for the computational domain. This issue is resolved at the end of this section by employing the Finite Difference Method (FDM) to solve the Reynolds equation and thereby obtaining an approximation of the boundary conditions for the computational domain.

On the other hand it is noted that a 'broad based' analysis in this case will be an inefficient way of studying the fluid behaviour. The operating conditions in the turbo machinery considered here remain fairly steady. Great care is taken in order to ensure this through proper control. If the operating conditions in these machines fluctuate the electricity generation and line frequency would vary. This sets this study apart from those done on automotive journal bearings, where sudden changes in the journal velocity and position are to be expected. This is not to say that a research in the transient dynamics of the fluid in this region would be fruitless. Rather it affirms the approximation's ability to capture the flow conditions in this region accurately enough to determine the influence of the coupled formulation.

The geometry used to approximate this section of the bearing is prismatic. The reasons for this choice are:

- A hexahedral mesh is much easier and quicker to generate in the OpenFOAM environment.
- The number of pressure correctors needed for a hexahedral mesh that is orthogonal is very low, thus computationally it is less resource intensive.
- The accuracy of the finite volume method is generally better when orthogonal meshes are used (Juretić & Gosman 2010).

Since the curvature of the bearing is therefore neglected, it is important to determine the dimensions of computational domain that would be a reasonable approximation. Note that when the dimensions of the section of the oil film considered is small, then the curvature of the journal and bearing is well approximated geometrically by the computational domain (see Figure 9).

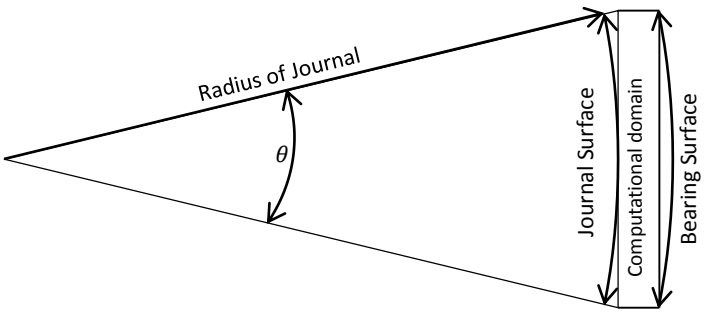

Figure 9: Geometry of computational domain approximating a section of the oil film.

If the angle is small (i.e. $\theta \ll 1\text{rad}$) then the following approximation applies:

$$\sin(\theta) \approx \theta \tag{4.2}$$

By looking at equation (4.2) for different values of θ it was found that if $\theta < 0.15$ then the error in the approximation is less than 0.5%. This implies that the difference between a straight line and a circle is less than 0.5% when the angle is smaller than 0.15. Using (4.2) this translates to a volume with a length of 3.75cm. Therefore if the volume has a length of less than 3.75cm the curvature of the bearing and journal can be neglected. Before the length of the volume is fixed the thickness of the fluid film is to be determined.

The thickness of the oil film in large bearings is difficult to determine, there is not a large body of literature available on the topic either. ESKOM indicated that the thickness should be about 1mm. In one article it was reported that the film thickness usually varies between 6-9.5mm (Lisyanskii et al. 2006). Turning to literature on automotive journal bearings it is seen that the ratio of the journal radius to the bearing radius is 0.9987. Applying this ratio to steam turbines it is seen that the corresponding film thickness is about 0.325mm. This is much smaller than the results reported by the above cited sources. The film thickness in the converging section is therefore selected to be 0.4mm. From the above cases in is evident that the film will not be thinner than this. This film thickness also allows the bearings to carry the typical weight of the rotors at the operating condition that were indicated by ESKOM (this conclusion is based on results obtained by Finite Difference solution of the Reynolds equation, this discretization is presented later in the section).

The remaining dimensions were set, based on the aforementioned discussion, as: a film thickness (R-direction) of c =0.4mm, the length (θ-direction) 5c (2 mm), and width (z-direction) 5c (2 mm). The aforementioned length and width was chosen since it was determined that this is the minimum length for which boundary effect can be neglect if the field variables are measured in the centre of the computational domain. The volume therefore had dimensions much smaller than that presented earlier in the section. The volume was therefore chosen sufficiently small to neglect the curvature of the bearing.

Next the fluid properties of the oil were determined. For the temperature dependence, the constants for the WLF-equation for the turbine oil are not known. ESKOM provided the fluid properties of the oil at three distinct temperatures. In order to determine the constants for the WLF-equation, (2.35) is cast in the form:

$$C_1 = \frac{(C_2 + T - T_0)}{T - T_0} \ln\left(\frac{\eta(T)}{\eta_0}\right) \tag{4.3}$$

Using the known viscosity data, two equations are found and can be solved simultaneously to find the constants of the WLF-equation for the oil in question. The constants for the oil were found to be C_1 = -5.898 and C_2 = -266.967. In order to confirm the validity of these constants, the shift factor (2.35) is applied to the zero shear viscosity:

$$\eta(T) = a_T \eta_0 \tag{4.4}$$

The results predicted by equation (4.4) are presented in table 18.

Table 20: Values predicted by equation (4.4)

T [K]	$\eta(T)$ mm²/s	Status of results
293.15	1.05E-02	Corresponds with given value
303.15	8.33E-03	Predicted by (4.4)
313.15	6.50E-03	Corresponds with given value
323.15	4.97E-03	Predicted by (4.4)
333.15	3.71E-03	Predicted by (4.4)
343.15	2.69E-03	Predicted by (4.4)
353.15	1.90E-03	Predicted by (4.4)
363.15	1.29E-03	Predicted by (4.4)
373.15	8.40E-04	Corresponds with given value
383.15	5.22E-04	Predicted by (4.4)
393.15	3.06E-04	Predicted by (4.4)

Comparing the viscosity predicted by the WLF-equation in table 20 to the know viscosity values at the various temperature, it is concluded that the values predicted by the WLF-equation using the calculated constants are accurate.

For the pressure dependence data form Li et al. (2000) is used. In their work they reported two constants that govern the pressure dependence. One constant applies to the viscosity directly and the other to the shear rate. The geometric mean of these two constants was taken in order to find a single constant (this can be done since the magnitude of the constants are not too far apart). The model used in this work applies the same shifting factor to the viscosity and the shear rate and therefore the aforementioned distinction made by Li et al. (2000) is neglected. This approach is followed by Wachs et al. (2002) and was adopted here. The constant used for the pressure dependence was calculated to be $\psi = 1.82 \times 10^{-8}$ Pa^{-1}. This constant is valid for dynamic pressures. OpenFOAM, however works with kinematic pressure, therefore the constant has to be divided by the density of the fluid in order to arrive at the kinematic pressure equivalent: $\psi = 1.4924 \times 10^{-5}$s^2/m^2. The density of the oil is chosen to be $\rho = 820$kg/m^3 as referenced in the aforementioned article by Li et al. (2000).

The constants used for the shear dependence was determined by using the constants for oil reported in an article by Li et al. (2000). In this article the model for shear dependence was different to the Carreau model used in the current work. The corresponding constants for the Careau model was determined by adjusting the constants *a* and *b* until the shearing of the fluid between the viscosity dependence models were less than 1% apart. The determined constants were $a = 0.3$ and $b = 0.25$ respectively.

The Giesekus model accounts for the shear thinning of the fluid. To this end the empirical constants of the viscoelastic model need to be chosen in order to give the same amount of shear thinning as the Carreau fluid. Using the equation (4.5), (Bird et al. 1977), which gives the viscosity of the fluid at a specific shear rate to the zero shear rate viscosity, the values of α,β and λ_1 were determined to be 0.5, 0.77 and 0.012 respectively.

$$\frac{\eta}{\eta_0} = \frac{1-\beta}{\beta} + \frac{\beta(1-f)^2}{1+(1-2\alpha)f} \tag{4.5}$$

where

$$\lambda_2 = \frac{\lambda_1 \eta_s}{\eta_p} \tag{4.6}$$

$$\beta = \frac{\eta_s}{\eta_s + \eta_p} \tag{4.7}$$

$$f = \frac{1-\chi}{1+(1-2\alpha)\chi} \tag{4.8}$$

$$\chi^2 = \frac{(1+16\alpha(1-\alpha)(\lambda_1\dot{\gamma})^2)}{8\alpha(1-\alpha)(\lambda_1\dot{\gamma})} \tag{4.9}$$

Finally the boundary conditions need to be determined. In order to determine the pressure boundary conditions the FDM was employed to discretize the classic Reynolds equation. Figure 10 shows an example of a FVM mesh where the nodes are indicated at the intersections of the lines.

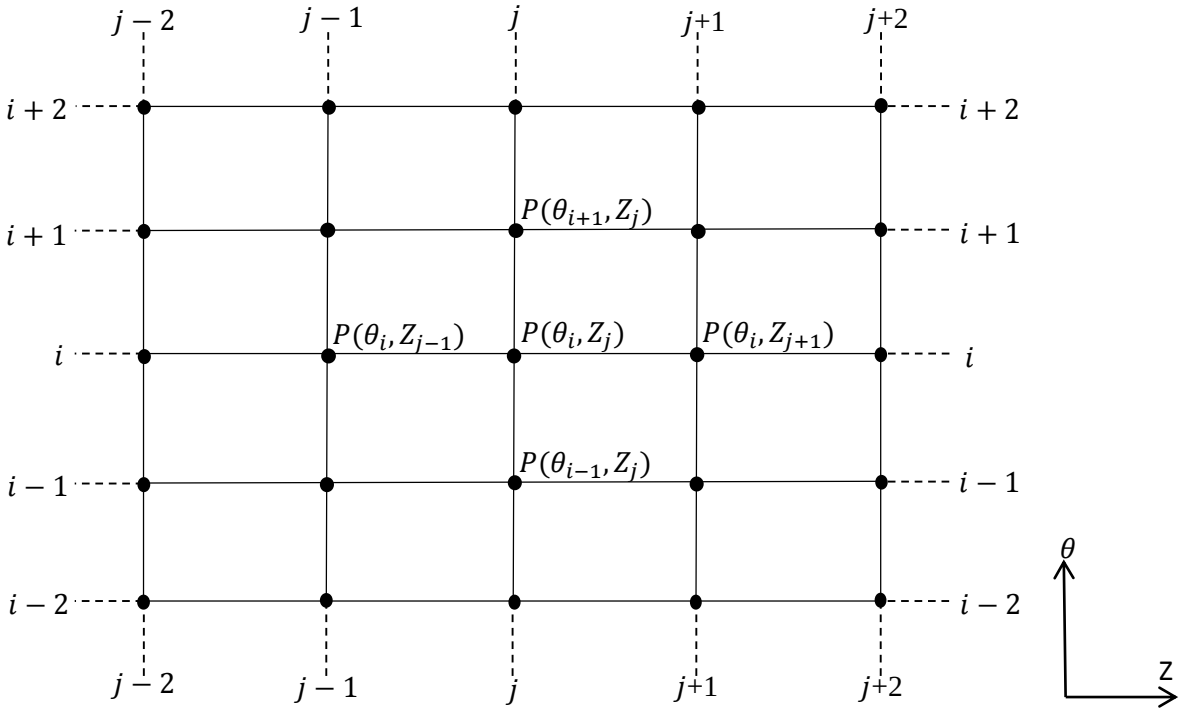

Figure 10: Finite difference mesh for solving the pressure distribution from Reynolds equation.

The pressure is computed at the nodes. This allows one to determine the values of the pressure at each boundary of the computational domain (see Figure 11). The nodes used to determine the boundary condition for the computational domain was determined by setting $P(\theta_i, Z_i)$ in Figure 11 equal to the node with the maximum pressure. The computational domain is therefore situated in the section of the bearing which is at the maximum pressure (both circumferentially and axially).

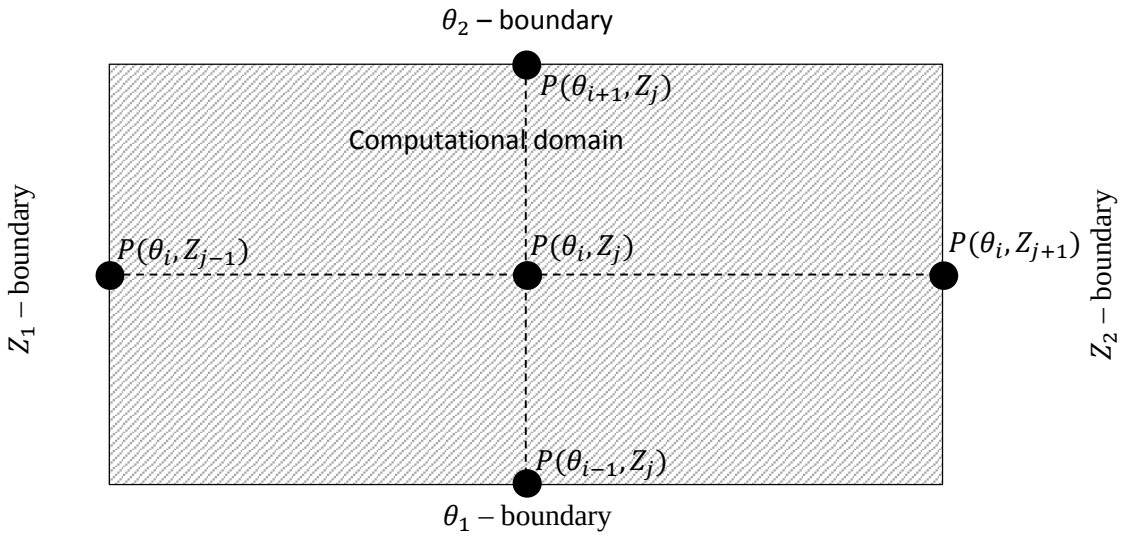

Figure 11: Top view of computational domain with nodes from finite difference domain indicated at the boundaries.

The pressure computed at the nodes is used as the average pressure on the boundaries of the computational domain. The discretized equations are presented as equation (4.10) to (4.14) below, (the functions $b_k(\theta_i)$ are renamed from equation (4.1)):

$$b_1(\theta_i)\frac{\partial p}{\partial \theta} + b_2(\theta_i)\frac{\partial^2 p}{\partial \theta^2} + b_3(\theta_i)\frac{\partial^2 p}{\partial z^2} = b_4(\theta_i) \tag{4.10}$$

$$b_1(\theta_i) = -3(1 + \epsilon\cos(\theta_i))^2(\epsilon\sin(\theta_i)) \tag{4.11}$$

$$b_2(\theta_i) = (1 + \epsilon\cos(\theta_i))^3 \tag{4.12}$$

$$b_3(\theta_i) = \left(\frac{R}{2L}\right)(1 + \epsilon\cos(\theta_i))^3 \tag{4.13}$$

$$b_4(\theta_i) = -\frac{6\eta\Omega R^2\epsilon}{c^2} sin\,(\theta_i) \tag{4.14}$$

Computing the pressure field from equation (4.10) and converting it to kinematic pressure, the pressures at the boundaries of the computational domain was found to be:

Table 21: Pressure computed by the FDM at the boundaries of the computational domain.

Boundary	Pressure computed at boundary
$\boldsymbol{p(\theta_1)}$	2.5350×10^4 m²/s²
$\boldsymbol{p(\theta_2)}$	2.5334×10^4 m²/s²
$\boldsymbol{p(z_1)}$	2.5355×10^4 m²/s²
$\boldsymbol{p(z_2)}$	2.5334×10^4 m²/s²

The discretised equations were solved by starting at an initial pressure field which is updated as the discretized equation is solved at each of the points in the domain. This process was iterated until the pressure field converged. Mesh independence was also established.

Since this case is only an approximation a constant pressure boundary condition was used at three of the four side walls. The z_2 boundary condition (see Figure 11) was set to be a zero gradient condition however. This was chosen in order to avoid large pressure gradients in the corners where the walls

meet. Although this does happen in the $z_1 - \theta_2$ corner, its effect on the flow is minimal. If another large gradient was also present in the opposite corner these effects start to affect the flow significantly. Another benefit of the zero gradient boundary condition is that a linear pressure distribution is computed on this boundary. This is closer to the actual flow conditions since the pressures at the faces will not remain constant in reality but should drop almost linearly from the high point to the low point.

Computed results from thermal profiles within the bearing have shown that the temperature in this region is almost entirely at the maximum temperature (Li, Davies, et al. 2000). The thermal boundary conditions at z_1 and θ_1 are set to be constant at 350 K. ESKOM indicated that the oil in the bearings is never allowed to go above 340 K. This value is measured after the fluid has left the bearing. The maximum value is therefore just an estimation of what is expected to be the maximum temperature in this region.

The top wall of the volume was set to move at 80 m/s as this corresponds to an angular velocity of 3000 rpm for the bearing in question. For the thermal boundary conditions the bottom wall was set to remain constant at the maximum temperature and the moving wall was set to remain constant at 300 K, slightly above room temperature. See section 2.2.2 for further details regarding thermal boundary conditions.

Finally the mesh density for both the strong and the weak coupling were seen to be the same. The coupling therefore did not seem to have an influence on the mesh density. The time step sizes were seen to be affected quite dramatically as the viscoelastic coupling was changed. This was however due to the instability of the Oldroyd-B model (see section 4.4 for more details on the time step sizes). The Meshes used are presented in table 22 below, mesh convergence was established for the last mesh.

Table 22: Mesh specifications for computational domain

	Number of Control Volumes		
	θ-direction	z-direction	R-direction
Mesh 1	20	20	10
Mesh 2	30	30	15
Mesh 3	40	40	20

4.2 Pressure dependencies a weak coupled formulation

In this section the fluid models are considered in the light of the pressure and shear rate dependence of the fluid. The pressure and shear rate dependencies of the viscosity introduces an additional non-linearity to the fluid problem. Describing a coupling as strong or weak is a rather subjective matter (Markert 2010). In the current study the pressure and shear rate dependencies are considered to introduce a weak coupling: the viscosity is determined by the field variables computed from the governing equations. The governing equation is then updated according to the newly calculated viscosity from its constitutive relation. The viscosity relation does not add an additional governing equation; rather it is added in order to complete the set of governing equations.

Two set of results are compared in this section as well as the next section: the viscous formulation and the viscoelastic formulation are compared separately. The comparison in both cases however is the

same: the difference between the different coupled or uncoupled formulations. The velocity profiles presented in sections 4.2 and 4.3 were measured at the centre of the computational domain. The magnitude of the velocity was presented. The velocity profiles however closely resemble the flow in the circumferential direction since the velocity of the flow in the axial direction is much smaller. The average velocity of the flow in the axial direction was 0.4 m/s.

For the comparison of the viscous formulations the uncoupled equation was solved using the average viscosity as computed when taking the pressure and shear rate dependencies into account. It therefore is a representative of models where one would adjust only the viscosity in order to account for the various dependencies.

The velocity profiles computed by the various viscous formulations are presented in Figure 12. The velocity profiles are plotted against the radial position (R) divided by the thickness of the fluid film (c).

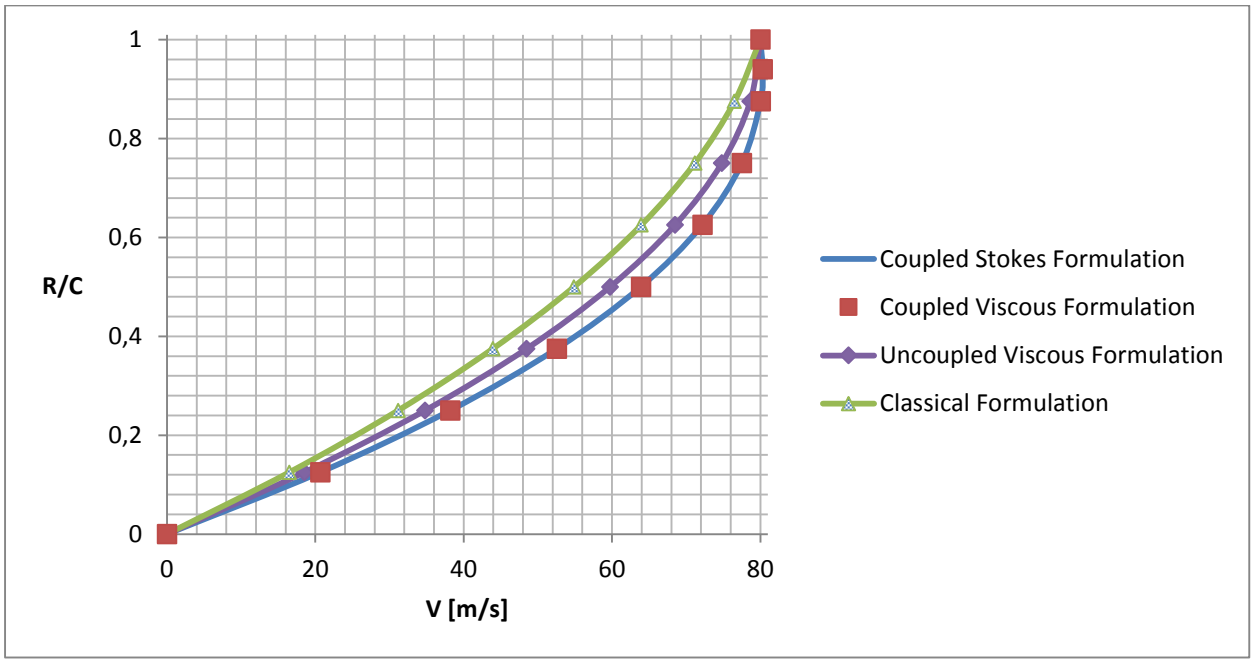

Figure 12: Velocity profiles computed using the viscous fluid and classical formulations.

The velocity profiles form the coupled Stokes and viscous formulations are almost identical. For this reason the velocity profile computed by the coupled Viscous formulation is plotted as discrete points on the velocity profile computed by the coupled Stokes formulation.

As a reference the problem was solved without adjusting the viscosity. This is representative of the result obtained with the classic formulation. Using the classical formulation as a reference, the differences between the uncoupled and coupled formulations are determined with respect to the classic formulation.

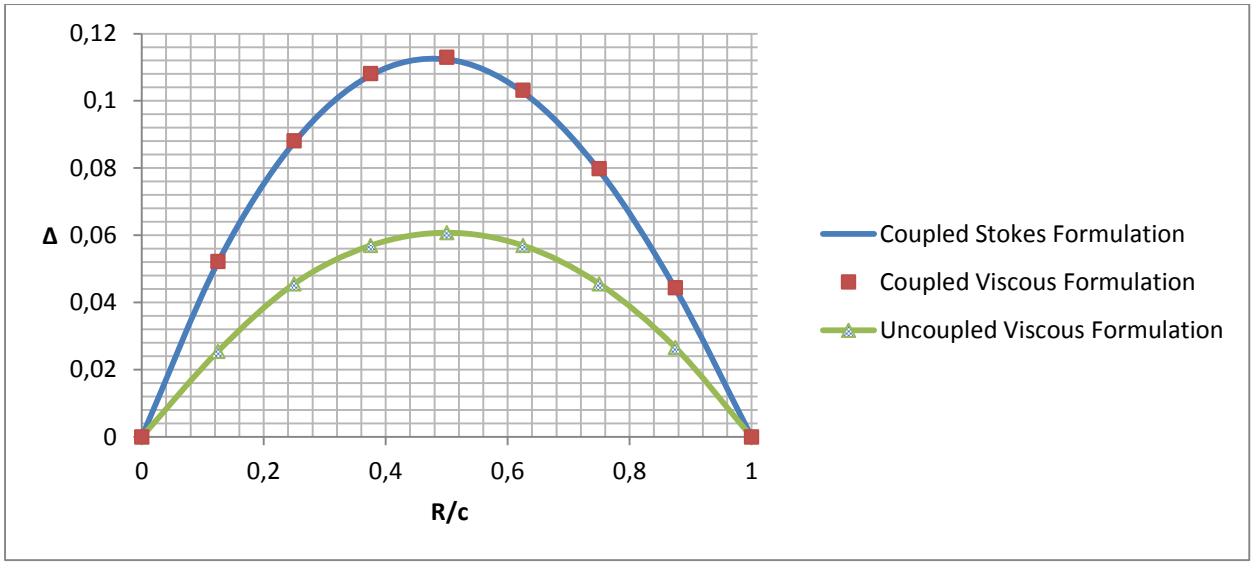

Figure 13: Difference between the velocity profiles computed by the viscous fluid and classical formulations.

Before the difference between the velocity profiles was taken the velocity profiles were divided by the velocity of the journal (the top moving wall of the domain). The absolute value of the differences was taken in order to eliminate the sign. The difference functions, equation (4.15), are computed and shown in Figure 13.

$$\frac{\|V(y) - V_{classic}(y)\|}{V_{journal}} = \Delta \tag{4.15}$$

From Figures 12 and 13 it is very clear that there was a significant difference between the coupled and uncoupled viscous formulations results. Although the difference between the coupled and uncoupled formulations is apparent from both of the mentioned figures, the different fluid models with a coupled formulation seem to be very similar.

The viscoelastic formulation was compared in the same way, although in this case the term weak coupling would not bear the same significance as in the viscous models cases. This is due to the stress field being strongly coupled with the momentum equation. The dependencies of the fluid were only allowed to influence the fluid properties; these are the viscosity and the relaxation time of the fluid. This means that the Oldroyd-B fluid formulation has a weaker coupling than the Giesekus fluid formulation when set up in this way. For this case the Oldroyd-B constitutive model was used as the simpler model and the fluid properties were assumed to be constant. The fluid properties were determined by averaging the values determined from the fully coupled case. Figure 14 shows the velocity profiles computed by the viscoelastic formulation. The classic formulation was included for the sake of comparing the results to that of the viscous formulation.

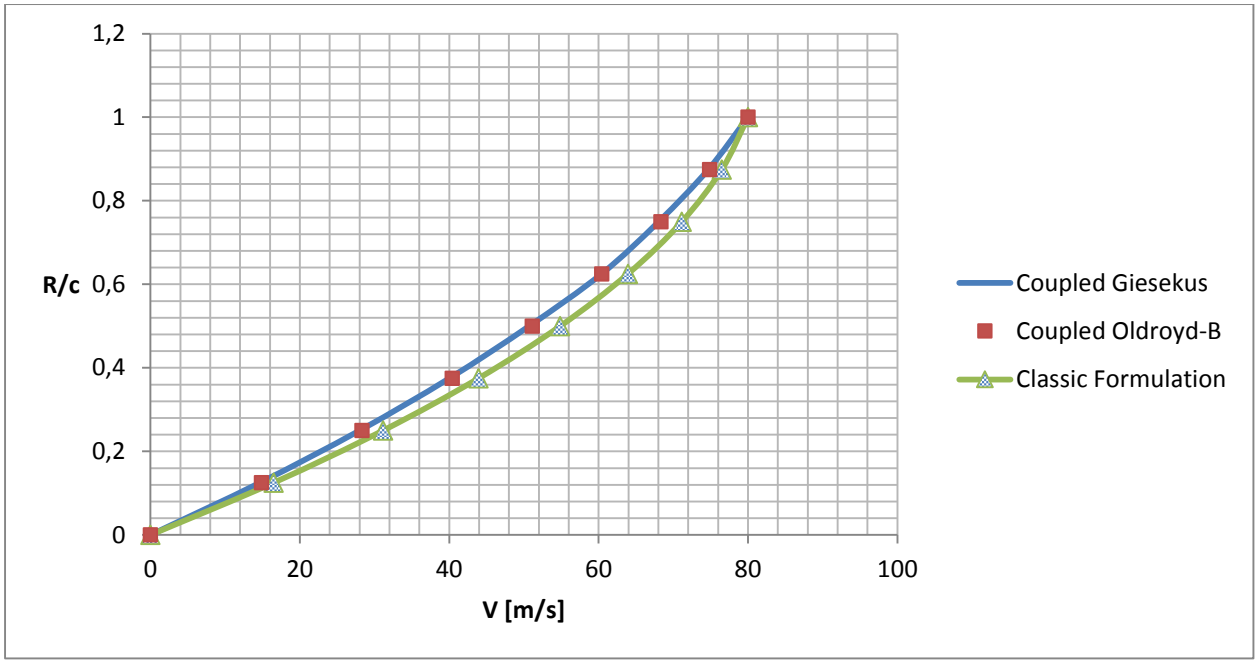

Figure 14: Velocity profiles computed using the viscoelastic fluid and classical formulations.

From Figure 14 it is firstly seen that the Oldroyd-B model gave almost identical results to the Giesekus model for this case. The difference between these two formulation in this case is, however, slightly larger than the two coupled viscous models. It is also seen from this figure that the viscoelastic fluid models predict results that were closer to the classic formulation of the problem than the viscous models in the case of a weak coupling. The comparison of the differences to the classical formulation is presented in Figure 15.

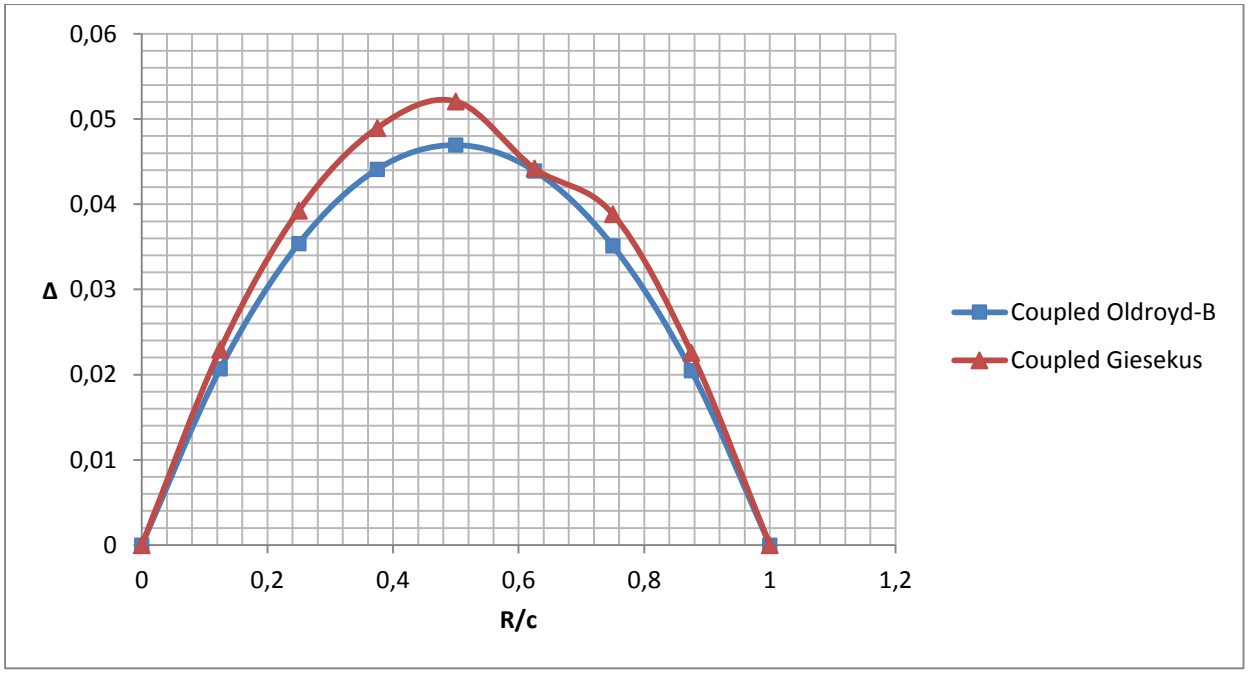

Figure 15 : Difference between the velocity profiles computed by the viscoelastic fluid and classical formulations.

Comparing Figures 14 and 15 with one another it is seen that the difference between the two viscoelastic formulations were greater than that of the viscous formulations. The viscoelastic

formulations, however, were much closer to the classical formulation than the viscous formulations. The difference function for the viscoelastic models had a different shape, as seen in Figure 15. This implies that the changes in fluid behaviour from the classical formulation to the two viscoelastic fluid models were not the same and that the change in the flow was not homogeneous. The difference function of the coupled Oldroyd-B formulation has a similar shape to the difference function of the viscous formulation (Figure 13). The coupled Giesekus did not follow this trend. This implies that the departure from the classical formulation when employing a coupled viscoelastic formulation was not analogous among the viscoelastic fluid formulations. This implies that the two viscoelastic formulations behaved differently in the presence multiple dependencies.

4.3 Thermal dependencies

In this section non-isothermal fluid models are considered. The fluid models are consequently considered as being strongly coupled. The strong coupling is introduced: firstly through additional governing equations, the energy equation and the stress constitutive relation for the viscoelastic formulation, and secondly through cross terms appearing in the different governing equations. Cross terms in this context include the viscous dissipation term (equation (2.32)), the viscosity dependence on temperature in the momentum equation (equation (2.39)), and the cross terms found in the governing equation of the stress field for the viscoelastic formulation (equations (2.13) and (2.17)).

The velocity profiles for the viscous formulation are presented in Figure 16. The uncoupled equations were computed similarly to those in the previous section: the values of the fluid properties were held constant. These values were determined by averaging the values determined form the fully coupled formulation.

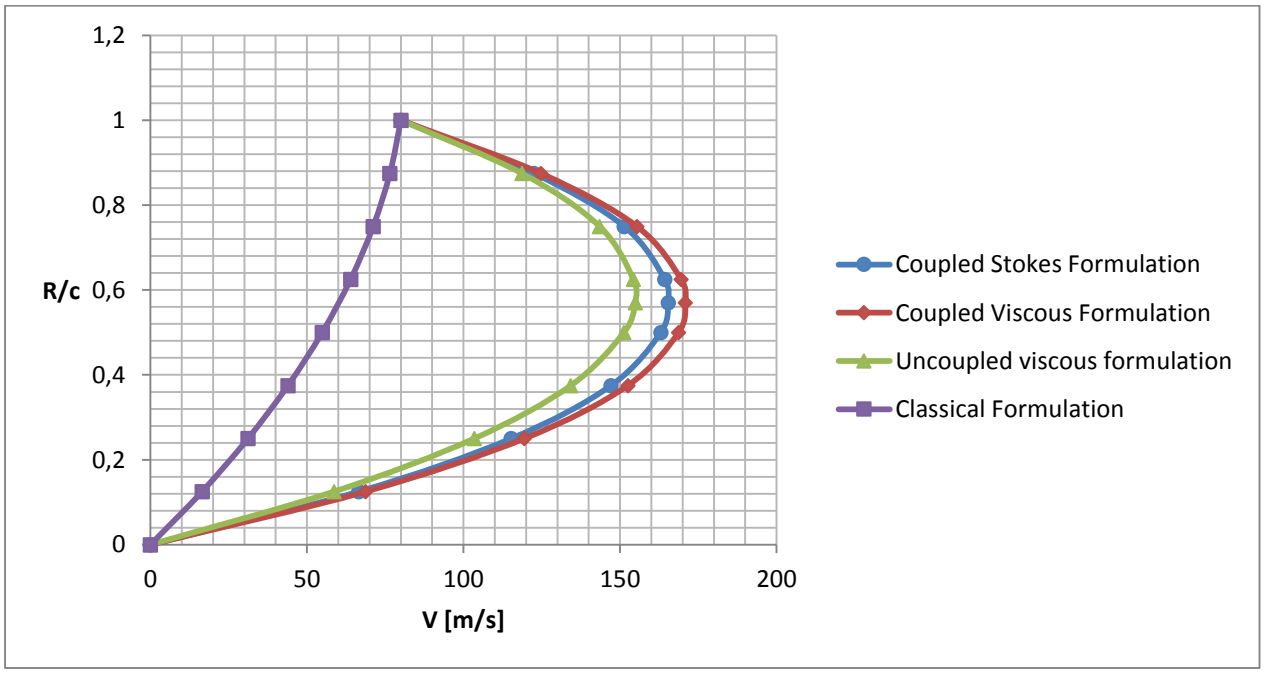

Figure 16: Velocity profiles computed using the viscous fluid formulations.

Using the same result for the classical formulation from the previous section, the differences between the velocity profiles were computed as before and are presented in Figure 17.

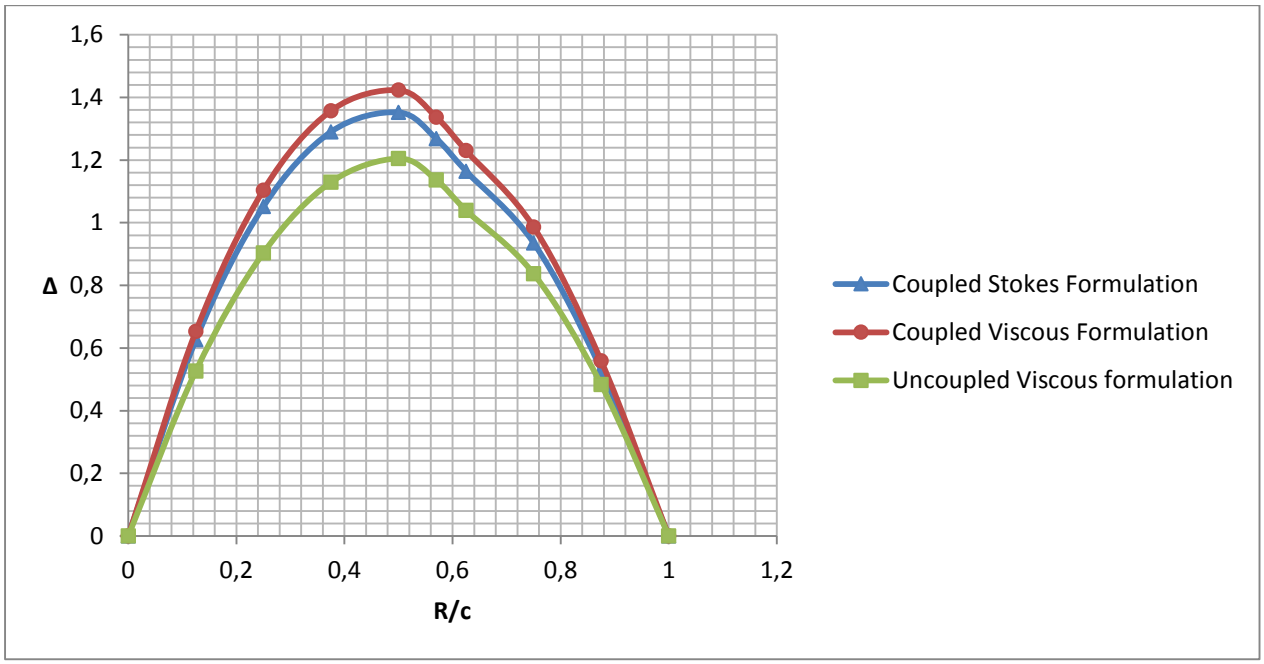

Figure 17: Difference between the velocity profiles computed by the viscous fluid formulations and classical formulations.

From Figures 16 and 17 it is clearly seen, as was the case for the weak coupling, that the coupling had a significant influence on the computed velocity profiles. By comparing Figures 13 and 17, specifically the magnitude of the differences, it is clear that the difference between the models were augmented through the stronger coupling. Another interesting result arises when comparing these two figures: the velocity profiles in the presence of the strong coupling are no longer alike as in the previous section. This implies that the strong coupling did not only introduce nonlinearities in itself, but also influenced the nonlinearities present. The different fluid models therefore behaved differently when the governing equations were coupled.

In Figure 13 the shape of the difference functions are similar to parabolas. In Figure 17 it is seen that in the presence of the stronger coupling the shape of the difference functions departed from the parabola-like shape. The change in shape of the difference functions from the weak coupling to the strong coupling is seen, however, to have changed in a similar fashion. Therefore, the departing from the parabola-like shape in Figure 13 and Figure 17 is unanimous among the models.

As in the previous section, the coupling of the viscoelastic formulation is not a comparison between a coupled or uncoupled formulation. Rather the comparison is between a weak and a strong coupled formulation. The coupling term in the constitutive relation for coupling this equation with the energy equation was set to zero in the weak coupling case. The temperature and shear dependencies of the properties were determined beforehand and were not updated in the solution procedure. The computed velocity profiles form the viscoelastic models are presented in Figure 18. The difference between the computed velocity profiles are more easily seen for the viscoelastic models in this section, compared to the previous section (see Figures 18 and 14). The difference however is not as

dramatic as for the viscous models. The reason for this is that the coupling is weaker rather uncoupled formulation as mentioned before.

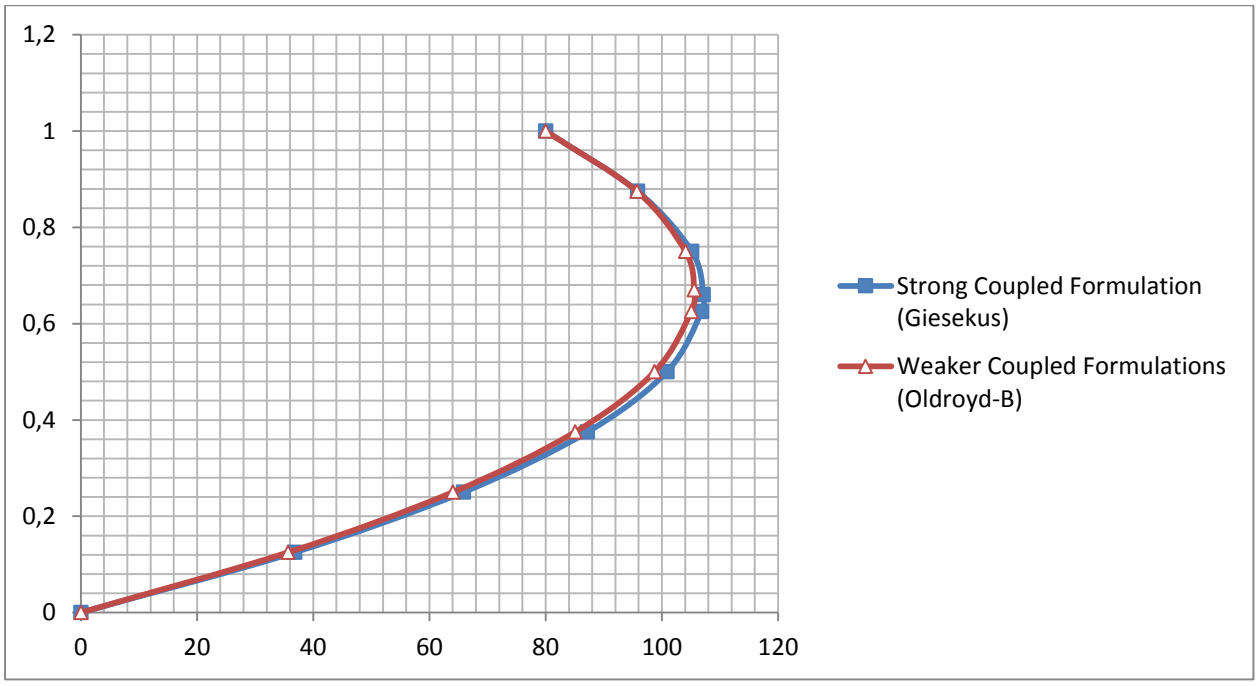

Figure 18: Velocity profiles computed using the viscoelastic fluid formulations.

The difference between the viscoelastic models and the classical formulation is presented in Figure 19. By comparing Figures 15 and 19 it is seen that the difference between the couplings of the viscoelastic models were less than for those presented in the previous section. The reason for the small change, in Figure 17, is due to the comparison between the two viscoelastic models being a comparison between a weakly coupled and strongly coupled formulation. For the viscous models the comparison is first between an uncoupled formulation and a weak coupled formulation and then to a strong coupled formulation.

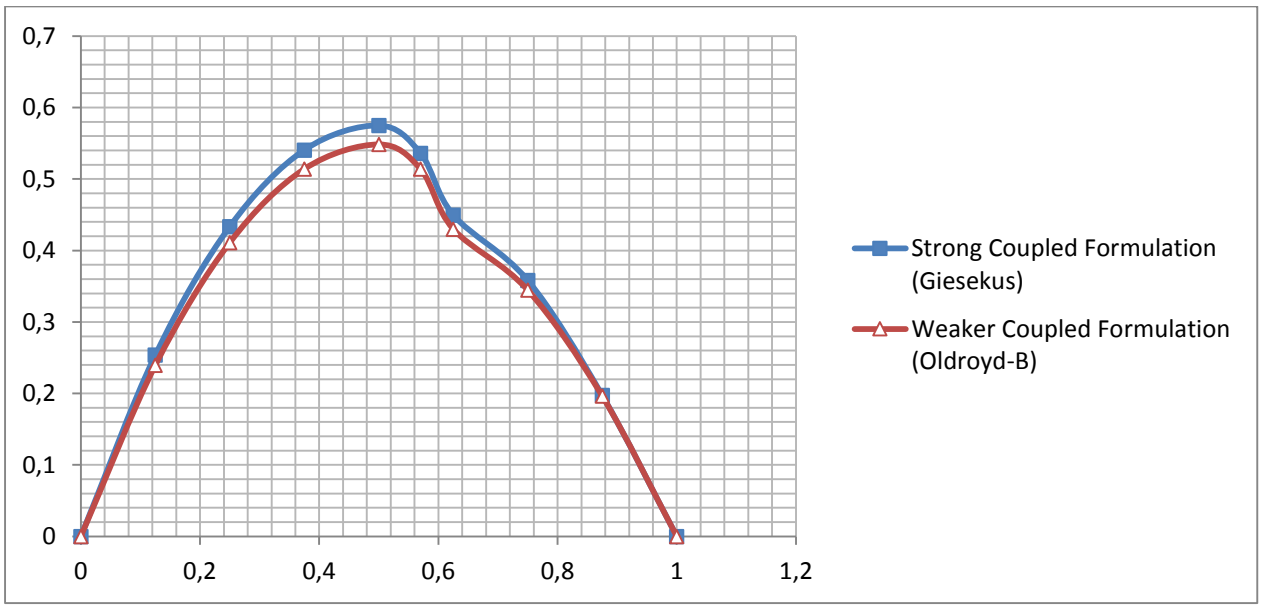

Figure 19: Difference between the velocity profiles computed by the viscoelastic fluid and classical formulations.

Comparing the viscous formulation and the viscoelastic formulation, results shown in Figures 16 and 18, it is seen that the character of the viscoelastic flow is substantially distinct for the viscous formulation. Not only do the magnitudes of the velocities differ dramatically, but the position of the maximum velocity is closer to the journal in the viscoelastic formulation compared to the viscous formulation.

The computed temperature profiles were compared and the percentage difference between the profiles is presented in Table 22.

Table 23: Percentage difference between the temperature profiles.

	Temperature difference [%]
Stokes Formulation	0.0068
Viscous Formulation	0.00079
Viscoelastic Formulation	0.0015

For this comparison the temperature profiles computed by the coupled formulations were compared to that computed by the uncoupled formulation.

The differences between the temperature profiles were negligible. The greatest difference between these various models was therefore seen in the velocity profiles.

4.4 Discussion

The context of this study is the diagnostics of large scale turbo machinery. In order to simulate reliable responses of the system reliable bearing models should be used. To this end the coupling of the governing equation were studied to determine their influence on the flow behaviour in the bearing. It has been shown that a coupled formulation of the fluid model has a significant effect on the fluid dynamics in the bearing.

The numerical case study considered the region in the bearing where the dependencies of the fluid model are the greatest. Comparison between the classical formulation and the various other formulations confirmed this. The influence of the dependencies themselves has been studied before, as was mention in section 1.2.2. The difference between the classical formulation and the various other models are therefore not surprising.

In the weak (section 4.2) and the strong (section 4.3) coupled formulation of the fluid models, it was shown that the coupling had a significant influence on the fluid behaviour. Therefore this study showed that despite the need to take into account the various fluid dependencies that influence the flow behaviour, there is a further need to take the interaction of these fluid properties with one another into account.

It was further shown therefore that when considering the influence of various dependencies that the superposition principle no longer holds: the influence of an isolated dependency in not the same as when it is in the presence of other dependencies. The most dramatic case of this is seen in section 4.3,

where the viscous models were compared to one another. The difference in the maximum velocity due to the coupling was up to 10%.

The viscous fluid formulation included the inertia terms whereas the Stokes fluid formulation did not. The influence of these terms in the case of the weak coupling does not seem to make any difference to the fluid behaviour. Moving to the case of the strongly coupled formulation the matter changes quite substantially with regards to the computed velocity profiles. It was shown that the influence of the coupling of the fields depends on the fluid model itself. This is seen very clearly in section 4.3, where the two coupled viscous models differed in maximum velocity with almost 4%.

This poses an interesting result: each case needs to be modelled individually. For large scale journal bearings one cannot simply adjust one model with say 20% since the viscosity changes that amount for the average temperatures encountered. The fluid model for the oil needs to be selected specifically to suit that oil. The governing equations would have to be coupled especially in the case of strong couplings where the coupled and uncoupled formulations showed significantly different results. These differences were not only in magnitude but in shape; implying a change in the characteristic of the flow. This change in the flow behaviour can only be accommodated by a coupled formulation. The extent of these changes also depends on the fluid model selected. This shows that selecting a fluid model to describe the oil film is not trivial as the coupled formulation of each of the models behaved differently.

In both Figures 15 and 19 it is seen that the viscoelastic models reacted differently to the coupling of the equations. The coupling in the Giesekus formulation was stronger than for the Oldroyd-B model in each of the cases presented. However, this difference in the coupling did not produce a homogenous change. Rather, the differences between the two formulations with regards to the classical formulation are quite distinct.

By comparing the results from the viscous and viscoelastic formulation it was showed that there is a dramatic difference. The shape of the velocity profiles as well as the magnitudes of the velocities is enormously different from one another. Going from the viscous to the viscoelastic formulation in the presented results were enormous, not only in terms of dependencies but also in general fluid behaviour. Neglecting the viscoelastic fluid behaviour can certainly not be rectified in a simple way. Not only is the velocity profiles dramatically changed but also the results show that the way in which the viscous and viscoelastic models respond to couplings is quite distinct.

By comparing the magnitudes of the difference functions in section 4.2 (see Figures 13 and 15) it was found that there is a significant difference between the coupled and uncoupled viscous formulations. In Figure 13 the magnitude of the difference of the coupled formulations were almost double that of the uncoupled formulation. This implies that in the region considered, neglecting the weak coupling would result in the same error as neglecting pressure effects.

This comparison for the strong coupling is much harder to make due to the dramatic difference between the viscous and viscoelastic formulations results. It is, however, seen that the differences for the coupled viscous formulations were less dramatic for the strong coupling. Although in this region the error of neglecting the coupling would result in 40% of the error when neglecting temperature and shear dependencies (although this is said in order to highlight the extent of the influence of the coupling, the author makes this statement not without some reservation. This is primarily due to the

dramatic change in flow conditions brought about when the dependencies are introduced. Although the influence is therefore highlighted it is done with the caution since it is a rough estimate). The departure from the classical formulation was not homogenous (Figure 17) as with the weak coupling (Figure 13). This implies a non-homogenous change in the fluid behaviour, the effects of which would have to be studied further as far as the impact on bearing operating conditions are concerned.

During this study it was also found that the uncoupled and coupled formulations have a significant effect on the numerical stability of the solvers: the uncoupled formulation being the more stable of the two. In conjunction to this it was also seen that the time step sizes needed for the uncoupled formulation to be stable was at least double or up to five times more in the viscoelastic cases.

For the viscoelastic case it was seen that the Giesekus model was much more stable than the Oldroyd-B model. Simulations with the test case presented in section 4.1 with the fully coupled Oldroyd-B model could not be completed due to the model being too unstable. The reason for the added stability of the Giesekus model is the additional term. When α is made small the instability of the Oldroyd-B model surfaces. The divergence of the model always originated from the constitutive models. The additional term in the Giesekus model adds a positive value to the diagonal of the system matrix. This improves the diagonal dominance of the system for the same reason the DEVSS (see section 3.1.2) improves the stability of the momentum equation.

The influence of the additional term in the constitutive relation coupling the stress and temperature fields seems to be negligible (see section 2.14 and 2.15). This is seen by comparing Figures 15 and 19. In Figure 15 this term is negligible, however in Figure 19 it is not. The difference between these two figures being as similar as they are implies the insignificance of this term in this study. This is not to say that this term is insignificant in general, it might even be significant under transient conditions (see section 5.1).

Chapter 5: Conclusion

In this study four distinct fluid models were implemented in the OpenFOAM environment. The fluid models have a coupled formulation and differ significantly in the degree of sophistication as far as the fluid behaviour each model can describe. The validity of each of the developed solvers was established by means of various analytical solutions.

The importance of studying the fluid behaviour in the presence of a coupled formulation of the fluid models has been highlighted. The fluid models which were developed and validated were then used to study the fluid behaviour in a bearing. This was done by looking at a specific region of the oil film. This region was specifically selected for this study since it was determined that this region would have the greatest presence and interaction of the various dependencies modelled.

In this region considered it was shown that the coupling of the fields has a significant effect on the fluid dynamics. The coupling itself introduces various complexities to the fluid behaviour which cannot be accounted for by merely adjusting the fluid properties. It was shown that in both the weak and strong coupled formulations a significant error is introduced when fluid properties are adjusted without regarding the interaction of the various dependencies.

In this study it was therefore clearly demonstrated than in order to accurately model the fluid behaviour in large scale journal bearings the coupling of the fields must be considered and accounted for. To the authors knowledge this research has not been conducted before. The ability to simulate a rotor bearing system accurately depends vitally on the accuracy of the bearing models. This in turn depends on the accuracy of the fluid models used to describe the oil film. If the various factors that influence the fluid dynamics in the oil film is not accounted for one cannot with any certainty diagnose any fault mechanism in the rotor-bearing system.

It is therefore concluded that the coupling, either weak or strong, of the fields, velocity, temperature and stress are essential to describe the fluid behaviour and characteristic in a large scale journal bearing accurately.

5.1 Recommendations for further research

The first matter to mention in regard to further research is experimental determination of the fluid properties. The fluid properties used in this study were merely estimations of the actual values, and greater accuracy is needed. Experimental data for large scale journal bearings are also needed in order to determine which fluid model is the best to predict the actual flow condition. These flow properties are not readily available in literature. This might even show the necessity of looking at more general viscoelastic models. As was shown in this study, the model used is very important in describing the fluid behaviour as each model could potentially behave differently in the presence of dependencies and couplings.

As mentioned in section 4.4 the change in flow behaviour when going form the weak to the strong coupling needs to be further investigated in order to determine the extent to which this change influences the bearing operating conditions.

Since numerical stability issues have already been encountered further research is required in the stabilising of the solvers, specifically with respect to the part of the constitutive relation that is evaluated implicitly for the viscoelastic fluid formulations. The larger the portion of the divergence of the polymer stress that is evaluated implicitly the more stable the scheme. This would be particularly important when considering transient boundary conditions.

The boundary conditions for the numerical case used in this study need to be improved. One of the first ways to do this is to use a linear pressure drop over all the boundary faces rather than constant values. Transient conditions can be included in various ways, but essentially one would want to change one of the three main driving forces of the flow: the axial pressure gradient, the circumferential pressure gradient and the rotation of the journal. The change could be oscillatory in nature, changing one of these three at frequencies in the order of the operating conditions of the system (this would typically be at 50Hz). However, it might also be interesting to look at how the models behaviour when very high frequency changes occur. The number of boundary conditions that are changed can then also be increased from one until all three of the aforementioned driving forces are changing at the same time. Another change that is worth looking into is sudden jump boundary conditions: where there is a sudden loss of pressure for instance. Studying the additional term coupling the stress and energy equation for the viscoelastic fluid formulation is important when the boundary conditions are transient. It is expected that this term will grow in it's significant with the addition of more transient dynamics due to the term being a time derivate.

The thermal boundary condition should also be improved. This was already noted in section 2.2.2. The implementation of a Robin's boundary condition seem the most logical way forward considering the results presented by X.K. Li et al. (2000).

The interpolation used at the boundaries also needs to be revised. In their work, Habla et al. (2012) showed the importance of this interpolation with regards to the stress field. This was not done in this study but this is surely necessary if one wants to improve the general accuracy of the results.

The response of the bearings were not considered in this study, however in the general context of this project the following points are worth mentioning as far as the response and dynamics of the system is concerned:

In order to study the response of the system the model must be extended to include dynamic motion of the journal. OpenFOAM can be used to do this without too much trouble as dynamics mesh libraries exist and incorporating them into solvers in not too complicated.

In order to model the dynamics of the journal properly a good cavitation model is needed. In the context of predicting the response of the system, a full two phase formulation is necessary. Together with the two phase model a compressible fluid model is needed. This might seem drastic; however the reason for this is bubble collapse. When the cavitation bubbles collapse a shock wave is formed in the film. The propagation of such a shock wave would be dependent on the density of the fluid and therefore a compressible fluid is necessary to accurately model the propagation of the shock wave through the film. In order to deal with the bubbles a Lagrangian formulation is also needed to track the bubbles as they move through the mesh and is able to predict the movement of a bubble from one control volume to another. Whether or not the Finite Volume Method (and therefore by

implication OpenFOAM) is the correct way to tackle this kind of problem is also matter that needs to be considered.

References

Avramov, K. V. & Borysiuk, O. V., 2011. Nonlinear dynamics of one disk asymmetrical rotor supported by two journal bearings. *Nonlinear Dynamics*, 67(2), pp.1201–1219. Available at: http://www.springerlink.com/index/10.1007/s11071-011-0063-x [Accessed January 9, 2013].

Bank, R. & Chan, T., 1994. A composite step bi-conjugate gradient algorithm for nonsymmetric linear systems. *Numerical Algorithms*, 7, pp.1–16. Available at: http://link.springer.com/article/10.1007/BF02141258 [Accessed May 26, 2014].

Bensow, R. & Bark, G., 2010. Simulating cavitating flows with LES in OpenFoam. *V European Conference on Computational …*, (June), pp.14–17. Available at: http://www.researchgate.net/publication/228406414_Simulating_Cavitating_Flows_with_LES_in_OpenFOAM/file/32bfe512c474492304.pdf [Accessed April 30, 2014].

Bird, R.B., Armstrong, R.C. & Hassager, O., 1977. Dynamics of polymeric liquids.

Bollada, P. & Phillips, T., 2007. On the effects of a compressible viscous lubricant on the loadâ€bearing capacity of a journal bearing. *… Journal for Numerical Methods in …*, (June), pp.1091–1120. Available at: http://onlinelibrary.wiley.com/doi/10.1002/fld.1545/abstract [Accessed March 6, 2013].

Bollada, P.C. & Phillips, T.N., 2012. On the Mathematical Modelling Viscoelastic Fluid. , 205, pp.1–26.

Bouaziz, S., Fakhfakh, T. & Haddar, M., 2012. Acoustic analysis of hydrodynamic and elasto-hydrodynamic oil lubricated journal bearings. *Journal of Hydrodynamics, Ser. B*, 24(2), pp.250–256. Available at: http://linkinghub.elsevier.com/retrieve/pii/S1001605811602412 [Accessed January 24, 2013].

Burden, R.L. & Faires, J.D., Numerical analysis. 2001. *Brooks/Cole, USA*.

Chen, C., 1998. Chaos in the Imbalance Response of a Flexible Rotor Supported by Oil Film Bearings with Non-Linear Suspension. , pp.71–90.

Chhabra, R.P. & Richardson, J.F., 2011. *Non-Newtonian flow and applied rheology: engineering applications*, Butterworth-Heinemann.

Christensen, R.M., 2013. *Theory of Viscoelasticity*, Courier Dover Publications.

Davies, a. R. & Li, X.K., 1994. Numerical modelling of pressure and temperature effects in viscoelastic flow between eccentrically rotating cylinders. *Journal of Non-Newtonian Fluid Mechanics*, 54(94), pp.331–350. Available at: http://linkinghub.elsevier.com/retrieve/pii/0377025794800308.

Faghri, A., Zhang, Y. & Howell, J.R., 2010. *Advanced heat and mass transfer*, Global Digital Press.

Favero, J. & Secchi, A., 2009. Viscoelastic flow simulation: development of a methodology of analysis using the software OpenFOAM and differential constitutive equations. *Computer Aided Chemical …*, pp.915–920. Available at:

http://www.sciencedirect.com/science/article/pii/S1570794609703736 [Accessed May 23, 2013].

Ferziger, J.H., Peric, M. & Leonard, A., 2008. Computational Methods for Fluid Dynamics. *Physics Today*, 50(3), pp.80–84.

Georgescu, A. et al., 2001. On special solutions of the Reynolds equation from lubrication. , 133, pp.367–372.

Gertzos, K.P., Nikolakopoulos, P.G. & Papadopoulos, C. a., 2008. CFD analysis of journal bearing hydrodynamic lubrication by Bingham lubricant. *Tribology International*, 41(12), pp.1190–1204. Available at: http://linkinghub.elsevier.com/retrieve/pii/S0301679X08000546 [Accessed January 24, 2013].

Giesekus, H., 1982. A simple constitutive equation for polymer fluids based on the concept of deformation-dependent tensorial mobility. *Journal of Non-Newtonian Fluid Mechanics*, 11(1), pp.69–109.

Gucnette, R. & Fortin, M., 1995. A new mixed finite element method for computing viscoelastic flows. , 60, pp.27–52.

Gwynllyw, D.R. & Phillips, T.N., 2008. The influence of Oldroyd-B and PTT lubricants on moving journal bearing systems. *Journal of Non-Newtonian Fluid Mechanics*, 150(2-3), pp.196–210. Available at: http://linkinghub.elsevier.com/retrieve/pii/S0377025707002303 [Accessed December 3, 2012].

Habla, F. et al., 2012. Development of a methodology for numerical simulation of non-isothermal viscoelastic fluid flows with application to axisymmetric 4: 1 contraction flows. *Chemical Engineering …*, 207-208, pp.772–784. Available at: http://dx.doi.org/10.1016/j.cej.2012.07.060 [Accessed May 31, 2013].

Habla, F., Marschall, H. & Hinrichsen, O., 2011. Numerical simulation of viscoelastic two-phase flows using openFOAM®. *Chemical Engineering …*, 66(22), pp.5487–5496. Available at: http://dx.doi.org/10.1016/j.ces.2011.06.076 [Accessed March 12, 2013].

Haosheng, C. & Darong, C., 2005. Modified Reynolds Equation for Non-Newtonian Fluid With Rheological Model in Frequency Domain. *Journal of Tribology*, 127(4), p.893. Available at: http://link.aip.org/link/JOTRE9/v127/i4/p893/s1&Agg=doi [Accessed January 24, 2013].

Jagadeesha, K.M. et al., 2012. 3D Surface Roughness Effects on Transient Non-Newtonian Response of Dynamically Loaded Journal Bearings. *Tribology Transactions*, 55(1), pp.32–42. Available at: http://www.tandfonline.com/doi/abs/10.1080/10402004.2011.626144 [Accessed January 24, 2013].

Juretić, F. & Gosman, a. D., 2010. Error Analysis of the Finite-Volume Method with Respect to Mesh Type. *Numerical Heat Transfer, Part B: Fundamentals*, 57(6), pp.414–439. Available at: http://www.tandfonline.com/doi/abs/10.1080/10407791003685155 [Accessed April 30, 2014].

Kayar, A.E.L. & Khalil, M.F., 1983. Two-dimensional finite difference solution for externally pressurized journal bearings of finite length. *Wear*, 84, pp.1–13.

Kohno, K., Takahashi, S. & Saki, K., 1994. Elasto-hydrodynamic lubrication analysis of journal bearings with combined use of boundary elements and finite elements. *Engineering Analysis with Boundary Elements*, 13(3), pp.273–281. Available at: http://linkinghub.elsevier.com/retrieve/pii/0955799794900531.

Kvitnitsky, Y., Kirkatch, N. & Poltavsky, Y., 1976. The solution of reynolds equation under natural boundary conditions for hydrodynamic journal bearings. *Wear*, 37, pp.217–231. Available at: http://www.sciencedirect.com/science/article/pii/0043164876900296 [Accessed April 29, 2014].

Li, W. et al., 2011. A novel nonlinear model of rotor/bearing/seal system and numerical analysis. *Mechanism and Machine Theory*, 46(5), pp.618–631. Available at: http://linkinghub.elsevier.com/retrieve/pii/S0094114X11000127 [Accessed May 30, 2013].

Li, X.., Gwynllyw, D.R., et al., 2000. On the influence of lubricant properties on the dynamics of two-dimensional journal bearings. *Journal of Non-Newtonian Fluid Mechanics*, 93(1), pp.29–59. Available at: http://linkinghub.elsevier.com/retrieve/pii/S0377025700001075.

Li, X.., Davies, a. . & Phillips, T.., 2000. A transient thermal analysis for dynamically loaded bearings. *Computers & Fluids*, 29(7), pp.749–790. Available at: http://linkinghub.elsevier.com/retrieve/pii/S0045793099000353.

Li, X.K. et al., 2011. On non-Newtonian lubrication with the upper convected Maxwell model. *Applied Mathematical Modelling*, 35(5), pp.2309–2323. Available at: http://linkinghub.elsevier.com/retrieve/pii/S0307904X10004130 [Accessed April 29, 2014].

Li, X.K., Davies, A.R. & Phillips, T.N., 1999. THREE-DIMENSIONAL EFFECTS IN DYNAMICALLY LOADED JOURNAL BEARINGS. , 341(October 1997), pp.311–341.

Lind, S. & Phillips, T., 2012. Bubble collapse in compressible fluids using a spectral element marker particle method. Part 2. Viscoelastic fluids. *… Journal for Numerical Methods in Fluids*, (June 2012), pp.1103–1130. Available at: http://onlinelibrary.wiley.com/doi/10.1002/fld.3701/full [Accessed March 7, 2013].

Lind, S.J. & Phillips, T.N., 2012. The effect of viscoelasticity on the dynamics of two gas bubbles near a rigid boundary. *IMA Journal of Applied Mathematics*, 77(5), pp.652–677. Available at: http://imamat.oxfordjournals.org/cgi/doi/10.1093/imamat/hxs041 [Accessed March 7, 2013].

Lind, S.J. & Phillips, T.N., 2011. The influence of viscoelasticity on the collapse of cavitation bubbles near a rigid boundary. *Theoretical and Computational Fluid Dynamics*, 26(1-4), pp.245–277. Available at: http://www.springerlink.com/index/10.1007/s00162-011-0227-9 [Accessed March 7, 2013].

Lisyanskii, A.S. et al., 2006. Generalization of the results from investigations on perfecting the design of journal bearings for large steam turbines for nuclear power stations. *Thermal engineering*, 53(2), pp.81–87.

Liu, H. et al., 2010. Application of Computational Fluid Dynamics and Fluid–Structure Interaction Method to the Lubrication Study of a Rotor–Bearing System. *Tribology Letters*, 38(3), pp.325–336. Available at: http://www.springerlink.com/index/10.1007/s11249-010-9612-6 [Accessed November 30, 2012].

Liu, K. & Grecov, D., 2011. Rheological and flow modelling of viscoelastic fluids between eccentric cylinders. *Applied Mathematical Modelling*, 35(4), pp.1603–1615. Available at: http://linkinghub.elsevier.com/retrieve/pii/S0307904X10003719 [Accessed April 29, 2014].

Luneno, J.-C. & Aidanpää, J.-O., 2010. Use of nonlinear journal-bearing impedance descriptions to evaluate linear analysis of the steady-state imbalance response for a rigid symmetric rotor supported by two identical finite-length hydrodynamic journal bearings at high eccentricities. *Nonlinear Dynamics*, 62(1-2), pp.151–165. Available at: http://www.springerlink.com/index/10.1007/s11071-010-9706-6 [Accessed January 9, 2013].

Majumdar, B.C., 1969. The numerical solution of hydrostatic bearings with several supply ports. , 14, pp.389–396.

Mang, T. & Dresel, W., 2007. *Lubricants and lubrication*, John Wiley & Sons.

Markert, B., 2010. Weak or strong: on coupled problems in continuum mechanics.

Moreira, M., Antunes, J. & Pina, H., 2000. A theoretical model for nonlinear orbital motions of rotors under fluid confinement. *Journal of fluids and structures*, pp.635–668. Available at: http://www.sciencedirect.com/science/article/pii/S0889974600902895 [Accessed April 29, 2014].

Mu, Y. et al., 2012. Modeling and simulation of three-dimensional planar contraction flow of viscoelastic fluids with PTT, Giesekus and FENE-P constitutive models. *Applied Mathematics and Computation*, 218(17), pp.8429–8443. Available at: http://linkinghub.elsevier.com/retrieve/pii/S0096300312001166 [Accessed March 12, 2013].

Mukherjee, A., 1974. An analytical solution of a finite bearing with an inclined journal. *Wear*, 29, pp.21–29.

Nagaraju, T., Sharma, S. & Jain, S., 2003. Performance of externally pressurized non-recessed roughened journal bearing system operating with non-Newtonian lubricant. *Tribology transactions*, (2003), pp.37–41. Available at: http://www.tandfonline.com/doi/full/10.1080/05698190490426007 [Accessed February 27, 2013].

Oliveira, P.J., Pinho, F.T. & Pinto, G. a., 1998. Numerical simulation of non-linear elastic flows with a general collocated finite-volume method. *Journal of Non-Newtonian Fluid Mechanics*, 79(1), pp.1–43. Available at: http://linkinghub.elsevier.com/retrieve/pii/S0377025798000822.

Omowunmi, S.C. & Yuan, X.-F., 2013. Time-dependent non-linear dynamics of polymer solutions in microfluidic contraction flow—a numerical study on the role of elongational viscosity. *Rheologica Acta*. Available at: http://link.springer.com/10.1007/s00397-013-0684-8 [Accessed March 12, 2013].

Owens, R.G. & Phillips, T.N., 2002. *Computational rheology*, World Scientific.

Pennacchi, P., Vania, A. & Chatterton, S., 2012. Nonlinear effects caused by coupling misalignment in rotors equipped with journal bearings. *Mechanical Systems and Signal Processing*, 30, pp.306–322. Available at: http://linkinghub.elsevier.com/retrieve/pii/S0888327011005127 [Accessed January 9, 2013].

Phillips, T.. & Williams, a. ., 1999. Viscoelastic flow through a planar contraction using a semi-Lagrangian finite volume method. *Journal of Non-Newtonian Fluid Mechanics*, 87(2-3), pp.215–246. Available at: http://linkinghub.elsevier.com/retrieve/pii/S0377025799000658.

Reddy, J.N., 2009. Principles of continuum mechanics.

Saad, Y., 2003. *Iterative methods for sparse linear systems*, Siam.

Singhal, G.C., 1981. Computation methods for hydrodynamic problems (Reynolds ' equation). , 13(3), pp.151–154.

Solghar, A.A. & Gandjalikhan Nassab, S. a., 2011. Thermohydrodynamic behaviors of finite journal bearings with cavitation. *Mécanique & Industries*, 12(1), pp.5–15. Available at: http://www.mechanics-industry.org/10.1051/meca/2011002 [Accessed January 24, 2013].

Stachowiak, G. & Batchelor, A.W., 2013. *Engineering tribology*, Butterworth-Heinemann.

Sun, J. & Changlin, G., 2004. Hydrodynamic lubrication analysis of journal bearing considering misalignment caused by shaft deformation. *Tribology International*, 37(10), pp.841–848. Available at: http://linkinghub.elsevier.com/retrieve/pii/S0301679X04000970 [Accessed May 26, 2014].

Szeri, A.Z., 2011. *Fluid film lubrication*, Cambridge University Press Cambridge.

Thomas, D.., Sureshkumar, R. & Khomami, B., 2004. Effect of inertia on thermoelastic flow instability. *Journal of Non-Newtonian Fluid Mechanics*, 120(1-3), pp.93–100. Available at: http://linkinghub.elsevier.com/retrieve/pii/S0377025704001107 [Accessed May 26, 2014].

Uhkoetter, S. et al., 2012. Development and Validation of a Three-Dimensional Multiphase Flow CFD Analysis for Journal Bearings in Steam and Heavy Duty Gas Turbines. In *ASME Turbo Expo 2012: Turbine Technical Conference and Exposition*. pp. 749–758.

Versteeg, H.K. & Malalasekera, W., 2007. *An introduction to computational fluid dynamics: the finite volume method*, Pearson Education.

Vignolo, G.G., Barilá, D.O. & Quinzani, L.M., 2011. Approximate analytical solution to Reynolds equation for finite length journal bearings. *Tribology International*, 44(10), pp.1089–1099. Available at: http://linkinghub.elsevier.com/retrieve/pii/S0301679X11000752 [Accessed November 7, 2012].

Wachs, A., Clermont, J.-R. & Khalifeh, A., 2002. Computations of non-isothermal viscous and viscoelastic flows in abrupt contractions using a finite volume method. *Engineering Computations*, 19(8), pp.874–901. Available at: http://www.emeraldinsight.com/10.1108/02644400210450332 [Accessed March 12, 2013].

Walters, K. et al., 1997. On the Importance of Non-Newtonian Effects in Journal Bearing Lubrication: A Numerical Approach. *SAE Technical Paper*.

Wang, X.-L., Zhang, J.-Y. & Dong, H., 2011. Analysis of bearing lubrication under dynamic loading considering micropolar and cavitating effects. *Tribology International*, 44(9), pp.1071–1075.

Available at: http://linkinghub.elsevier.com/retrieve/pii/S0301679X11001277 [Accessed January 24, 2013].

White, F.M., 2006. *Viscous fluid flow*, McGraw-Hill New York.

Zhmayev, E., Zhou, H. & Joo, Y.L., 2008. Modeling of non-isothermal polymer jets in melt electrospinning. *Journal of Non-Newtonian Fluid Mechanics*, 153(2), pp.95–108.

Appendix A: Notes on the finite volume method and OpenFOAM

OpenFOAM is a finite volume based numerical solver, originally designed to solve partial differential equations.

A.1 Finite Volume method

The finite volume method refers to the discretization of a domain into a number of finite volumes. OpenFOAM uses a collocated finite volume method: all the variable's values are stored at the centre of a cell, or at the node. This technique is usually adopted for unstructured grids. In this case the domain is described in generalized coordinates and contra-variant vectors and tensors are used. This greatly complicates the equations. Due to the unstructured nature of the mesh pressure oscillations are no longer a concern (Ferziger et al. 2008).

The first step is to integrate the conservation equation over an arbitrary control volume; generally this is of the form (Versteeg & Malalasekera 2007):

$$\int_{CV} \frac{\partial}{\partial t}(\rho\phi)dV + \int_{CV} \nabla\cdot(\rho\phi u)dV = \int_{CV} \nabla\cdot\big(\Gamma\,\nabla(\phi)\big)dV + \int_{CV} S_\phi\, dV \qquad \text{(A.1)}$$

the integrals are taken over the entire control volume as indicated by the subscript CV at the bottom of the integral. ϕ is the transported property. The diffusivity of a property is accompanied by a proportionality constant that relates the rate of transfer of the property to the gradient of that property. Finally S_ϕ is a source or sink of the transported property ϕ.

Using Gauss' divergence theorem the governing equation can be transformed to flux integrals across the control surface rather than looking at the control volume as a whole:

$$\int_{CV} \frac{\partial}{\partial t}(\rho\phi)dV + \int_{CS} (\rho\varphi\bar{u})\cdot\bar{n}\,dA = \int_{CS} (\Gamma\,\nabla(\phi))\cdot\bar{n}\,dA + \int_{CV} S_\phi\, dV \qquad \text{(A.2)}$$

The terms on the left hand side expresses the change in the scalar variable in the control volume with respect to time, and the convective flux across the control surface into and out of the control surface respectively. On the other side the terms represent the diffusion of the scalar property into and out of the control volume across the control surface, and the generation of the scalar property in the control volume respectively.

In orthogonal meshes the convective and diffusion terms are easily discretize since the area vector will always be in the same direction as one of the base vectors of the domain. However in general meshes are not orthogonal and to resolve these terms require some effort, introducing additional terms in the discretized equation.

The equation is now discretized by summing the total flux across the surfaces due to convection and diffusion and approximating the two volume terms that remain. The integrals are replaces with finite summations and therefore the system is discretized. The finite volume method therefore recast the partial differential equations into a system of algebraic equations of the form:

$$A\bar{x} = \bar{b} \tag{A.3}$$

This can then be solved by the numerical solvers discussed in section (A4).

A.2 Piso Algorithim

OpenFOAM uses the Pressure Implicit with Splitting of Operators (PISO) algorithm to solve the pressure and velocity fields. The PISO algorithm is a prediction and correction algorithm. Usually the PISO algorithm will comprise of one prediction step and two correction steps, however in OpenFOAM the amount of correction steps can be specified, usually ranging between 2 to 20 steps.

Once discretized the linear momentum equation is of the form (Ferziger et al. 2008):

$$A_p^{u_i} u_{i,p}^{m^*} + \sum_l A_l^{m^*} u_{i,l}^{m^*} = Q_{u_i}^{m-1} - \left(\frac{\delta p^m}{\delta x_i}\right)_p \tag{A.4}$$

The coefficients $A_p^{u_i}$, where p refers to an arbitrary node, are the coefficients of the matrix A in (A3). These coefficients are dependent on the velocity field, making the algebraic system of equations nonlinear. The index *i* in the summation refers to all neighbouring cells. $Q_{u_i}^{m-1}$ refers to the source terms of momentum other than pressure (pressure is treated in a conservative manner by evaluating pressure as a surface trace rather than a body force, this reduces numerical errors due to interpolations required when modelling pressure in as a body force) , which can also be nonlinear due to its possible dependence on the velocity field.

The superscript m refers to the outer iteration time step: Two sets of iterations are performed, inner iterations, which solve the linearised equations and the outer iterations which update the coefficients of the matrix and linearise the equation again for the next inner iteration loop. The pressure is treated implicitly, meaning that the pressure used in the solving of the equation corresponds to the pressure at that time step; this is opposed to explicit evaluation which uses the pressure at the previous time step. The different from of the gradient operator acting on the pressure field used in this equation indicates that it is a discretized gradient.

The superscript for the velocity field m^* indicates that the velocity field is not yet divergence free: Since the problem being considered has incompressible flow it follows from the continuity equation (2.3) that the velocity field must be divergence free. This gives the criteria when evaluating the velocity field. In the inner iterations the equations is subjected to this condition and then iterated until conservation of mass is achieved.

The PISO algorithm uses two correction terms, one for velocity and one for pressure, defined as:

$$p^m = p' + p^{m-1} \quad \text{(A.5)}$$
$$u_p^m = u_p' + u_p^{m-1} \quad \text{(A.6)}$$

By using this corrector and making the assumption that the neighbouring cell's corrections have no influence on the pressure correction (which is not easy to justify, the same assumption is made to derive the relation between the velocity and pressure correction terms in the SIMPLE algorithm) Poisson's equation for pressure correction arises:

$$\frac{\delta}{\delta x_i}\left[\frac{\rho}{A_p^{u_i}}\left(\frac{\delta p'}{\delta x_i}\right)\right]_p = \left[\frac{\delta\left(\rho u_i^{m^*}\right)}{\delta x_i}\right]_p \quad \text{(A.7)}$$

Solving this equation in the inner iteration loop gives a pressure correction which is then used to determine the pressure field implicitly. Since (A.7) follows from the continuity equation it follows that once the above equation is satisfied and the corrections is applied the velocity field will be divergence free.

After this the velocity correction is determined the velocity field is corrected by using:

$$u_{i,P}' = \hat{u}_{i,P}' - \frac{1}{A_p^{u_i}}\left(\frac{\delta p'}{\delta x_i}\right)_p \quad \text{(A.8)}$$

This equation follows from the momentum equation when substituting in the correction terms. The first term on the right hand side is the velocity sources excluding pressure as well as the influence of neighbouring cells.

Once the continuity equation has been satisfied the pressure and the velocity field now obey the conservation of mass restriction imposed but does not satisfy the linear momentum equation. In order for the momentum equation to be solved the outer iteration loop (which iterates the nonlinear problem) must be solved. After each outer iteration the coefficients of the matrix are updated according to the available information and according to the constraint of conservation of linear momentum. Continuing the above procedure yields a velocity and pressure field that obeys all the necessary conservation laws within the convergence criteria.

A.3 Preconditioners

A preconditioner is any implicit or explicit modification of a linear system of equations which allows one to solve the system quicker and/or more accurately. Although this is the goal of preconditioners, this is not necessarily always the case and easier solutions cannot be guaranteed by just applying a preconditioner.

The two preconditioners that are applied in this study is: DICPreconditioner (Simplified diagonal-based incomplete Cholesky preconditioner), which is applied to symmetric matrices, and the DILUPreconditioner (Simplified diagonal-based incomplete LU preconditioner), which is applied to asymmetric matrices.

Although the word preconditioner is used in the OpenFOAM computational environment it is very closely related to the corresponding LU and Cholesky factorisations.

For LU factorization Gauss elimination is used to find the upper triangular matrix corresponding to the matrix A. For this process to be successful the matrix A must be an M-matrix (Saad 2003):

1. $a_{i,i} > 0 \; for \; i = 1, \dots, n$
2. $a_{i,j} \leq 0 \; for \; i \neq j; \; i, j = 1, \dots, n$
3. A is non-singular
4. $A^{-1} \geq 0$, which means that every entry of the inverse of the matrix is nonnegative.

If these conditions hold then the matrix A will be reduced into an upper triangular matrix through Gauss elimination. The goal of LU factorization is therefore the factorization of the matrix A in the product of the matrices L and U. In the case of a preconditioner this is not done exactly, rather an approximation of L and U is found therefore yielding:

$$A = LU - R \tag{A.9}$$

where R is the matrix that contains all the terms that was dropped during Gauss elimination (this dropping of terms are done according to a specified zero pattern that is predefined and eases the computational time of the Gauss elimination). This matrix has the property of having only nonnegative entries. This is the incomplete factorization of A, it can be shown that this is a regular splitting of A; which means that LU is non-singular and the matrices $(LU)^{-1}$ and R all have nonnegative entries (Saad 2003).

Since on the other the Choleshy factorization is applied to symmetric matrices this preconditioner tries to cast the matrix into the form:

$$A = LL^t - R \tag{A.10}$$

In practice OpenFOAM would give a warning if a symmetric preconditioner was applied to an asymmetric matrix, therefore it is not necessary before hand to determine this property of the matrix. It is commonly seen that the matrices of scalar variables tend to be symmetric whereas the vector variable tend to have asymmetric matrices.

A.4 Solvers

The solvers implemented in OpenFOAM are listed in the manual. The ones of interest are:

The PBiCG (Preconditioned Bi-Conjugate Gradient) and PCG (Preconditioned Conjugate Gradient) solvers.

These solvers can be implemented as either direct or iterative solver, and are used to solve the linear system of equations (A.3).

The dimensions of A correspond to the number of degrees of freedom in the computational domain. When there is therefore a large computational domain (which is most definitely the case with the current problem) direct solvers are no longer an option since they require an immense amount of memory and therefore altogether uneconomical.

Boundary value problems usually results in matrices that contain a large amount of zeroes, this makes iterative solvers the preferred choice if the matrix is converted to a sparse matrix (Burden & Faires 2001). The implementation of these solvers in OpenFOAM is therefore iterative.

The two solvers (PBiCG and PCG) are used to solve the velocity, pressure and stress fields respectively. The reason for using two solvers lies in the difference in nature of the solvers themselves. The PCG solver is used to solve systems such as (A.3) where A is a positive definite matrix. By definition A must therefore be a symmetric matrix (Burden & Faires 2001). The PBiCG on the other hand is a natural generalization of the PCG solver as this solver is applied to the same system however the matrix A need not be positive definite. In fact this solver reduces to the PCG solver if A is a positive definitive matrix (Bank & Chan 1994).

Precondition has a significant effect on computational time as it generally reduces the number of iterations, if the preconditioning was selected well (a good preconditioning would be one that allow for faster more accurate computations). Suppose A is ill conditioned, merely applying the conjugate gradient method results in the solution being more susceptible to rounding errors, increasing the computational time required to meet convergence criteria (Burden & Faires 2001).